

**Discovery of Small Molecule Regulators of Insulin
Degrading Enzyme via Computational Screening Approach**

by

Ezgi Dağyıldız

**Thesis Submitted to the
Graduate School of Engineering
in Partial Fulfillment of the Requirements for
the Degree of**

**Master of Science
in
Chemical and Biological Engineering**

Koç University

August, 2010

Koç University
Graduate School of Sciences and Engineering

This is to certify that I have examined this copy of a master's thesis by

Ezgi Dağyıldız

and have found that it is complete and satisfactory in all respects,
and that any and all revisions required by the final
examining committee have been made.

Committee Members:

Seda Kızılel, Ph. D. (Advisor)

Metin Türkay, Ph. D. (Co-Advisor)

İbrahim Halil Kavaklı, Ph. D.

Cory D. Dunn, Ph. D.

Alkan Kabakçioğlu, Ph. D.

Date: _____

to my family...

ABSTRACT

Insulin-degrading enzyme (IDE) is an allosteric Zn^{2+} metalloprotease involved in the clearance of various physiologically relevant peptide substrates including amyloid beta ($A\beta$), and insulin that play key roles in Alzheimer's disease (AD) and type 2 diabetes mellitus (T2DM), respectively. Several evidences suggest that IDE dysfunction may be responsible in the pathogenesis of these chronic diseases. Therefore, the regulation of IDE might be an alternative approach for the treatment of both AD and T2DM. It should be possible to enhance the catabolism of $A\beta$ which is the major component of plaques that are observed in the brains of AD patients and insulin by increasing the activity of IDE. Crystal structure of IDE revealed that N-terminal domain of IDE has a highly conserved exosite which is ~ 30 Å away from the catalytic region. This specific site allows the anchoring of the N-terminus of IDE substrates in the substrate binding chamber and orients them to the catalytic site. Additionally, a 9-amino acid long peptide, bradykinin is known to bind to the exosite and enhances the activity of IDE. On the basis of this finding, a computer-aided small molecule discovery protocol involving molecular dynamics, structure-based virtual screening with docking simulations targeting to the IDE exosite has been used for screening compounds that might regulate the catalytic function of IDE from a compound library.

ÖZETÇE

İnsülin parçalayan enzim (IDE), 2. Tip şeker ve Alzheimer hastalıklarında önemli rol oynayan sırasıyla insülin ve amyloid- β proteinlerinin kandan temizlenmesinde görev alan alosterik bir Zn^{2+} metalloproteazdır. Çeşitli bulgular IDE'nin işlev bozukluğunun bu kronik hastalıkların patogenezinde etkili olabileceğini göstermektedir. Bu bağlamda IDE'nin katalitik fonksiyonunu düzenlemek bu hastalıkların tedavisi için kullanılabilir alternatif bir yaklaşımdır. Alzheimer hastalarının beyinlerinde oluşan plakların en temel maddesi olan A β proteinin ve insulinin parçalanma hızlarının artırılması IDE enziminin katalitik fonksiyonunun artırılması ile mümkün kılınabilir. IDE'nin kristal yapısı bu enzimin N-terminalinde ve katalitik bölgeden ~ 30 Å uzakta bulunan exosite bölgesinin, IDE substratlarının kesilecek kısımlarını katalitik bölgeye yönlendiren düzenleyici bir özelliği olduğunu göstermiştir. Buna ek olarak, 9 amino asitlik bir peptid substrat olan bradykinin'in de IDE'ye exosite bölgesinden bağlanarak IDE'nin aktivitesini arttırdığı bilinmektedir. Bu bulgular dahilinde IDE'nin katalitik fonksiyonunu aktive eden düzenleyici moleküllerin tasarımı için moleküler dinamik simülasyonu, yapıya dayalı sanal tarama ve exosite bölgesini hedef alan moleküler kenetlenme simülasyonlarını da içeren bir protokol uygulanarak bir molekül veritabanı taranmıştır.

ACKNOWLEDGEMENTS

There are a number of people I am deeply grateful without whom this thesis would not be completed.

I would like to express my deep and sincere gratitude to my advisor Dr. Seda Kızılel and Dr. Metin Türkay for their great guidance, patience and continuous support during my graduate study. Also, I would like to thank my thesis committee member Dr. İ. Halil Kavaklı, Dr. Alkan Kabakçiođlu and Dr. Cory D. Dunn for their critical reading and useful comments.

I would like to thank my research group friends, Onur Dađlıyan and Bilal akır, It would not be possible to finish this thesis without their help.

I wish to thank my friends Selin Özdiñ, Yeliz Aka, Bahriye Cesaret, Eda Bektař, Seil Uluřık, Gzde zbek, Ceren Tzmen, Onur Dađlıyan, Uđur Kaplan, Mehmet Ali Yatbaz, Nil Ezgi Diñer, Selmi Bozbađ, Bilal akır, Enis Demir, Sibel Kalyoncu, Erdal Uzunlar, Fatma Virdil, Filiz Sayın, Bora Kabatepe for their valuable friendships and for sharing me great moments.

I owe my loving thanks to Tarık for always believing in me and for his encouragement.

Finally, I would like to thank my wonderful family Nesteren Dađyıldız, İbrahim Dađyıldız, my sister Sidar Dađyıldız Thams and my brother in law Chris Thams for their continuous support, patience and guidance during every step of my education.

TABLE OF CONTENTS

| | |
|---|-----------|
| List of Tables | x |
| List of Figures | xi |
| Chapter 1: Introduction | 16 |
| Chapter 2: Literature Review | 20 |
| 2.1. Alzheimer's Disease | 20 |
| 2.1.1 Amyloid β peptide | 21 |
| 2.1.2 Genetics of Alzheimer's disease | 24 |
| 2.1.3 Treatment Strategies of Alzheimer's disease | 26 |
| 2.2. Type II diabetes mellitus (T2DM) | 27 |
| 2.2.1 Insulin signalling | 28 |
| 2.3. Diabetes and dementia..... | 29 |
| 2.3.1 Epidemiology | 29 |
| 2.3.2 Pathological links between AD and T2DM | 30 |
| 2.3.3.1 Insulin Resistance & Hyperinsulinemia | 30 |
| 2.3.3.2 Glucose and energy metabolism impairment | 32 |
| 2.3.3.3 Amyloidogenesis..... | 33 |
| 2.3.3.4 Molecules linking both of them | 34 |
| 2.3.3.4.1 GSK | 34 |
| 2.3.3.4.2 Insulin Degrading Enzyme (IDE)..... | 35 |

| | |
|---|-----------|
| 2.4. Structure Based Drug Design for AD and T2DM..... | 37 |
| 2.4.1 Drug Design | 37 |
| 2.4.2 Structure Based Drug Design..... | 39 |
| 2.4.3 Target Identification: IDE | 42 |
| 2.4.4 Target Structure..... | 42 |
| Chapter 3: Computational Method | 48 |
| 3.1 Molecular Dynamics (MD) Simulation..... | 48 |
| 3.1.1 NAMD..... | 48 |
| 3.1.2 MD Setup..... | 50 |
| 3.2 Protein-Small Molecule Docking..... | 51 |
| 3.2.1 AutoDock..... | 53 |
| 3.2.2 AutoDock Docking Setup..... | 54 |
| Chapter 4: Results and Discussion | 58 |
| 4.1 Analysis of Molecular Dynamics Simulation..... | 58 |
| 4.2 Validation of AutoDock with Molecular Docking Studies for the Previously Found IDE Regulators..... | 61 |
| 4.3 Virtual Screening and Detailed Docking Results..... | 65 |
| 4.3.1 Virtual Screening Results..... | 65 |
| 4.3.2 Detailed Docking Results, Selection and Elimination of the Candidates..... | 66 |
| 4.3.3 Computational Analysis of the Novel Compounds | 100 |
| 4.5.4 Discussion | 122 |

| | |
|-------------------------------|------------|
| Chapter 5: Conclusions | 127 |
| Supplementary | 130 |
| Bibliography | 131 |
| Vita | 152 |

LIST OF TABLES

| | | |
|------------|---|----|
| Table 4.1: | Residual RMSD values for IDE exosite (336-342 & 359-363)..... | 60 |
| Table 4.2: | Binding and Docking Energies of bradykinin and selected compounds..... | 65 |
| Table 4.3: | Binding and docking energy scores of virtual screening and detailed docking of the selected 38 candidates..... | 67 |
| Table 4.4: | Physicochemical properties of top selected candidates..... | 71 |
| Table 4.5: | IDE regulation of compounds selected from Ambinter Compound Library that showed effective binding and docking scores in virtual screening and detailed docking..... | 91 |
| Table 4.6: | 2D Structures of the selected candidates..... | 92 |

LIST OF FIGURES

| | | |
|-------------|--|----|
| Figure 2.1: | Systematic Diagram of the “amyloid cascade hypothesis” | 25 |
| Figure 2.2: | Hypothesized stages of neurodegeneration | 37 |
| Figure 2.3: | The process of structure-based drug design | 40 |
| Figure 2.4: | Secondary structure representation of the IDE..... | 43 |
| Figure 2.5: | Interactions between A β and IDE..... | 44 |
| Figure 2.6: | Detailed interaction of the N-terminus of amylin, A β 1–42, IGF-II and TGF- α with the exosite of IDE..... | 45 |
| Figure 2.7: | Surface representation of IDE (a). Interactions between bradykinin and the exosite of IDE (b)..... | 47 |
| Figure 4.1: | Time dependence of the root mean square deviations (rmsd) for the 1.2-ns MD trajectory of IDE (2G47-without amyloid- β fragment..... | 58 |
| Figure 4.2: | IDE exosite colored by the average RMSD per residue | 59 |
| Figure 4.3: | Docked Conformation of bradykinin within IDE exosite. a) Interactions between full bradykinin and the exosite of IDE. b) Interactions between N-terminus of bradykinin and the exosite of IDE..... | 62 |
| Figure 4.4: | Docked Conformation of compound Ia1 and Ia2 within IDE exosite. Interactions between a) Ia1 and b) Ia2 and the exosite of IDE..... | 64 |
| Figure 4.5: | Docked Conformation of compound 8-171972 within IDE exosite. Interactions with exosite of IDE..... | 73 |
| Figure 4.6: | Docked Conformation of compound 1-100872 within IDE exosite. Interactions with exosite of IDE..... | 74 |
| Figure 4.7: | Docked Conformation of compound 4-131929 within IDE exosite. Interactions with exosite of IDE..... | 75 |

| | |
|---|----|
| Figure 4.8: Docked Conformation of compound 3-122109 within IDE exosite. Interactions with exosite of IDE | 76 |
| Figure 4.9: Docked Conformation of compound 1-16588 within IDE exosite. Interactions with exosite of IDE | 77 |
| Figure 4.10: Docked Conformation of compound 8-141265 within IDE exosite. Interactions with exosite of IDE | 78 |
| Figure 4.11: Docked Conformation of compound 3-116810 within IDE exosite. Interactions with exosite of IDE | 79 |
| Figure 4.12: Docked Conformation of compound 5-108909 within IDE exosite. Interactions with exosite of IDE | 80 |
| Figure 4.13: Docked Conformation of compound 1-168108 within IDE exosite. Interactions with exosite of IDE | 81 |
| Figure 4.14: Docked Conformation of compound 9-1674 within IDE exosite. Interactions with exosite of IDE | 82 |
| Figure 4.15: Docked Conformation of compound 2-12104 within IDE exosite. Interactions with exosite of IDE | 83 |
| Figure 4.16: Docked Conformation of compound 1-102877 within IDE exosite. Interactions with exosite of IDE | 84 |
| Figure 4.17: Docked Conformation of compound 1-11351 within IDE exosite. Interactions with exosite of IDE | 85 |
| Figure 4.18: Docked Conformation of compound 1-180914 within IDE exosite. Interactions with exosite of IDE | 86 |
| Figure 4.19: Docked Conformation of compound 9-102548 within IDE exosite. Interactions with exosite of IDE | 87 |

| | |
|--|-----|
| Figure 4.20: Docked Conformation of compound 4-131363 within IDE exosite. | |
| Interactions with exosite of IDE | 88 |
| Figure 4.21: Docked Conformation of compound 4-100665 within IDE exosite. | |
| Interactions with exosite of IDE | 89 |
| Figure 4.22: Docked Conformation of compound 1-11207 within IDE exosite. | |
| Interactions with exosite of IDE | 90 |
| Figure 4.23: Selected IDE regulators (a) front view, (b) side view..... | 100 |
| Figure 4.24: The structure of IDE catalytic chamber and selected representative compounds (colorful sticks) docked to the IDE exosite (red cartoon) | 101 |
| Figure 4.25: Docked Conformation of compound 8-141267 within IDE exosite. | |
| Interactions with exosite of IDE | 102 |
| Figure 4.26: Docked Conformation of compound 8-171299 within IDE exosite. | |
| Interactions with exosite of IDE | 103 |
| Figure 4.27: Docked Conformation of compound 9-151914 within IDE exosite. | |
| Interactions with exosite of IDE | 104 |
| Figure 4.28: Docked Conformation of compound 9-147338 within IDE exosite. | |
| Interactions with exosite of IDE | 105 |
| Figure 4.29: Docked Conformation of compound 3-114154 within IDE exosite. | |
| Interactions with exosite of IDE | 106 |
| Figure 4.30: Docked Conformation of compound 9-14137 within IDE exosite. | |
| Interactions with exosite of IDE | 107 |
| Figure 4.31: Docked Conformation of compound 1-16593 within IDE exosite. | |
| Interactions with exosite of IDE | 108 |
| Figure 4.32: Docked Conformation of compound 9-151856 within IDE exosite. | |
| Interactions with exosite of IDE | 109 |

| | |
|---|-----|
| Figure 4.33: Docked Conformation of compound 3-113780 within IDE exosite. | |
| Interactions with exosite of IDE | 110 |
| Figure 4.34: Docked Conformation of compound 3-135627 within IDE exosite. | |
| Interactions with exosite of IDE | 111 |
| Figure 4.35: Docked Conformation of compound 9-1573 within IDE exosite | |
| Interactions with exosite of IDE | 112 |
| Figure 4.36: Docked Conformation of compound 3-137443 within IDE exosite. | |
| Interactions with exosite of IDE | 113 |
| Figure 4.37: Docked Conformation of compound 9-134343 within IDE exosite. | |
| Interactions with exosite of IDE | 114 |
| Figure 4.38: Docked Conformation of compound 1-180918 within IDE exosite. | |
| Interactions with exosite of IDE | 115 |
| Figure 4.39: Docked Conformation of compound 8-456 within IDE exosite. | |
| Interactions with exosite of IDE | 116 |
| Figure 4.40: Docked Conformation of compound 3-110732 within IDE exosite. | |
| Interactions with exosite of IDE | 117 |
| Figure 4.41: Docked Conformation of compound 4-106854 within IDE exosite. | |
| Interactions with exosite of IDE | 118 |
| Figure 4.42: Docked Conformation of compound 3-114848 within IDE exosite. | |
| Interactions with exosite of IDE | 119 |
| Figure 4.43: Docked Conformation of compound 2-114522 within IDE exosite. | |
| Interactions with exosite of IDE | 120 |
| Figure 4.44: Docked Conformation of compound 1-11728 within IDE exosite. | |
| Interactions with exosite of IDE | 121 |

Figure 4.45: Adopted computational strategy for the discovery of Alzheimer and T2DM

Regulators..... 122

Chapter 1

INTRODUCTION

Discovery of new therapeutic chemicals is the main concern in the pharmaceutical industry. It is estimated that on average 14 years are needed to obtain an approved drug from a lead compound [1], and as expected, the enormous costs associated with this process are the main challenges of this industry. Current efforts are generally directed towards eliminating this economic pressure [2]. As a consequence, this need forces scientists to develop alternative computational tools to identify lead compounds in a shorter timeline with higher quality and a reasonable cost.

In the process of drug discovery, the critical step is the identification of the proper lead compound for a given target molecule. In the traditional drug discovery, these novel hits are identified by the high-throughput screening (HTS) of large chemical libraries [3]. However, these systematic experimental processes generally require difficult, tiring and careful synthesis of putative structures or trial and error based screening of products which lead to high costs. In addition to this, the requisite specificity cannot be easily achieved [4]. As a consequence, computational methods are becoming increasingly important as plausible and supplementary alternatives to HTS [5]. Virtual screening which can be defined as the computational analysis of databases of chemical compounds to identify possible drug candidates for a specific pharmaceutical target is emerged as a cost-effective approach among the computational methods [3, 6]. With the help of this method a small subset of compounds can be selected for further analysis, which in turn decreases the required cost [5].

Enormous advances in genomics, proteomics, bioinformatics and structural biology (X-ray and NMR) that allow visualizing molecular structure have provided numbers of new

targets for further investigation through lead identification. Virtual screening which is either ligand-based or receptor-based plays an important role for the lead discovery [2]. In the ligand-based approach, the possible hits are identified based on chemical and physical similarities with the known ligands that are likely to interact with the target [3]. On the other hand, receptor-based approach uses the information about the structure of the target molecules. Docking small-molecule compounds from databases to known structure targets can be utilized to discover novel leads. After that, these leads can be selected based on their docking energies for further experimental testing (*in vitro* and *in vivo* studies to assay the actual activity of the lead) [7]. While computational approaches in fact are not reliable as experimental research, it cannot be disregarded that they are the important guides for the experimentalists in the design of compounds in a more rational way [4].

Treatment of many diseases is mainly provided by targeting the proteases. One such protease, insulin-degrading enzyme (IDE), is the potential target for both diabetes and Alzheimer's disease (AD). IDE, is a Zn^{+2} metalloprotease, and is involved in the clearance of insulin, and amyloid- β ($A\beta$), that are peptides associated with Type 2 diabetes and Alzheimer's disease, respectively [8]. AD is the most common form of dementia and affects significant number of people aged over 85. As a definition, it is a progressive and fatal brain disorder that gradually destroys a person's memory, and ability to think, learn, reason, make judgments, communicate, carry out daily activities; moreover it can ultimately lead to severe dementia, and death [9]. Today, current drug therapies for AD offer a small symptomatic benefit; however do not inhibit or delay the permanent and tenacious neuropathology of the disease. Researches indicate that the pathology of this disease is associated with $A\beta$ peptide-containing senile plaques. These plaques are composed of fibrils formed by the aggregation of short peptides, which are mostly $A\beta_{1-40}$ (the most common $A\beta$ peptide and is fairly soluble in water and aqueous media) and $A\beta_{1-42}$ (represents about 5–10% of total $A\beta$ produced from cell cultures and in the brain of animal

models) [10]. IDE naturally degrades this protein that accumulates abnormally in AD. Type 2 diabetes mellitus (T2DM) is one of the most common metabolic disorder, and affects 250 million people worldwide. It is defined as the reduced sensitivity of muscle, liver and fat cells to insulin, in other words, the cells develop insulin resistance. Evidences suggest that T2DM may lead to heart disease, kidney failure and also dementia [11]. People with this disease are more likely to develop AD within several years. Similarities have been identified between these two common disorders; extracellular senile plaques (SPs) which are mainly composed of β -amyloid aggregates, intracellular neurofibrillary tangles (NFTs) that are abnormal forms of tau protein, degeneration, high cholesterol levels, age dependency, and insulin signaling abnormalities [12].

The link between insulin and $A\beta$ metabolism is regarded as the key subject for a better understanding. The level of $A\beta$ is regulated by a number of degradative proteases (IDE, neprilysin, endothelin -converting enzyme 1 and 2) that provide its clearance [13, 14]. IDE is the major enzyme that degrades insulin with high affinity. It has been found that insulin competes with $A\beta$ for IDE, and IDE prefers insulin. This finding suggests that insulin inhibits the extracellular degradation of $A\beta$ by IDE in case of a concomitant increase in both insulin and $A\beta$ level, because IDE preferably degrades insulin at this condition [12]. Recent studies have indicated that, IDE hypofunction causes a significant decrease in $A\beta$ degradation, and a similar deficit in insulin degradation, which then may lead to AD and T2DM, respectively [11, 15]. Consistent with these reasons, preventing $A\beta$ formation or accelerating its degradation by modulating the IDE activity may represent a novel therapeutic approach for AD and also for T2DM.

The regulation of IDE with drug-like compounds is becoming very attractive strategy for the treatment of AD and T2DM. Cabrol et al. [16] introduced two novel compounds that stimulate the proteolysis of only short peptides of IDE synergistically with ATP using high-throughput screening. To our knowledge, these two molecules are the only drug-like

molecules that activate IDE. In a recent study [17], a set of IDE peptide-inhibitors were designed to regulate the catabolism and activity of insulin. A short peptide substrate bradykinin was discovered to regulate the activity of IDE with a selective binding to the “exosite” region of IDE [18]. However, this peptide had low affinity to exosite and this observation resulted with the idea that a more efficient molecule binding to the exosite could be utilized to increase the activity of IDE.

In this study, the aim is to design small molecules that target and regulate IDE activity for the treatment of AD by using the structure based drug design approach. Consistent with the previous studies, it is suggested that small chemical compounds that bind to the “exosite” would have the possible regulatory role in substrate binding and subsequent cleavage by IDE. In order to realize this goal, structure based virtual screening is conducted to identify small novel compounds that enhance the activity of IDE. After the molecular dynamics simulations of IDE, approximately one million chemical compounds are virtually screened using the docking software Autodock 3.0.5. Our study suggests a systematic approach with a virtual screening targeting the exosite of IDE, and that the proposed novel compounds can be initiators for the lead optimization studies. In addition, molecular docking calculations performed for bradykinin at the IDE exosite demonstrate similar interaction sites with the IDE crystal structure. Molecular dynamics and molecular docking calculations are also carried out to have a closer insight into the interaction between the exosite residues and previously found small molecular weight compounds [16].

In this thesis, Chapter 2 provides necessary background and literature review on the AD, T2DM, their common properties concerning the A β degradative enzyme, IDE, and the computational methods in structure-based drug design. Chapter 3 consists of the employed computational methods with the necessary biological information on the IDE docking site. Results and discussions are given in Chapter 4; and then Chapter 5 is dedicated to some important conclusions about this study and recommendations on future research.

Chapter 2

LITERATURE REVIEW

2.1. Alzheimer's Disease

Dementia is characterized as a syndrome of elderly having a set of symptoms affecting intellectual and social abilities severely which impede daily functioning. Today, 24-30 million people have dementia; but this number is expected to increase to 81-100 million in 2040 [19]. Alzheimer's disease (AD) is the most prevalent form of dementia and described as an age-related neurodegenerative disorder characterized by the progressive memory loss, inevitable behavioral changes and deterioration of cognitive function necessary to maintain an independent daily life [13]. These changes are attributed to the progressive dysfunction and death of neurons caused by a physiological normal peptide deposition. Significant increase in the prevalence of this disease can be attributed to an increase in the worldwide average public life time, which is most likely resulted from improved quality of life and availability of medical care. Therefore, AD has become one of the most serious diseases for this century and it is estimated to increase over the next decades with the aging of the populations [9]. From this point of view, this unraveling disease has given rise to a major serious public health, social and economic burden that must be eradicated. Therefore, it is worthwhile to understand the key pathological, epidemiological and molecular genetic factors. Recent evidences suggest that both environmental and genetic factors as well as "age" play a significant role in the pathology of AD [20].

2.1.1. Amyloid β peptide

The pathology of Alzheimer's disease (AD) was first recognized by Alois Alzheimer in 1907 [21]. The "amyloid cascade hypothesis" predicts that accumulated amyloid- β peptide ($A\beta$) oligomerizes and gradually develops fibrils in the brain and; this is the key event for an early evidence of the neuronal degeneration that leads to dementia [22]. Main neuropathological symptoms of this disease include extracellular senile plaques (SPs), intracellular neurofibrillary tangles (NFTs) and perivascular deposits within the specific brain regions (hippocampus and cerebral cortex) [22, 23]. SPs are composed of β -amyloid aggregates of 40–43 amino acids (called $A\beta_{1-40}$, $A\beta_{1-42}$, or $A\beta_{1-43}$ according to the number of amino acid residues), whereas NFTs arise from pathological protein aggregates of hyperphosphorylated tau protein [12, 24]. The link between the $A\beta$ elevation and the phosphorylation of tau has been identified in the study of Zheng et al.; it is found that $A\beta$ stimulates tau phosphorylation in rat primary septal cultures [25].

In essence, $A\beta$ is ubiquitously cleaved from a large type-1 integral transmembrane protein, termed APP (amyloid precursor protein). Even though the physiological role of APP is not clearly understood, it is believed that it is involved in cell adhesion, cell/cell and cell/matrix interactions, neurite outgrowth and neuron viability [23]. For instance, deletion of the APP gene in mice particularly has an adverse effect on the locomotor behavior in their later adult life and leads to cerebral gliosis [26]. This finding indicates that APP affects the nervous system depending upon the age. In another study, it has been observed that the decreased levels of soluble APP can lead to neurotoxicity in the brain [27], that is, APP must serve important functions in normal metabolism and development.

Early studies elucidate that APP can undergo degradation through 2 different proteolytic processing pathways. Enzyme α -secretase mediated pathway does not involve in the pathogenesis of AD; because produces the large neuroprotective soluble N-terminal sAPP α and C83 membrane-bound C-terminal fragments. Whereas, cleavage by β - and then γ -

secretases gives rise to soluble N-terminal sAPP β and A β peptide fragment which may in turn senile plaques over time [28, 29]. In other words, anti-amylogenic APP degradation by α -secretase is found to be the major route concerning the significant decrease in A β formation [30], whereas β -secretase activity heterogeneously generates N-terminus A β fragments of the 4 kDa A $\beta_{1-40/42}$ and the 3 kDa A $\beta_{11-40/42}$ [31].

It has been suggested that normally APP processing fragments have enriching properties in the neuronal system; however during the early stages of cerebral dysfunctioning, these beneficial effects may shift through disruptive ones such as abnormal oligomerization of A β peptide fragments that lead to dementia [32]. Cleavage products of this process have important physiological roles in adhesion, neurotrophic and neuroproliferative activity, membrane-to-nucleus signaling and intercellular communication [33].

A β can appear in three different forms in the brain; membrane associated, aggregated and soluble. Membrane associated A β is generally found in healthy individuals; on the other hand, aggregated and soluble forms are said to be toxic and neurodegenerative and found in patients diagnosed with AD [10]. A key event in AD pathogenesis is the tendency of the core amyloid protein to convert itself from the soluble monomeric form into smaller aggregates such as soluble oligomers and fibrils by structural transition from their normal α -helix fold (monomeric) into β -sheet (oligomeric) secondary structure [12, 32, 34]. In the early studies, it has been found that Alzheimer's brains have water soluble A β peptide levels are six times higher than that of normal brains, whereas the level of insoluble aggregates is 100 times higher [35]. Plaque formation after β -amyloid deposition has been assumed to occur in a staging manner, from diffuse deposits (preamyloid plaques) to more impact dense core forms [36].

A β is a physiological peptide, and steady state anabolism and catabolism rates provide its normal level in the brain. A recent study concerning the analysis of A β levels in the cerebrospinal fluid (CSF) of healthy 23-45 year-old men and women has shown that the

anabolism and the catabolism rates are 7.6%, 8.3%, respectively. This finding has revealed that A β can also be found in normal aged brains; but its clearance mechanism precludes its accumulation during its correct functioning [37]. Even a slight change in this balance may result in toxic peptide deposition, then oligomerization, and ultimately neuronal dysfunction [38]. These peptides generally composed of 39 to 43 amino acids; and can exist as monomers, dimers, and higher oligomers; however further aggregation leads to fibrillation [39]. The two major forms of amyloid peptides are A β_{1-40} and A β_{1-42} , but yet the former is the most abundant type corresponding to 90% of overall A β peptides. A β_{1-42} is more hydrophobic and has higher tendency to fibrillate in a concentration-dependent manner than A β_{1-40} , that is, it is the major risk factor of developing plaques [36]. It has been revealed that during the early onset of AD, the most deposited protein is in the longer form and not neuritic; but then promotes the further deposition of both the long and the short forms of A β resulting in toxic senile plaques formation [9]. On the other hand, it is also believed that the level of A β_{1-40} is more relevant with cognitive impairments occur in AD [40]. In addition to this, recent data have demonstrated that the value of A β_{1-42} /A β_{1-40} correlates better with the AD pathology, and would allow an early diagnosis at an early stage of the disease [41]. For instance, an experimental *in vivo* study on transgenic mice has showed that elevated A β_{1-40} production inhibits A β_{1-42} -linked amyloidosis and therefore speculates that neurotoxicity is related to aggregation state of amyloid peptides [42]. In other words, an alteration from the longer forms to the shorter ones or decreasing the ratio of A β_{1-42} to A β_{1-40} would alleviate their toxicity.

Based on various studies, there are different potential suggestions about how β -amyloid causes nerve cell degeneration; it may promote abnormal phosphorylation of tau by affecting cell membrane receptor, it may give rise to oxidative stress by binding to a 'receptor for advanced glycation end products' (RAGE) or by generating free radicals and reactive oxygen species, and it may render neurons more vulnerable to environmental

disturbances by increasing harmfully calcium levels, and by destabilizing neuronal calcium homeostasis, it may also increase other molecules toxicity such that excitatory amino acids, and finally may cause DNA damage [43, 44, 45, 46, 36]. These characteristics fit neatly with the major risk factors for AD, such that age and expedited production of heterogeneous amyloid peptides.

2.1.2. Genetics of Alzheimer's disease

As in most cases of neurodegenerative disorders, Alzheimer's disease is a multi-faceted malady resulted from both genetic and environmental factors. There are two types of AD, late-onset sporadic (LOAD) and early-onset familial (FAD). The former is the most common type affecting more than 15 million people worldwide, by contrast the latter only comprises the 10% of all AD cases, which are resulted from missense mutations on the specific genes [29, 47, 48]. The cause of sporadic AD is not clearly known, presumably because of diverse genetic and external influences; whereas early-onset FAD is known to be arisen from mutations in the APP and presenilin genes, both linked to A β metabolism [29]. Molecular genetic studies have identified four principal genes acknowledged to play effective role in the disease; genes encoding amyloid precursor protein (APP), presenilin-1 (PSEN1), presenilin-2 (PSEN2), and gene encoding apolipoprotein E, (APOE). Mutations on the first three genes are inherited in autosomal dominant manner as in the case of FAD. Several different missense mutations have been discovered in exons 16 and 17 of the APP coding gene in early-onset FAD cases [47], and resulted in over-expression of A β ₁₋₄₂ or seldomly a mutated isoform of A β ₁₋₄₀ with higher amyloidogenic properties. Apart from that, 50% of FAD cases result from PSEN1 and PSEN2 mutations on chromosomes 14 and 1, respectively, which induce especially the formation of A β ₁₋₄₂ as in the case with APP mutations, and also increase the ratio of A β ₁₋₄₂ to A β ₁₋₄₀ in the brain by altering the APP mechanism through a direct effect on the γ -secretase [49, 50, 13]. Besides, APOE, a carrier

of cholesterol in the blood, is also found in AD brains senile plaques, and genetic studies suggest that chromosome 19q12–q13 locates near the APOE gene and it is susceptible for AD. However, no clear information has yet been obtained corresponding to the link between this protein and AD; APOE should somehow influence the production, distribution, or clearance of the A β peptide [47]. An additional aspect of genetics is related to chromosome 21 that correlates Down’s syndrome (DS) to AD. Individuals having chromosome21 trisomy, in other words, have an extra copy of chromosome 21, are believed to develop AD at a very early age; because APP gene locus exists at this part. Unsurprisingly, DS patients are found to have high levels of A β peptide, and amyloid deposits [23, 9]. All these four genes share a common feature that they all alter the A β levels by modulating the APP processing which is the key matter in AD pathology.

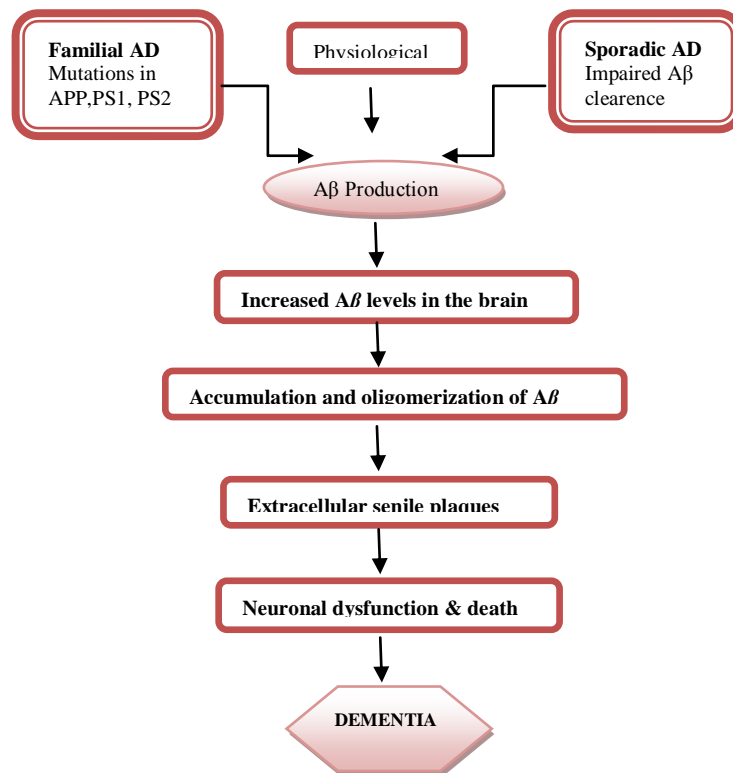


Figure 2.1: Systematic Diagram of the “amyloid cascade hypothesis” [51].

2.1.3. Treatment Strategies of Alzheimer's disease

Although a significant treatment has not been developed for the prevention or progression of AD, there are several strategies proposed for the AD treatment. These include anti-inflammatory approaches [52], tau pathology approaches [53], apolipoprotein E (APOE) related treatment approaches [54], metabolic dysfunction approaches [55, 56], A β -targeted therapeutic approaches [50], development of β - and γ - secretase inhibitors [57], usage of β -sheet breakers, NMDA-receptor blockade, cholesterol-lowering drugs, use of antioxidants, metal chelators, anti-inflammatory agents [58, 59], inhibitors of τ phosphorylation, activators of phosphatases, neuroregeneration by neurotrophic factors and immunophylline ligands, gene therapy and human embryonic stem cells for the supply of neuronal cells [60, 61, 62]. Among them, A β -targeted therapeutic approaches are still in the center of AD treatment methods.

There are several A β -targeted therapeutic strategies including modulation of A β production, blocking of A β aggregation, A β -targeted immunotherapy, and enhancement of A β degradation [50]. One of the first efforts of drug development for the modulation of A β production is the inhibition of γ -secretase [63]. However the inhibition of γ -secretase also affects the Notch1 cleavage resulting with the blockage of thymocyte differentiation and splenic B-cell maturation and causing of intestinal goblet-cell metaplasia in adult animals [64, 65]. Eisai developed a γ -secretase modulator E2012 that is still in the phase of clinical development [63]. Another A β modulation strategy is the design of β -secretase inhibitors; however there is only one clinical report about a β -secretase inhibitor [66]. The second A β -targeted strategy, inhibiting A β aggregation, which can prevent the formation of toxic oligomers and plaques, is an approach getting more attractive in recent years. A very few aggregation inhibitor candidates have been determined so far, however these inhibitor candidates did not demonstrate efficacy or desirable pharmacodynamic effects. [67, 68]. The third approach, A β -targeted immunotherapy is becoming more popular, and there are

three discovered drug candidates in Phase III trials: Bapineuzumab [69, 70], Solenezumab [71] and Intravenous immunoglobulin G [72, 73]. Nevertheless there are many debates about the usage of immunotherapy, since some lethal side effects were observed in some phases. Hence Phase III results are needed to evaluate the efficiency of immunotherapeutics. The last approach, the enhancement of A β clearance is a quite reasonable approach, since some important enzymes such as neprilysin, plasmin and insulin degrading enzyme (IDE) involved in the A β degradation have been identified in recent years [14].

2.2. Type II diabetes mellitus (T2DM)

T2DM is one of the main threats to human health in the modern times affecting 250 million people around the world, and it is the fourth leading cause of death worldwide corresponding to 3 million deaths annually. Unsurprisingly, economic burden that it leads is enormous. People with T2DM often suffer from cardiovascular diseases, kidney failure, blindness, high cholesterol levels and sometimes stroke [11, 12]. In addition, recent evidences suggest that there is a strong connection between T2DM and AD, that is to say, people suffer from T2DM is more likely to develop AD [11, 12, 74, 75, 76]

It has been stated that 90-95% of diabetes cases correspond to T2DM, and it is defined as noninsulin-dependent diabetes mellitus [77, 78]. People with T2DM develop hyperinsulinemia and insulin resistance at the early stages of disease; and hyperglycemia with glucose intolerance will dominate later on. Normally, postprandial blood glucose levels trigger insulin release from the pancreatic β -cells, and then released insulin stimulates glucose uptake by the peripheral tissues (liver, fat, muscle) and inhibits glucose production simultaneously. However, in T2DM patients, insulin loses its ability to stimulate glucose utilization and pancreas fails to produce adequate insulin to decrease high levels of unutilized glucose or produces higher than its normal levels, which in turn lead to insulin resistance, hyperinsulinemia, hyperglycemia and glucose intolerance [11, 79, 80].

Not all patients with insulin resistance and hyperinsulinemia will develop glucose intolerance and diabetes, but most of them will, depending on genetic and non-genetic factors [80]. Consequently, the early stages of T2DM are characterized by elevated plasma levels of both insulin and glucose.

2.2.1. Insulin signalling

Insulin signalling starts with binding of insulin to its receptor (IR), which stimulates tyrosine kinase activity. This further leads to autophosphorylation on tyrosine residues. The lipid kinase phosphatidylinositol 3-kinase (PI3K), mitogen-activated protein kinase (MAPK) signalling cascades are activated by insulin, and the meantime, PI3K signaling, which converts phospholipid phosphatidylinositol 4,5 bisphosphate (PIP₂) to phosphatidylinositol 3,4,5 trisphosphate (PIP₃), can also be activated by insulin receptor substrates (IRS) 1 and 2. The MAPK pathway is not very sensitive to insulin, so that PI3K is related to almost all insulin metabolic actions. Furthermore, PIP₃ stimulates protein kinase B (PKB), through the plasma membrane, where it activates glycogen synthase kinase-3 (GSK3) [81, 11]. In insulin signaling, GSK3 hyperphosphorylates and inhibits glycogen synthase (GS) by casein kinase 2 (CK2). GSK3 may become inactivated by phosphorylation of PKB in response to insulin, but this activates GS which in turn regulates the glycogen synthesis. In this manner, GSK3 generally opposes the actions of insulin, by inhibiting glycogen synthesis, glucose uptake, and also by altering the expression of genes regulated by insulin [82, 83].

It is suggested that, insulin produced by pancreatic β -cells pass through the brain by blood transmission and activate the IR in the brain, therefore regulates synaptic function, neurotransmission, neuronal growth, neurite and energy metabolism in the cortex and hippocampus; thereby, it is asserted that it should play an important role in learning and

memory [11]. Consistent with these suggestions, insulin resistance of these brain regions may also conduce hyperinsulinemia and finally T2DM.

2.3. Diabetes and dementia

2.3.1. Epidemiology

Numerous longitudinal epidemiological studies have asserted that there are strong similarities between the pathogenesis of AD and T2DM; and the incidence of AD is 2 to 3 times higher for T2DM patients [11, 12, 84]. For instance, diabetes was given as a risk factor of AD with a ratio of 2.18 in the study of Yoshitake et al. [85]. A comparative investigation on 34 - 65 years aged people suffering from T2DM relative to healthy aged-matched controls has revealed that patients with T2DM has slower psychomotor speed (the amount of time takes a person to process a signal, prepare a response and execute that response, than control people) [86]. In another longitudinal study, 1301 healthy people aged 75 years or older were examined during the following 6 years; 260 of them were developed AD, and T2DM was found to be associated with an increased risk of AD with a ratio of 1.3 [87]. In another study, 6370 healthy, elderly people were investigated for 2 years; it was observed that diabetes doubled the risk of development of AD with a hazard ratio of 1.9 [75]. In the survey of Luchisger et al. 149 people developed dementia, including 137 cases of AD among 683 subjects aged 65 years and older, and it showed that the risk of developing AD was increased with a ratio of 39% for the people having also hyperinsulinemia [88]. Additionally, 41 middle-aged non-dementia subjects having T2DM were compared with 47 age-, education-, and gender-matched controls in a survey; it was concluded that the decreased verbal declarative memory performance was likely consistent with the existence of T2DM [89]. More epidemiological studies have shown similar results. 2574 elderly non-demented Japanese–American men were followed for 3 years in a study with the objective of determining the relationship between diabetes, APOE ϵ 4 genotype

and development of dementia. This study indicated that diabetes was associated with a ratio of 1.5 for developing dementia and presence of the APOE ϵ 4 allele increased this risk to a ratio of 4.4 [85].

All these studies constitute the evidence for the link between diabetes and dementia, specifically T2DM and AD. Cognitive functions found to be affected in T2DM are given as verbal and nonverbal memory, attention, processing speed and executive function [83].

2.3.2. Pathological links between AD and T2DM

Various studies have shown that AD and T2DM underlie similar pathological processes including; aging-related processes, degeneration, high cholesterol levels, metabolic disorders, energy metabolism impairment, degenerative processes, β -amyloid aggregation, second messenger system abnormalities such as glycogen synthase kinase 3 (GSK3) over activity, glyceraldehydes derived advanced glycation end products (AGEs), increased oxidative stress and increased inflammation response, association with cardiovascular disease, blood vessel abnormalities, and correlation with the Apolipoprotein E (APOE) ϵ 4 allele [12]. Most important ones will be described in this study in accordance with insulin signalling.

2.3.2.1. Insulin Resistance & Hyperinsulinemia

Nutritional signaling is crucial for the neuronal growth and activates neurochemical reactions between brain structures assigned in feeding and energy, glucose and fat metabolism. In this sense, insulin has an important regulatory function [90]. The main pathological link between AD and T2DM is that both disorders are associated with the insulin signaling malfunctioning in peripheral and central nervous system (CNS) tissues. As indicated in earlier sections, insulin acts as a neuromodulatory protector against toxins and stress induced apoptosis during development [91]; therefore playing a significant role

in neuronal growth and survival. The insulin resistance syndrome is generally found in T2DM and known as the consequence of impaired signaling relevant to the insulin receptor (IR) and many post-translational modifications. It can be characterized as persistent chronic peripheral insulin elevations, reduced brain insulin levels and insulin activity, plus it may trigger age-related memory impairment and AD [92, 12, 93]. In a study of aging in Northern New York City, hyperinsulinemia and T2DM have found to associate with a higher risk of AD [94]. Peripheral hyperinsulinemia may inhibit brain insulin production which in turn results in impaired insulin related metabolism in the brain [80]. For evidence, AD patients were found to have lower than normal CSF levels of insulin, resulting in the suggestion that AD can be named as 'type 3 diabetes' [11]. In another study, memory is facilitated with low doses of insulin injection for normal older adults; but a subgroup of patients with AD who are believed to have insulin resistance syndrome require higher insulin doses to generate the same facility [95]. A high fat diet was applied to a transgenic mouse model of AD (Tg2576) to induce peripheral insulin resistance; therefore basal signaling (phosphorylation of IR, PKB and GSK3, as well as PI3K activity) was found to be decreased in the cerebral cortex, and the degree of neuropathology was increased. In other words, peripheral insulin resistance (pre-diabetes) triggers neuronal insulin resistance and generally leads to the molecular pathology of AD [96]. Also, peripheral high dose insulin injection in mice results in a rapid and dose-dependent tau phosphorylation in the CNS [97]. Alternatively, cholesterol levels also play a significant role in AD and abnormal levels are considered as a risk factor, separately hypercholesterolemia is also a crucial risk factors of T2DM [98]. Important to note that hyperinsulinemia associated with insulin resistance may likely result in reduced insulin transport across the blood brain barrier [99].

2.3.2.2. Glucose and Energy Metabolism Impairment

Most of the energy generated in the brain is obtained through the oxidation of glucose which has the modulatory effect in growth factor signal transduction pathways involved in cell division, cell signaling, and functional modulation of proteins. Therefore glucose availability is deterministic for the overall efficiency of the cellular energy metabolism [100, 12]. Reminiscently, insulin is involved in the regulation of glucose utilization in CNS.

Abnormal glucose levels are caused by insulin resistance which normally increases with age, and also by hyperinsulinemia to overcome insulin resistance in tissues [101]. In the brain, energy and glucose homeostasis is performed via accurate insulin signaling through the IRS/PI3K pathway [90]. For instance, through the usage of insulin antibodies insulin action in nucleus was hindered, unsurprisingly this phenomenon decreased the level of insulin receptors, and inhibited insulin-dependent activation of PI3K in order to suppress endogenous glucose production [102].

Cognitive impairment, found in both AD and T2DM patients, is a notable degenerative cause of impaired glucose mechanism, and increases with age [86]. Chronic hyperglycemia is considered as one of the major determinants of cognitive decline [83]. A recent study suggests that T2DM or impaired fasting glucose might be present in up to 80% of patients with AD [103]. In addition to this, acute glucose administration may facilitate memory of AD patients, and when fasting of plasma glucose is maintained, acute insulin administration facilitates memory of AD patient. [12].

The negative effects of hyperglycemia are mediated through the formation and accumulation of advanced glycation end products (AGEs), a heterogeneous group of molecules that have side groups irreversibly added to them [12]. Chronic hyperglycemia basically leads to AGEs formation and related oxidative stress. Accelerated AGEs production is also found in all types of A β plaques and NFTs in people suffering from AD

[104] and they might be involved in the elevated amyloid- β production and formation of NFTs. Moreover, nerves of the diabetes are under risk of accumulation of these molecules, which are observed in an experimental study on diabetic rats [105]. So, it can be concluded that physiological activities of AGEs are involved in pathogenesis of both T2DM and AD.

In addition to hyperglycemia, hypoglycemia, a common side effect of diabetes treatment, is also believed to play a significant role in cognitive impairment [12, 83]. Difficulty in concentrating, drowsiness, and incoordination are the main complications resulted due to hypoglycemia in the neuronal system [83].

2.3.2.3. Amyloidogenesis

Both AD and T2DM are considered as amyloidogenesis related disorders. Accumulation of A β is found in people suffer from AD, and similarly amyloid deposits in islets of Langerhans and lead to loss of β cells [106, 12, 84]. As noted before, A β is the cleavage product of its precursor protein, APP, on the other hand, islet amyloid is derived from islet amyloid polypeptide (IAPP), which has 90% structural similarity with APP. Similar to A β ₁₋₄₂, IAPP has tendency to form early intermediate assemblies as spherical oligomers [107]. In accordance with the facts that IAPP deposits are found in pancreatic islets of diabetes, and IAPP and APP have similar physiological properties, there is considerable evidence to suggest that AD and T2DM are inter-related disorders [103, 108, 109, 110]. In addition to amyloid precursor protein similarities, excessive hyperinsulinemia and neuronal insulin resistance is known to involve in undesired elevated β -amyloid peptide formation which in turn contribute to age-related memory impairment [111], similarly peripheral hyperinsulinemia is also found to increase inflammation in the central nervous system, and then induce elevated A β formation [92]. From another perspective, direct relationship between insulin resistance and A β toxicity is suggested depending on the fact that the A β oligomers persistently suppress IR expression on neuronal surface and lead to insulin

resistance [84]. In addition to the direct effect of insulin on amyloid metabolism, its additional secondary effect via glucose homeostasis may also contribute to amyloidogenesis [83]. Moreover, it is believed that there is a link between cholesterol and APP mechanisms; a reduction in cellular cholesterol availability would result in decreased A β formation [112]. Thereby, decreased prevalence of AD is associated with the usage of statins for hypercholesterolemia [47, 113, 114].

2.3.2.4. Molecules linking both of them

2.3.2.4.1. GSK3

Glycogen synthase kinase 3 (GSK3) is a serine/threonine protein kinase that is known for phosphorylation and thus inactivating glycogen synthase, and highly conserved in all eukaryotes. The consequence of GSK3 phosphorylation usually ends up with the inhibition of the substrate. There are evidences that GSK3 plays a central role in AD in a number of different ways (Fig. 2.2). Firstly, deregulated GSK3 activity has been reported in brain tissues of AD patients [83, 115]. Secondly, GSK3 is implicated in the hyperphosphorylation of tau, the primary constituent of tangles that are found in people suffer from AD. Moreover, GSK3 activity enhances APP proteolytic processing and directly promotes A β peptide production. Additionally, an important link has been suggested between GSK3 and insulin signaling; insulin signaling induces the phosphorylation and inhibition of GSK3 [116]. Therefore, it can be asserted that reduced insulin signaling resulted from insulin resistance found in T2DM patients would lead to an overall increase in GSK3 activity, which in turn provokes not only plaque formation by elevated A β peptide production, but also, tau phosphorylation that result in tangle formation [83, 11]. These findings are in accordance with the reduced PKB activity and increased GSK3 activity in AD [117].

2.3.2.4.2. Insulin Degrading Enzyme (IDE)

Insulin degrading enzyme (IDE) was discovered in 1949 by the physician and biochemist I. Arthur Mirsky [118]. IDE, which is also known as EC 3.4.24.56, insulin protease, insulysin, or insulinase [51], is an evolutionarily conserved zinc 110 kDa metalloprotease responsible for insulin degradation as the name implies [119, 120]. Inhibition of its activity by antibody injection into hepatoma cells reduces insulin degradation [121], while over-expression of IDE increases insulin degradation [122]. In addition to insulin, IDE has been shown to cleave several other peptides of diverse sequence with a propensity to form β -pleated sheet-rich amyloid fibrils, including A β , glucagon, amylin, insulin-like growth factor II, atrial natriuretic peptide, calcitonin, β -endorphin, transforming growth factor α , and the intracellular domain of APP (AICD) [123, 124]. Moreover, IDE expression and activity significantly decreased by aging; and this is consistent with the fact that diabetes and AD are age related chronic diseases [125].

IDE is taking significant attention as being the major enzyme of insulin and amyloid- β peptide degradations that constitute the pathogenesis of T2DM and AD, respectively. IDE is expressed in the human brain by cortical and subcortical neurons and found throughout the body [126], but cytoplasm, cell surface, mitochondria and peroxisomes of cells are the main IDE locations [12, 127]. Microglial cells secrete IDE to the extracellular space in the brain, therefore allow A β peptide degradation. However, IDE can only degrade soluble monomeric forms of amyloid peptides, not the oligomeric ones [128, 12]. Human genetic studies have previously reported that, there is a genetic linkage and association of late-onset AD with IDE, on chromosome 10q23–24 [127, 129]. Moreover, IDE region on chromosome 10q has been also found to be involved in the T2DM [130, 131].

IDE relates insulin signaling disorders and the amyloid cascade hypothesis. It is known that the affinity for the binding of insulin to IDE is much greater than the one for the A β peptide; therefore hyperinsulinemia in people T2DM competes with A β and sequesters IDE

[39, 15]. This phenomenon potentially results in a relative deficiency of IDE, reduced A β peptide clearance and many of the pathological features of AD [83]. IDE activity has been demonstrated to be abnormally lower in transgenic mouse models fed a high fat diet [96] and in people suffering from AD [132]. For instance, significant reductions in hippocampal IDE expression and IDE mRNA levels have been detected in AD patients, as compared to age-matched controls [95]. In addition, naturally occurring partial lost-of function IDE mutation in GK rats (an animal model of T2DM) has been shown to trigger T2DM and AD symptoms such as hyperinsulinemia, glucose intolerance and impaired degradation of A β , respectively [133, 134]; and similar responses have also been observed in the case for genetically modified mice that lack the gene for IDE [15, 96]. On the contrary, increased A β clearance has been detected in transgenic mice that overexpress IDE in neurons [8]. A nucleotide polymorphism of the human IDE gene is found to be linked to T2DM [136] which is relevant to the early genetic studies [130, 131]. Epidemiological [114], and animal [137, 138] studies suggest that deregulation of cholesterol mechanism may increase amyloid- β generation. A cholesterol enriched diet and subsequent hypercholesterolemia has recently found to decrease IDE, and trigger high levels of A β in rabbit hippocampus [139]. There is also evidence showing that cholesterol co-localizes with fibrillar A β in the amyloid plaques of transgenic mice [140]. All these findings suggest that plasma A β elevations prevent its transport from brain to periphery, while insulin resistance and hyperinsulinemia result in insulin depletion in the brain. Afterwards, elevated insulin competes with A β and lower IDE and this promotes A β accumulation. This cycle starts with dysfunctioning in A β clearance through the periphery as stated before, and results in AD pathology [92].

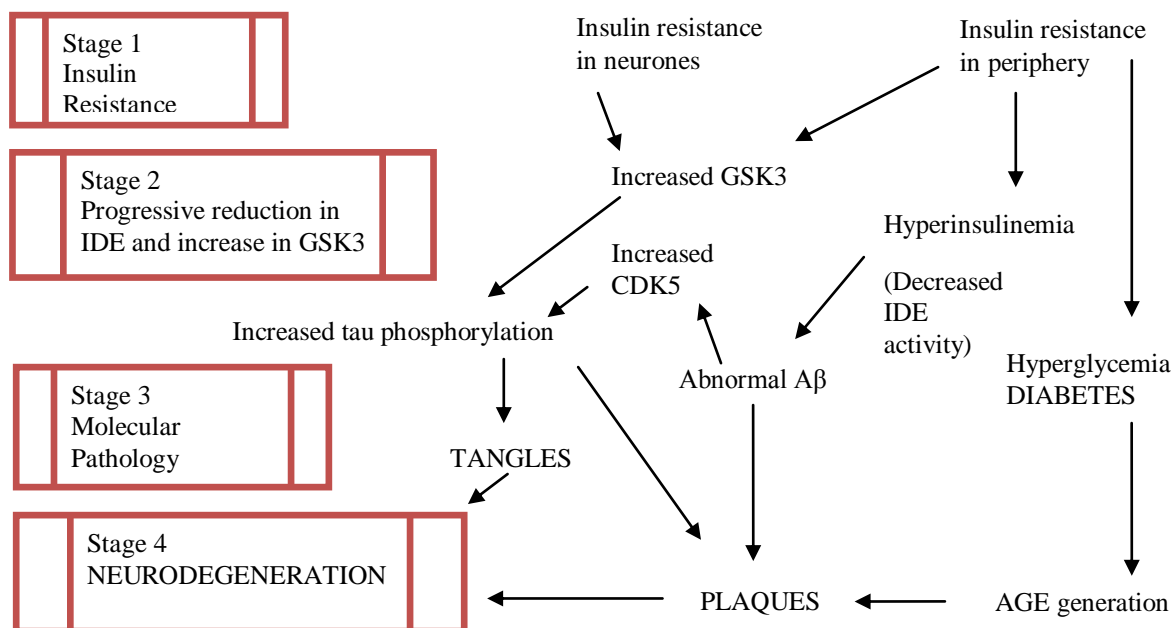


Figure 2.2: Hypothesized stages of neurodegeneration. Abbreviations; IDE, insulin-degrading enzyme; CDK5, cell cycle dependant kinase 5; AGE, advanced glycation end products [11].

In addition, APOE- ϵ 4 allele is known to reduce the expression of IDE [141]; and diabetes that posses this allele will likely to develop AD [142].

2.4. Structure Based Drug Design for AD and T2DM

2.4.1. Drug Design

Today, one of the most challenging tasks of science is the development of new drugs. The difficulty starts with selecting the biological target that involves in the specific metabolic pathways, then defining the disease-protein relations [143]. Designing a drug takes approximately 14-16 years and costs about US\$ 800 million [144]. This high cost is the result of intensive R&D investments, necessary technologies, management skills and excessive interdisciplinary work [145]. In order to deal with this complex and high cost required process, various experimental and computational techniques have been developed

[144]. About 20 years before, the most used method for the discovery of new lead compounds was the high-throughput screening (HTS) which is defined as the physical screening of large libraries of chemicals against a biological target [146, 147]. However, HTS is found unfavorable due to its low hit rates and related significant costs [147]. To decrease these experimental costs and to reduce time; more cost-efficient, faster computational methods and also algorithms are developed thanks to the tremendous amounts of information from genomic and proteomic studies [143]. These advances enable virtual visualization of protein structures that allow design of potential ligands specific for a protein target.

Computational tools identify the strength of established bonds between the target molecule and several ligands by using visualization programs, so that provides the understanding of protein-ligand interactions [4, 145]. In order to select promising, biologically active drug candidates; large compound databases are screened by applying such methods. This technique is nominated as virtual screening (VS) [145, 147]. In contrast to HTS, as the VS uses computer programs, it requires either the three-dimensional (3D) structure of the macromolecular target or at least a reference ligand with a known bioactive role specific for the receptor target molecule [147]. This is the fundamental difference that forms two approaches for VS. The former is defined as structure-based virtual screening (SBVS) that ranks the potential drug candidate molecules depending on their complementarities to the binding site, and the latter is ligand-based virtual screening (LBVS). In LBVS no information is required about the macromolecule; on the other hand, a known biologically active ligand provides the selecting criterion to form compound databases that may act in a similar manner [148].

In the field of VS, there is the possibility to screen also the molecules that do not exist physically. By means of purchasing and synthesizing, these compounds can be obtained [5]. Therefore, the possibility to come up with a promising result is higher than the older

technologies. Moreover, this approach decreases the cost required for drug discovery by eliminating the experimental deficiencies involved; such as limited solubility and aggregate formation [147]. Consequently, VS limits the possible candidates at the initial screening without testing experimentally and invests money.

2.4.2. Structure Based Drug Design

SBVS begins with obtaining the 3-D structure of the target macromolecule by NMR, X-ray crystallography or homology modeling, and identifying the ligand binding pocket on it. Generally, the target site is a pocket with a variety of potential hydrogen bond donors, acceptors, and hydrophobic characteristics [149]. It can be the active site of the protein, as in the case for discovery of inhibitory based drug candidates; or another site that takes charge in the binding or recognition process [150]. Molecular dynamics simulation can preferably be used for analyzing the dynamic characteristics of the target binding site [149]. Afterwards compounds are docked sequentially onto this selected binding site within the macromolecule, and their best docking conformations among many orientations that structurally and chemically fit the target site are selected based on a scoring function. Scoring functions estimate the binding energy of each ligand pose based on their steric and electrostatic interactions within the target site iteratively. Based on previous conformations of the ligands, a new conformation is generated and is accepted or rejected by doing comparison with respect to their resulting score between these two conformations. This process iterates until it produces the best scoring conformation [4]. The goal is to determine the most promising candidates in large compound libraries. Exceptionally, compounds that did not exist in the top scoring ones are also selected after detailed visual analysis by looking at their conformations other than the best scoring one [151, 144, 2]. *In vitro* and *in vivo* studies are crucial at the last step to assay the actual activity of the lead designed molecule for the specific application [4].

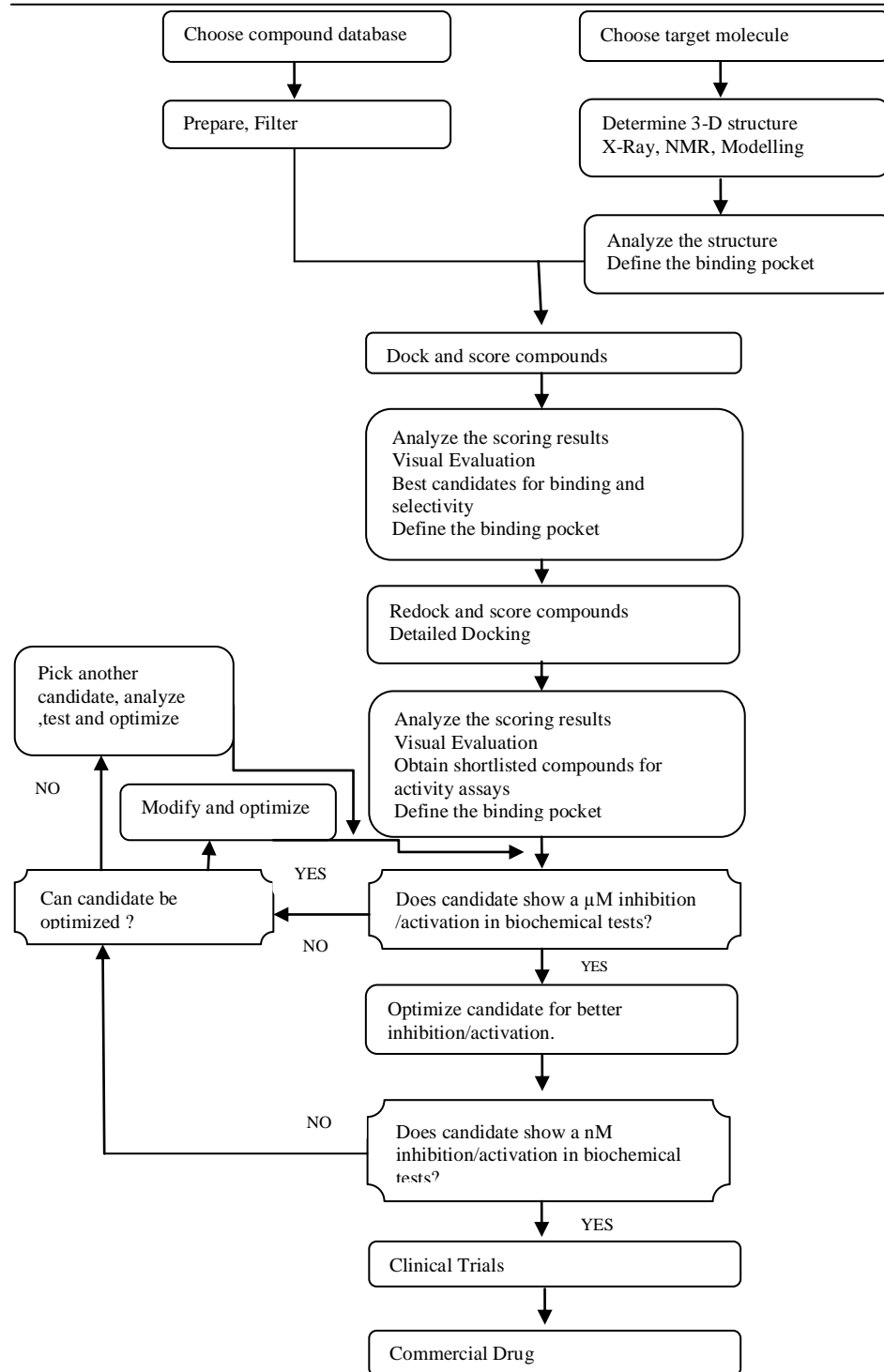


Figure 2.3: The process of structure-based drug design [149].

There are three types of scoring functions, first of which is force-field scoring function [152], where binding affinity is approximated by the strength of non-bonded interactions by computing total hydrogen, van der Waals and electrostatic interactions between protein and ligand. The second is empirical scoring function [153] based on approximations similar to force-field functions, explores the number of hydrogen bonds, hydrophobic contacts, hydrophilic contacts and number of immobile rotatable bonds, and the third one is the knowledge based scoring function [148], which is based on statistical observations of atomic interaction-pair potentials.

Another important issue in SBVS is the selection of an appropriate docking program. These programs differ in the search algorithms, ligand and/or protein flexibility, the scoring functions. Systematic methods, such as incremental construction algorithms explore all degrees of freedom in a molecule by breaking the ligand at rotating bonds. This procedure creates various fragments, and then these fragments are docked rigidly in the binding pocket up to a point where the realistic entire ligand is obtained. FlexX, Hammerhead, DOCK, Surflex and SLIDE implement this kind of search algorithm [2, 4, 5]. Stochastic methods such as Monte Carlo and genetic algorithms (GA) optimize the flexible small molecule conformation within the binding site by generating low energy conformations of ligands. GA does this by considering the biological competition and population dynamics principles. GOLD, AutoDock, ICM and Glide which require parallel processing to perform faster implement stochastic methods [2, 4, 5].

SBVS is generally preferred when the target protein structure at high atomic resolution is available rather than LBVS [148]. The accuracy of the results depends on the quality and the number of information about the target molecule [145, 147]. After selecting the top scoring candidates, some of them are eliminated based on common filtering protocols. The fundamental elimination criteria include drug-like properties. Drug like compounds, characterized as orally bioavailable compounds, generally obey Lipinski's rule-of-five

which comprises the set of rules based on molecular weight, lipophilicity and hydrophobicity [154].

2.4.3. Target Identification: IDE

Amyloidosis resulted from the accumulation of the amyloid- β protein in the form of insoluble plaques in the brain involves in the AD pathogenesis. Unstable anabolism and catabolism rates of this protein mainly lead to its accumulation. Intensive work is concentrated on the understanding of defects or abnormalities of the enzymes that are responsible for A β degradation. Among them, IDE is taking great attention as being also known by its ability to rapidly degrade insulin. This property makes this enzyme critical for both AD and T2DM. Consequently, for the treatment of these chronic diseases, IDE is regarded as a potential new target.

2.4.4. Target Structure

The crystal structures of human IDE in complex with A β (1-40), insulin B chain, amylin, and glucagon [119, 155, 156] have provided the first structural information about this evolutionarily conserved zinc metalloprotease and give significant insights about its unusual substrate recognition mechanism. The active site of IDE consists of an inverted zinc-binding sequence His-Glu-aaaa-His (HEXXH) in which the two histidines coordinate the zinc ion binding and the glutamate residue involves in the catalytic activity [119, 120, 156]. Substrate binding does not depend on the existence of the zinc ion; it only coordinates the catalysis [157].

IDE is such a compelling enzyme that has a strange structure. It has four homologous domains that share 15–24% sequence similarity in which two of them form a functional unit by getting together due to their high affinity to each other [157].

Structural and biochemical analysis reveal that this enzyme is organized in two domains (IDE-N and IDE-C) that connect with each other by an extended 28 amino acid residues loop, and has a large catalytic chamber with a total volume of $16,000 \text{ \AA}^3$ that can degrade a different ranges of peptide substrates less than 70 amino acid residues [119, 158]. The unique electrostatic nature of this internal cavity is important for the recognition and catalysis activity of IDE. IDE-N is predominantly negative; on the other hand IDE-C is positive which is also known to be involved in the regulation of IDE activity [157, 159, 160].

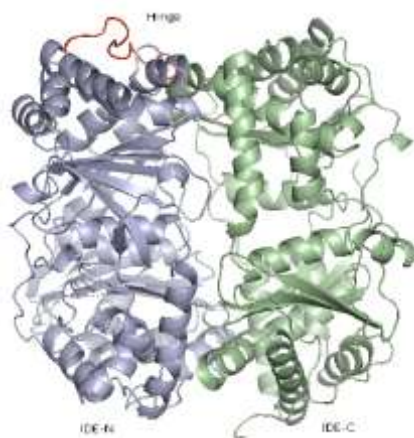


Figure 2.4: Secondary structure representation of the IDE. N-terminal domain, C-terminal domain, and, hinge region are shown as blue, green, and red respectively.

Other than these properties of the IDE structure, IDE also has an evolutionary conserved site, named exosite, which is located approximately 30 \AA away from the zinc ion bound at the catalytic center [18](see Fig 2.7). It has been observed that exosite is highly involved in the substrate recognition mechanism of IDE by anchoring the N-termini of its substrates [156, 159, 18, 161]. It has been hypothesized that substrates position their cleavable regions to the close proximity to the catalytic chamber and allow their N-terminus having β -strand conformations to form hydrogen bonding with β -sheet of IDE substrate binding chamber.

This mechanism is assumed to ensure initial cleavage by IDE and the substrates undergo a conformational switch upon binding to the catalytic chamber. This cleavage is expected to occur at least 10 amino acids away from the N-terminal end of its longer substrates [119, 161].

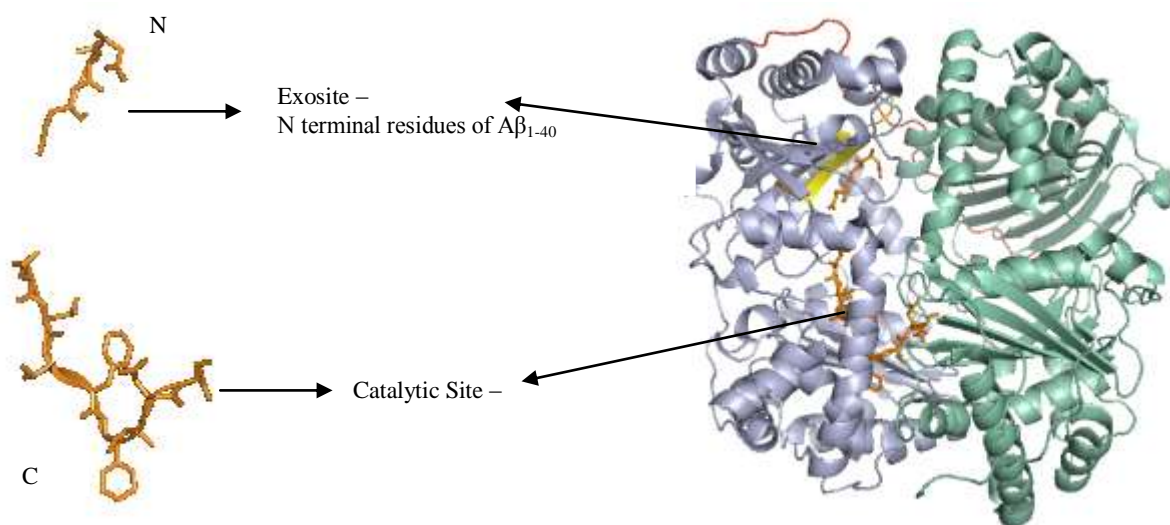


Figure 2.5: Interactions between Aβ and IDE. Right panel: surface representation of IDE in complex with Aβ₁₋₄₀ (PDBID 2G47). IDE-N and IDE-C are depicted as gray and green, respectively. The hinge region of IDE is depicted as a red ribbon, and Aβ₁₋₄₀ is depicted as sticks with carbon, nitrogen, and oxygen atoms colored orange, blue, and red, respectively. Catalytic site and exosite are indicated (exosite as yellow surface). Left panel: details of Aβ₁₋₄₀ conformation as observed in PDB ID 2G47 (depicted as orange sticks), their N and C terminals bound to IDE exosite and catalytic site respectively [119].

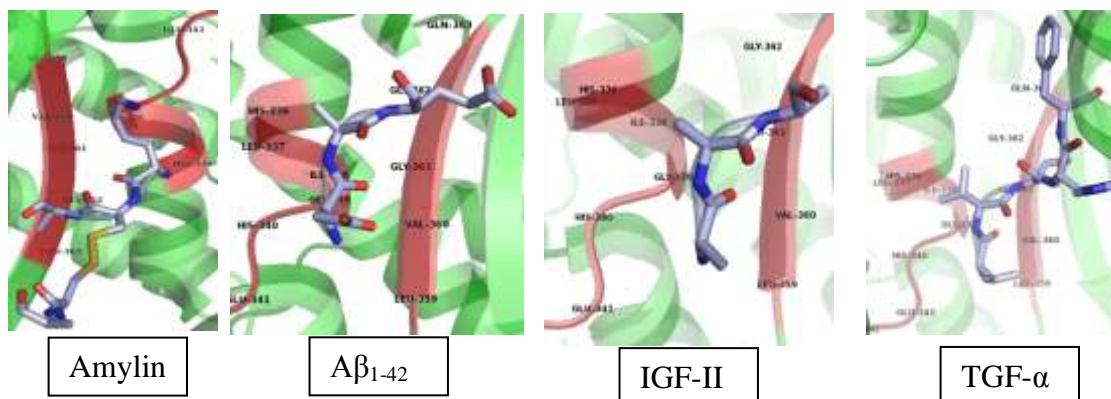


Figure 2.6: Detailed interaction of the N-terminus of amylin, $A\beta_{1-42}$, IGF-II and TGF- α with the exosite of IDE [161].

Crystal structure experiments of IDE complex with its substrates; amylin, $A\beta_{1-42}$, IGF-II and TGF revealed that the amino acid residues 336-342 and 359-363 of IDE are involved in interactions with the N-terminal ends of its substrates (see Fig 2.6) [18]. The binding of $A\beta_{1-40}$ to IDE exosite is found to be virtually identical with that of $A\beta_{1-42}$ [161].

IDE substrates do not share an obvious sequence similarity between each other; however one remarkable common property is their ability to form amyloid fibrils during cleavage [162]. Apart from insulin and $A\beta$, several other molecules such as; glucagon, atrial natriuretic factor, transforming growth factor α , TGF- α , insulin-like growth factor, (IGF)-II, atrial natriuretic peptide, β -endorphin and dynorphins, and amylin have been shown to serve as substrates of IDE [163].

The structures of IDE in complex with $A\beta$, glucagon, insulin, amylin and bradykinin reveal that the shape, size, charge distributions, conformational flexibility, and exosite binding ability of these substrates contribute to the substrate recognition and binding mechanisms of IDE [156, 159, 18, 161]. Besides, IDE can have at least two different conformations; denoted as “open” and “closed”. In the open state, substrates can freely enter the catalytic cavity. The stable closed state entraps the substrates inside to perform

hydrolysis, and it is significant for the catalytic function. Therefore, it is estimated that the enzyme activity depends on the stabilizing factors of this closed state [155, 156]. During the catalytic cycle, IDE would be in its substrate-free closed state, due to a thermodynamic perturbation or other unknown event(s), enzyme rearranges itself and yields an open state in order to promote the substrate access to the catalytic site. Once the substrate is entrapped inside the catalytic chamber, IDE-substrate complex switches back into a closed state to allow substrate cleavage. N-terminal end of the substrate becomes anchored to the exosite of IDE, then undergoes a secondary structure rearrangement to fit into the catalytic site. At the final step IDE releases the proteolytic fragments [119].

Extensive interaction between IDE-N and IDE-C act like a 'latch' to stabilize the closed conformation, and a mutation that destabilizes this interaction significantly increases the catalytic function of IDE [156]. The catalytic site of this structurally distinctive enzyme has two pieces; one half is from N-terminal and the other half is from C-terminal. This mechanism render this site as a moving active site during IDE's catalytic cycle [17]. Recently, a short peptide substrate bradykinin has been found to enhance the activity of IDE by only binding to the exosite and not to the catalytic site, which suggested low affinity of bradykinin for IDE and how the binding of short peptides at the exosite would regulate substrate recognition [18]. Interactions between bradykinin and residues 336-342 and 359-363 of IDE can be seen in Figure 2.7-b. This study suggests that the binding of small molecules to exosite would facilitate the switch of the closed conformation to the open conformation which is because small molecules could even enter in the partially open cavity [18]. In a recent study, parallel high-throughput screening is conducted in the absence and presence of ATP, and two lead compounds are identified -Ia1 and Ia2-that significantly stimulated IDE proteolytic activity synergistically with ATP [16].

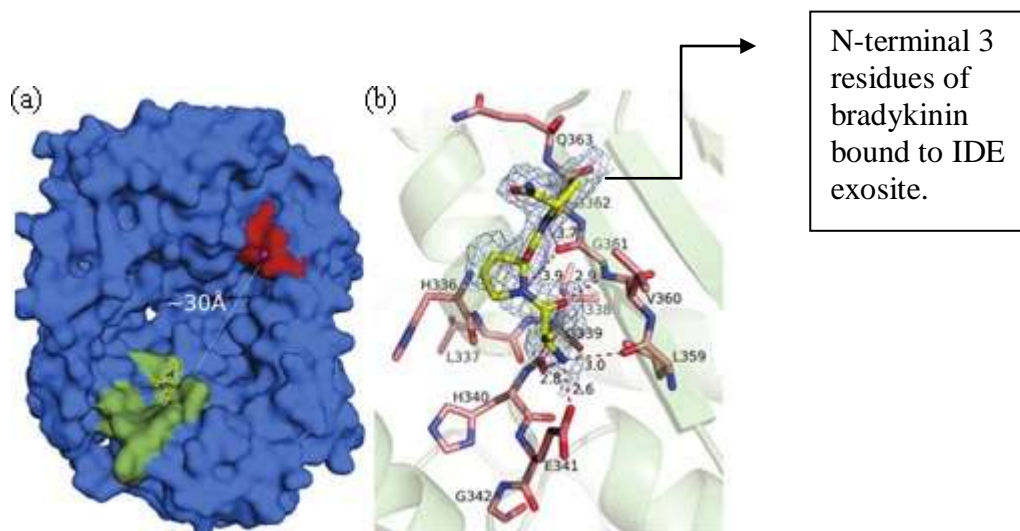


Figure 2.7: (a) Surface representation of IDE. Active site, catalytic zinc and exosite (336-342 and 359-363 of IDE) are represented as red surface, magenta sphere and green surface, respectively. N-Terminal bradykinin is shown as yellow sticks, and distance from active site to exosite is shown as a dashed line (30 Å). (b) Interactions between bradykinin and the exosite of IDE. The N-terminal residues Arg(Ala)¹-Pro²-Pro³ of bradykinin are shown as yellow sticks. Protein residues belonging to the exosite are shown as salmon sticks, while their secondary structures are shown as green cartoon. Hydrogen bonds are shown as dashed lines[18].

Chapter 3

COMPUTATIONAL METHODS

3.1. Molecular Dynamics Simulations (MD)

Molecular dynamics simulations lean upon the theory that the motions at the microscopic level such as motions of atoms and molecules generate the macroscopic property of a sample. In accordance with this concept, MD simulations are widely used to obtain information on the time dependent dynamic behavior of proteins by numerically integrating the Newton's equation of motion [143, 164]. It can be stated that MD generates the link between the molecular structure, function and dynamics [165]. Additionally, the effects of solvent molecules, temperature changes and pressure on protein structure and also the stability of the biomolecular system can be examined through this computational method [166, 167]. Thus, in order to investigate the biological systems dynamics (i.e. protein folding, protein-protein interactions...) molecular dynamics simulations combined with other computational approaches gain attention [167]. Commonly used programs for MD simulations for biological systems are Amber [168], CHARMM [169], GROMOS [170], and NAMD [171, 172].

3.1.1. NAMD

NAMD is a parallel molecular dynamics tool that enables high-performance simulation of large biomolecular systems. AMBER and CHARMM force field parameters are used in NAMD simulations. These force fields include 2-, 3-, 4-body interactions, electrostatic and van der Waals interactions [172]. NAMD is generally used with its coupled molecular

graphics software, VMD, which allows to prepare the input files for the MD simulations, and to analyze the simulation [172].

In MD simulations, it has been postulated that the atoms of a biopolymer move according to the Newtonian equations of motion [172].

$$F_i = m_i a_i = m_i \frac{d^2 r_i}{dt^2} = -\frac{\partial U}{\partial r_i} \quad (3.1)$$

In this equation m_i represents the mass of atom i , r_i is its position, and U is the total potential energy. Potential energy is evaluated depending on all atomic positions, thereby, represents the motion of atoms [172].

Newtonian equations of motion is computed iteratively for each atom in the system to determine atomic trajectories (positions and velocities); the equation also allows for evaluation of the electrostatic forces through the particle mesh Ewald method. Initial coordinates of the molecule are determined by its structure file; thereby the initial velocities (v_i) are also computed by calculating the expected value of the kinetic energy. Afterwards, the coordinates and the velocities of the atoms from the previous step are used to determine the new coordinates iteratively, and this process is repeated through the final step by solving Newtonian equations of motion [172]. The velocity Verlet method [173] is used as a numerical integrator. The potential energy (U) which is the most essential part of the MD simulation is designated by the force field parameters. U is given as a sum of bonded and non-bonded interaction potentials.

$$U = U_{bondstretching} + U_{bending} + U_{torsional} + U_{Lennard-Jones} + U_{electrostatic} \quad (3.2)$$

The first three terms describe the bonded interactions such that bond stretching (3.3), bending (3.4) and torsional interactions (3.5); and the rest are the non-bonded interactions. The bonded terms are applied to each covalent bond between a pair of atoms sharing a single atom, to each angle between adjacent bonds and to each dihedral between pairs of atoms separated by three covalent bonds with the central bond subject to the torsion angle ϕ [167].

$$U_{bondstretching} = \sum_{bonds} K_b (b - b_o)^2 \quad (3.3)$$

$$U_{bending} = \sum_{angles} K_\theta (\theta - \theta_o)^2 \quad (3.4)$$

$$U_{torsional} = \sum_{dihedral\ angles} K [1 + \cos (n - \delta)] \quad (3.5)$$

The non-bonded terms, Lennard-Jones potential (3.6) and electrostatic interactions (3.7) are computed by considering all atoms except those attached through one or two covalent bonds. For instance, Lennard-Jones potential term approximates the Van der Waal's forces [167].

$$U_{Lennard-Jones} = \sum_{non-bonded\ pairs} \frac{A}{r^{12}} + \frac{B}{r^6} \quad (3.6)$$

$$U_{electrostatic} = \sum_{non-bonded\ pairs} \frac{q_1 q_2}{\epsilon r} \quad (3.7)$$

3.1.2. MD Setup

MD simulation is carried out by using the NAMD software, version 2.6 [172] with the PARAM22 version of the CHARMM [174] force field. In order to run any MD simulation,

NAMD requires at least four documents; (i.) a PDB, Protein Data Bank, file which stores atomic coordinates and/or velocities for the system, (ii.) a PSF, or Protein Structure file, which stores structural information of the protein, (iii.) a force field parameter file, which is a mathematical expression of the system potential, and (iv.) a configuration file, which is used for the simulation submission. Coordinate of the initial structure is obtained from Protein Data Bank (PDB code 2G47) [156]. The reported structure is catalytically inactive IDE mutant IDE-E111Q [175] in complex with amyloid- β peptide ($A\beta_{1-40}$) at 2.1 Å. The bound amyloid- β peptide is then discarded from the structure to obtain solely IDE PDB. VMD is used to prepare protein structure file (PSF) for NAMD simulation. Using *psfgen* package, atoms and residue names are replaced with ones recognized by NAMD. After preparation of the PSF, IDE is solvated in rectangular box including TIP3P water molecules. Distances between the edge of the water boxes and the closest atom of solutes were at least 10 Å. Counter ions were added to neutralize the systems. According to the relevant configuration files (Supplementary 6-7), first the system is minimized through 10000 steps by fixing the backbone fixed, and then backbone atoms are relaxed through another 10000 steps. Next, the system is heated to 310 K with 15 K increments (10ps simulation at each temperature increment). After the equilibration of the system, molecular dynamics simulation was carried out with constant temperature (310 K) and pressure control using Langevin piston method. The time-step of the simulation was set to be 2 fs and, the bonded interactions, the van der Waals interactions (12 Å cut-off), and the long-range electrostatic interactions with partial-mesh Ewald (PME) were included in the calculations to define the forces acting on the system. The damping coefficient was set to be 5 ps⁻¹ using Langevin dynamics to handle pressure control. The simulation was carried out for 1.2 ns, and the final stable structure was used later in the docking calculations. The structure file of the macromolecule for the molecular docking and virtual screening was derived from result of the MD simulation.

3.2. Protein-Small Molecule Docking

Docking techniques are designed to generate a comprehensive set of conformations of the receptor and the ligand complex in order to select the top scoring ones that ensure stability [143]. In general, docking study aims to generate the accurate structural modeling and the correct prediction of activity in a reasonable time [164]. The molecular docking problem can be viewed as an optimization problem predicting the “best-fit” orientation of the protein-ligand complex [176], where the objective function is the minimization of the free energy of the system. The accurate prediction of the binding pose is of great importance in structure based drug design. The docking process is regarded as a multi-step process in which the degrees of complexity increase with each step [164]. The process of binding a small molecule to its receptor protein depends on several entropic and enthalpic factors that affect the interactions between them [143]. Especially, hydrogen bonds and lipophilic contacts contribute to these interactions. Besides, solvation and desolvation effects that exist either in the ligand and the protein binding site are important for the binding process [177]. Flexibility and mobility of both ligand and receptor, interactions between the protein and the surrounding water molecules, further influence the binding process and its quantitative description [143].

In early docking algorithms both the target receptor and the ligand act as rigid bodies; and the main selection criterion was the geometric complementarity of the ligand to the binding site. This algorithm is more suitable for large database screening due to its faster docking process; however all conformational space cannot be sampled with docking due to its limited degrees of freedom. Programs “DOCK” and “GOLD” can be given as examples for this type of search algorithm [178].

Recently, more flexible docking algorithms are produced in which either the receptor or the ligand or both of them are flexible. But more often, the protein receptor is set as the

rigid body and the flexible ligand searches the most optimum configuration. Even though it is not suitable for large compound library screening due to its long processing times, the results are more accurate with respect to the rigid receptor based algorithms. More recently, Autodock 4 is created which provides the flexibility of both the ligand and the receptor molecules [178].

In regard to the receptor macromolecule representations, there are three basic docking methods: atomic, surface and grid [179]. Among them, grid representation is mostly preferred for energy calculations. It allows creating potential energy grids of receptor's energetic contributions in order to consider them during ligand scoring [180, 164].

3.2.1. AutoDock

In this study Autodock docking program is selected among several popular docking softwares such as GOLD, FlexX, Dock, which is a flexible ligand docking tool as mentioned before; because its scoring function is verified its better performance over those of other programs tested in several target proteins [181]. Autodock which is a suite of automated docking tools that predicts protein–ligand conformations, offers several alternatives for search algorithms including Monte Carlo Simulated Annealing, Genetic Algorithm and Lamarckian-Genetic Algorithm. The fundamental base of the genetic algorithms (GA) depends on the evolution of a population through genetic operators with mutations and crossovers. GA process starts by generating a random population of individuals (genes) in which each gene corresponds to a different conformation of the docked molecule. Then, the creation of the next generation based on the best solutions from the previous population is performed depending on several genetic parameters such that phenotypic mapping, fitness evaluation, natural selection, crossover, mutation, elitist selection and number of evolutionary rounds. Then energy minimizations are performed and individuals having lowest energy are transferred to the next generation of

conformations [178]. As a macromolecule representation type, Autodock uses the precalculated potential energy grid points to perform docking. [147]. The scoring consists of electrostatic, Lennard-Jones, hydrogen bond, solvation, and torsional entropy terms.

In this study AutoDock 3.05 [182] is used since it uses Lamarckian-Genetic Algorithm as the stochastic search method which offers high degrees of freedom. In the case of molecular docking, ligand's state variables, translation, orientation, and conformation of the ligand according to the protein, constitute the genes. During this process, pairs of individuals are mated randomly, which is nominated as crossover and some offspring resulted from this crossover process can go under mutation. During mutation, randomly selected genes are changed by a random amount. Fitness which is defined as the total interaction energy of the ligand with the protein (docking energy) is evaluated using the energy function. Therefore, selection of the offspring is dependent on the individuals fitness score [182]. This approach exists both in the "genotypic space" and "phenotypic space". In genotypic space, mutations and crossover production occur, while in phenotypic space energy functions are optimized. The acquired phenotypic advantages are then transferred to the genotype. In this regard, a ligand's state corresponds to a genotype and the atomic coordinates correspond to phenotype. Then the energy minimization is performed. Finally, rankings are done based on geometrical and energetic constraints. Ligands or conformations with better geometrical fit and lower estimated binding energy are ranked higher. [178].

AutoDockTools package scripts are used to convert structures of compounds to AutoDock 3.05 format and to prepare proteins. AutoDock is employed in the generation of grid files for each type of atom in the ligand by using AutoGrid component. In this concept, every atom is assigned a non-bonded interaction potential with the protein and electrostatic potentials.

3.2.2. AutoDock Docking Setup

To run a docking algorithm Autodock requires four types of input files: the PDBQS file for the protein, the PDBQ file for the ligand, the GPF file to create the active site grid parameter files and the DPF file containing the docking parameters.

To prepare the macromolecule valid for Autodock, PDBQS file was generated by adding first the polar hydrogen atoms to the PDB structure obtained from MD simulation. Since the MD simulation already added the polar hydrogens to our structure, only the non-polar ones were merged. Then, the Kollman charges were added; yet macromolecule was protein, and the final structure was stored in the PDBQS file.

Next, the PDBQ files were prepared for the each ligand molecule, in this case, for a commercial compound database, Ambinter, to perform virtual screening and also for molecular docking study of bradykinin, Ia1 and Ia2. First all hydrogen atoms were added. Since bradykinin is a peptide, again the Kollman charges were added; for the rest of the ligands that were chemical compounds, instead of Kollman charges, Gasteiger charges were added. After that, non-polar hydrogens were merged for all ligands. In Autodock, carbons were treated as planar and non-planar depending on the angle between consecutive C atoms; then the torsional freedom of the bonds were marked and recorded in the PDBQ file for the flexible ligand docking.

For the grip maps, GPF files were prepared in order to define the docking site. The residues 336-342 and 359-363 of the target macromolecule, IDE, were taken as the target for docking, as these were defined to constitute the exosite region of IDE. Crystal structure experiments revealed that the exosite residues of IDE are involved in interactions with bradykinin which has found to be an activator of IDE by only binding to the exosite and not to the catalytic site [18]. This has suggested the idea that the binding of small compounds to this region would have the regulatory effect on IDE activity. Consistent with these findings, in our study, exosite was modeled as the target docking site. This docking site

was modeled as a box, and the resulting grip map comprised the grid center coordinates of this box, the grid size as number of points, the spacing between two grid points, and the number of the grid files based on each atom type present in the ligands that would be created.

Throughout the study, two different grid files were generated; the first set is designed for a relatively coarse docking, and second is designed for a fine docking. For virtual screening, low resolution grid maps are created to ease docking simulation in a shorter time. For this purpose, map size is defined as 60x60x60, spacing is kept as default 0.375 Å. Fine docking setup, involving high resolution grip map, was prepared within 126×126×126 grid points having 0.180 Å spacing parameter for the detailed docking which allows the study of ligand-protein interactions in detail. Since, virtual and detailed docking processes were performed over several thousands of compounds, grid maps were generated for atom types present in all compounds. Samples of this GPF files for both virtual screening and detailed docking can be found in Supplementary 6-7.

For the next step, the DPF file was prepared which contained the setup for the run parameters of the Lamarckian-Genetic Algorithm such as: population size, number of generations, number of runs, crossover rate, mutation rate and number of evaluations. In the DPF file, the run parameters adopted for the coarse docking for virtual screening were as follows; population size was 50, number of generations was 27,000, crossover rate was 0.8, mutation rate was 0.02, number of runs was 10, and number of evaluations was 1000000. For the fine docking in detailed docking study, population size was kept 250, number of generations was 50000, crossover rate was 0.8, mutation rate was 0.02, number of runs was 256, and number of evaluations was set at 15,000,000. DPF file samples can also be found in Supplementary 8-9.

Important to note that, for the virtual screening pre-filtering protocol was applied first on the ligand set to save from the computational time, since docking process would last longer

for larger compounds. Molecular weight threshold was set to be 550 g/mol in virtual screening in order to select drug-like compounds which were able to cover the exosite region. After running Autodock, based on energetic and geometrical constraints, estimated binding and docking energies were obtained. As it is known that the native conformation of the ligand should correspond to a global minimum of the docking energy function, lower estimated energies were accepted. Finally all figures were rendered using PyMOL version 0.99.

Chapter 4

RESULTS AND DISCUSSION

4.1. Analysis of Molecular Dynamics Simulation

Molecular dynamics simulation is applied for 1.2 ns and it is observed that we have a stable IDE structure at physiological conditions. Root mean square deviation (RMSD) is obtained for every frame by aligning the final conformation of IDE at the corresponding frame to the initial structure (Fig. 4.1). Graph includes both equilibration and main simulation steps. The equilibration takes place in the first 0.4 ns time period.

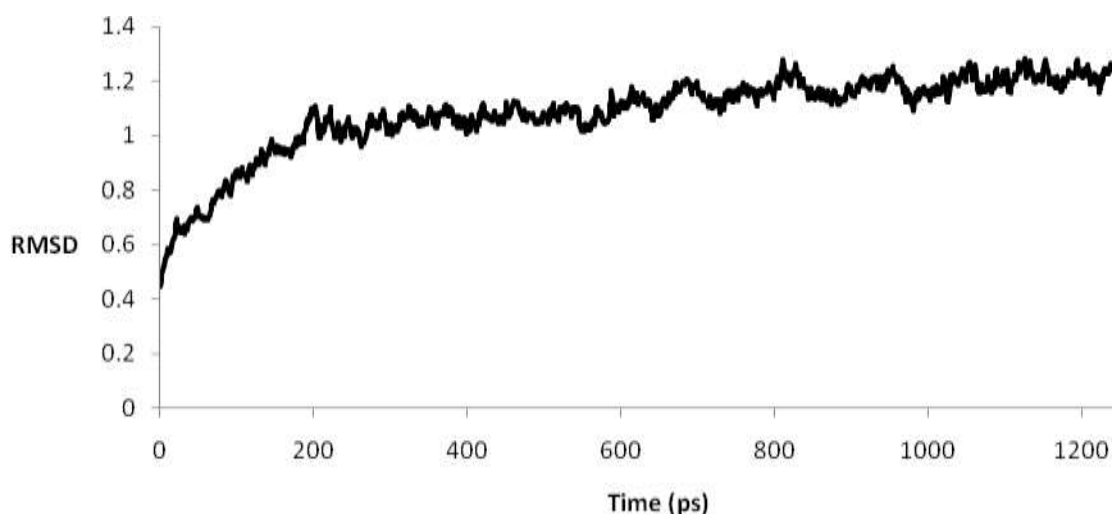


Figure 4.1: Time dependence of the RMSD for the 1.2-ns MD trajectory of IDE (2G47-without amyloid- β fragment).

As explained before, first, the backbone of the protein is fixed and only hydrogen atoms are allowed to move and position themselves in a minimum energy confirmation; and then

the fixed-backbone system is allowed to move without pressure control. Finally, the whole system is heated up with 15 K increments slowly up to 310 K. IDE shows expected solvation, heating and relaxation behavior in the equilibration steps where, no deformation was observed. The simulation shows a slight increment after minimization up to approximately 0.4 ns. In the main simulation, RMSD continues to increase during the first 0.8 ns and then any significant deviations during the rest of the simulation are not observed which demonstrates the convergence of RMSD and the stability of the given structure within 1.2 ns time period. This behavior is significant for accuracy of the structure based drug design. Instability and deformations in throughout the structure build hinders a reliable rigid binding pocket model for the docking studies to find effective regulatory hits.

In order to understand the stability of the equilibrated exosite residues, the residual RMSD of these residues are calculated and analyzed (Supplementary 5). The RMSD range is between 0.4 and 0.9 which corresponds to lower mobility. Residues between 338 and 358 correspond to the loop region where no hydrogen bonding patterns exist as α -helices and β -sheets; therefore this part is expected to be less stable according to secondary structure elements. However in our enzyme, loop region also has small RMSD values, and it is quite stable. The highest mobile residue among others is observed to be Glu³⁶³ which is located at the end of the β -sheet secondary structure. This moderate mobility can also be ignored (Table 4.1).



Figure 4.2: IDE exosite colored by the average RMSD per residue.

Table 4.1: Residual RMSD values for IDE exosite (336-342 & 359-363).

| Residue | RMSD |
|----------------|-----------------------|
| 336 | 0.495924666525 |
| 337 | 0.563022822143 |
| 338 | 0.657464245957 |
| 339 | 0.660268033542 |
| 340 | 0.503175357978 |
| 341 | 0.486161972085 |
| 342 | 0.54808005194 |
| 343 | 0.676422337692 |
| 344 | 0.537686347962 |
| 345 | 0.376894267897 |
| 346 | 0.459154407183 |
| 347 | 0.300692200662 |
| 348 | 0.494027515253 |
| 349 | 0.59317573905 |
| 350 | 0.426192124685 |
| 351 | 0.435855483013 |
| 352 | 0.509076019127 |
| 353 | 0.751319477955 |
| 354 | 0.295074981948 |
| 355 | 0.388941844305 |
| 356 | 0.27105530103 |
| 357 | 0.485222955545 |
| 358 | 0.323070593178 |
| 359 | 0.32914053897 |
| 360 | 0.444338738918 |
| 361 | 0.500776390235 |
| 362 | 0.758700420458 |
| 363 | 0.926659286022 |

The mobility of each residue located in the exosite depending on Beta-Color scale based on beta value of the PDB file is also visualized in Figure 4.2. In the Figure above, red denotes residues which moved less during equilibration. Blue denotes more mobile residues, while values near the middle of the scale are green. For the IDE exosite RMSD per residue is less therefore, no blue or green color is appeared. Therefore, the final structure at the end of the MD simulation is applicable for the molecular docking calculations.

4.2. Validation of AutoDock with Molecular Docking Studies for the Previously Found IDE Regulators

In an attempt to validate our docking strategy to enable docking and selection of molecules through virtual screening, we tried to implement docking studies of recently published compounds, Ia1, Ia2, and known small substrate bradykinin by AutoDock before virtual screening.

Docking analysis of bradykinin is conducted at the exosite of IDE to ensure the reliability of the docking process initially. Docking conformation of bradykinin is illustrated in Figure 4.3. The crystallization experiments with IDE and bradykinin showed that three residues at the N-terminus of bradykinin (Arg¹-Pro²-Pro³) bounded to exosite residues. The side chain of the N-terminal arginine was not visible; therefore alanine was replaced for that invisible arginine [18]. The backbone N and C atoms of Arg¹ and Pro² of bradykinin formed hydrogen bonds with the backbone carbonyl O atom of Leu³⁵⁹ and amino group of Gly³⁶¹, respectively. Gly³⁶¹ also favorably interacts with N atom of Pro³ side chain within a 3.89 Å (3.7 Å in previous publication [18]). Another strong hydrogen bonding is also mediated between the carboxyl oxygen of Glu341 and the side chain N of Arg¹. Additionally, Arg¹⁰ is in contact with Ala⁴²¹. Moreover, hydrogen bonding is also formed between Arg¹⁰ and Ser⁶¹⁷, Lys⁶³². Residue Ser⁷ interacts with Ala⁶¹¹, Leu⁶¹⁶, and

Ser⁶¹⁷ that exist within the α -helix segment and β -sheet secondary structure found in domain 3, near the exosite region (Fig. 4.3).

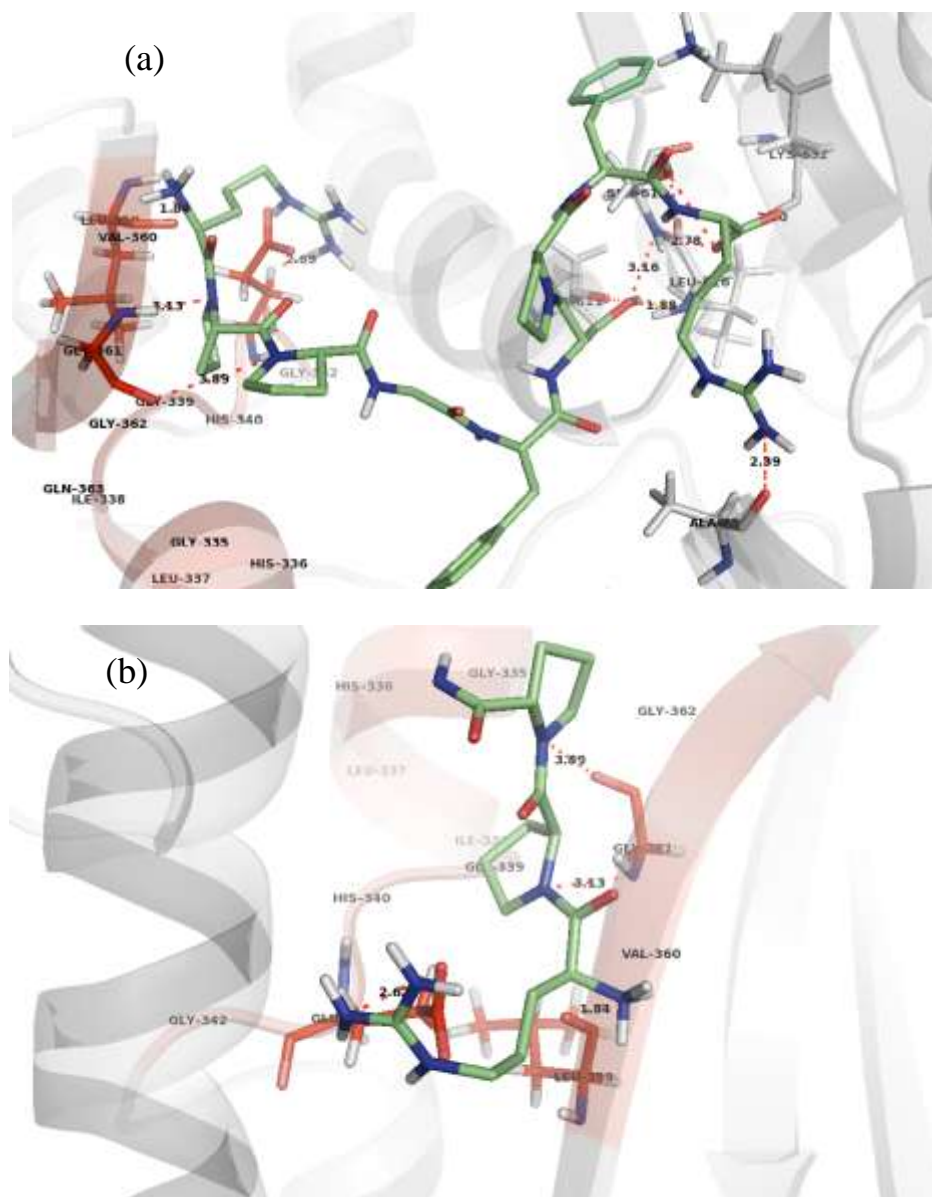


Figure 4.3: Docked Conformation of bradykinin within IDE exosite. a) Interactions between full bradykinin and the exosite of IDE. b) Interactions between N-terminus of

bradykinin and the exosite of IDE. The exosite residues are shown as red and bradykinin is illustrated by using stick representation with green color. Hydrogen bonds are shown as red dashed lines.

Next, we performed molecular docking calculations with two additional small molecules, which were recently demonstrated to enhance the catalytic activity of IDE [16]. The characterization of degradation of fluorogenic peptides has shown that these two small molecules were capable of enhancing the activity of IDE in the presence of ATP and other small substrates (Supplementary 2). The binding and docking energies for these additional compounds are listed in Table 4.2, and their corresponding docking conformations in the IDE exosite derived from their minimum energy snapshots are displayed in Figures 4.4a and 4.4b. Molecular docking calculations demonstrated that compound Ia1 makes polar interactions with the Asn³²⁹, Gly³³¹, His³³², Gln³⁶³, Tyr⁴⁴⁴ of IDE residues. Polar nature of Tyr⁴⁴⁴ and Asn³²⁹ allow them to make polar interactions with the N atom of the compound Ia1. Even though these residues are not located at the IDE exosite, these interactions may provide additional stability to the docking position onto the exosite, which resulted in lower binding energy. The compound also makes polar interactions with Gly³³¹, His³³², Gln³⁶³. Former two residues have not been reported as exosite residue; however they exist on the same helix-loop segment. Side chain N atom of His³³² is in contact with the O atom of the ligand, and the other O atom of the same aromatic ring that exists in the ligand makes two hydrogen bonds with the side chain amine group of the polar Gln³⁶³ residue and the carboxylic O atom of Gly³³¹.

Compound Ia2 is found to make hydrogen bonding interaction with two exosite residues, namely, with carboxyl oxygen atoms of Gly³³⁹ and Glu³⁴¹ (Fig. 4.4b). We found that, the binding and docking energies for this compound is higher than that of compound Ia1.

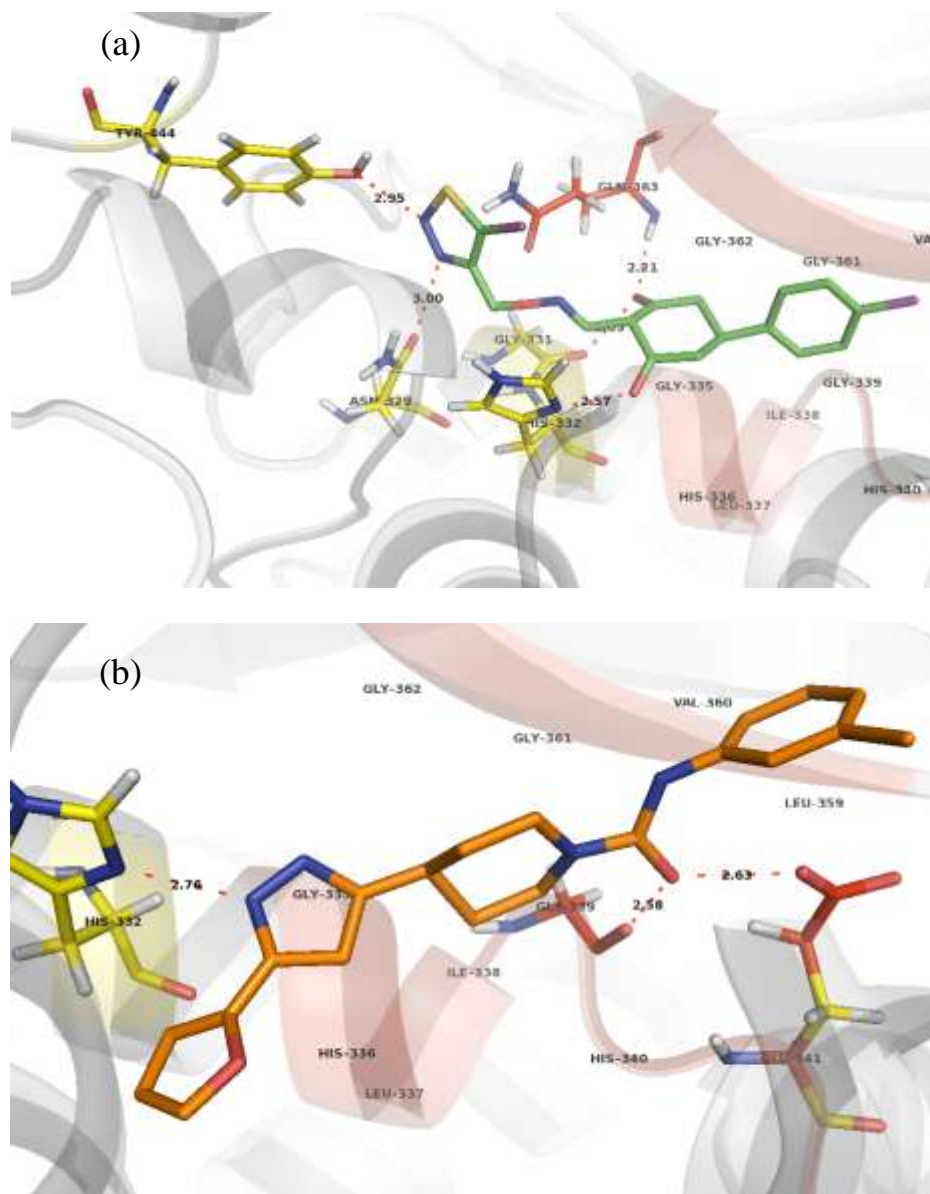


Figure 4.4: Docked Conformation of compound Ia1 and Ia2 within IDE exosite. Interactions between a) Ia1 and b) Ia2 and the exosite of IDE. The exosite residues are shown as red. Hydrogen bonds are shown as red dashed lines.

Table 4.2: Binding and Docking Energies of bradykinin and selected compounds. (The common interaction sites within exosite (336-342, 359-363) are represented as red color)

| | BINDING ENERGY (KCAL/MOL) | DOCKING ENERGY (KCAL/MOL) | INTERACTIONS |
|-------------------|--|--|---|
| BRADYKININ | -5.66 | -15.91 | Glu³⁴¹, Leu³⁵⁹, Gly³⁶¹ , Ala ⁴²¹ , Ala ⁶¹¹ , Leu ⁶¹⁶ , Ser ⁶¹⁷ , Lys ⁶³² |
| IA1 | -9.68 | -11.31 | Asn ³²⁹ , Gly ³³¹ , His ³³² , Gln³⁶³ , Tyr ⁴⁴⁴ |
| IA2 | -7.97 | -9.38 | His ³³² , Gly³³⁹, Glu³⁴¹ |

4.3 Virtual Screening and Detailed Docking

4.3.1. Virtual Screening Results

Following the success of the control dockings performed with bradykinin and Ia1-Ia2, VS calculations were performed with the same IDE grid file obtained from MD derived crystal structure model. The Ambinter Library, chosen as an initial database for lead compound identification, is composed of 9,000,000 compounds. Among them more than 1,000,000 were selected randomly and analyzed for the virtual screening purposes on a computational grid. In virtual screening, pre-filtering protocol was applied first on the ligand set to save from the computational time, since docking process would last longer for larger compounds. Molecular weight threshold was set to be 550 g/mol in order to select drug-like compounds which were able to cover the exosite region. After running Autodock, based on energetic and geometrical constraints, estimated binding and docking energies were obtained. As it is known that the native conformation of the ligand should correspond to a global minimum of the docking energy function, lower estimated energies were accepted.

The docked conformations were evaluated by their mean estimated docking and binding energy scores, which were then used to form a preliminary ranked list. On the basis of the initial ranking, 300 compounds were selected as virtual hits. Docking conformations within the exosite and hydrogen bonding with these residues were also considered during this selection process. Additionally, some highly scored compounds were found to possess long aliphatic structures with many rotatable bonds resulting in high torsional freedom. Therefore, compounds having high torsional freedom and long hydrocarbon chains, generally flexible and hydrophobic, were eliminated during this initial step.

Binding and docking energies of selected candidates were in range of -9 kcal/mol to -13 kcal/mol. The top-ranked compounds from the virtual screening were chosen for further study.

4.3.2. Detailed Docking Results, Selection and Elimination of the Candidates

After this initial ranking, the selected compounds were then redocked in a more detailed manner with increased grid resolution in order to ensure the accuracy. Among those, 38 of them were selected as shown in Table 4.3 with respect to their estimated minimum energy scores of their lowest energy conformations.

Table 4.3: Binding and docking energy scores of virtual screening and detailed docking of the selected 38 candidates

| COMPOUND ID | VIRTUAL SCREENING | | DETAILED DOCKING | | INTERACTIONS |
|-------------|---------------------------|---------------------------|---------------------------|---------------------------|--|
| | BINDING ENERGY (KCAL/MOL) | DOCKING ENERGY (KCAL/MOL) | BINDING ENERGY (KCAL/MOL) | DOCKING ENERGY (KCAL/MOL) | |
| 8-171972 | -12.79 | -13.62 | -13.21 | -14.13 | -- |
| 8-141267 | -10.64 | -11.97 | -12.99 | -14.89 | His ³³² , His ³³⁵ , His ³³⁶ , Gly ³⁶¹ |
| 1-100872 | -10.34 | -12.07 | -12.65 | -14.39 | -- |
| 8-171299 | -11.34 | -14.14 | -12.22 | -14.9 | Gly ³³¹ , His ³³² , Gln ³⁶³ |
| 4-131929 | -10.77 | -12.38 | -12.19 | -13.94 | His ³³² , His ³³⁶ |
| 9-151914 | -10.92 | -13.6 | -12.18 | -15.26 | Asn ³²⁹ , Gly ³³¹ , His ³³² , His ³³⁶ , Gly ³⁶¹ , Gln ³⁶³ , Asn ⁴¹⁸ |
| 3-122109 | -11.77 | -13.7 | -12.17 | -14.23 | Gly ³³¹ , Gly ³³⁵ , Gln ³⁶³ |
| 9-147338 | -9.71 | -13.85 | -12.06 | -15.14 | Gly ³³⁹ , Gly ³⁶¹ , Gln ³⁶³ |
| 3-114154 | -11.48 | -11.11 | -11.84 | -11.54 | His ³³² , Gln ³⁶³ |
| 1-16588 | -11.04 | -13.35 | -11.78 | -13.82 | Gly ³³¹ , His ³³² , His ³³⁶ |
| 8-141265 | -10.36 | -12.3 | -11.77 | -13.95 | His ³³² , Gln ³⁶³ |
| 9-14137 | -11.08 | -12.67 | -11.77 | -14.23 | His ³³² , Gly ³⁶¹ , Gln ³⁶³ |
| 1-16593 | -10.86 | -13.24 | -11.76 | -14.06 | Gly ³³¹ , His ³³² , His ³³⁶ , Gly ³³⁹ , Gly ³⁶¹ , Gln ³⁶³ , Tyr ⁶⁰⁹ |
| 3-116810 | -11.05 | -12.49 | -11.73 | -12.76 | Gln ³⁶³ |
| 5-108909 | -11.54 | -13.65 | -12.72 | -13.89 | His ³³² , His ³³⁶ |
| 9-151856 | -10.57 | -13.2 | -11.57 | -13.95 | His ³³² , Gly ³³⁹ , Gln ³⁶³ , Tyr ⁶⁰⁹ |
| 3-113780 | -11.26 | -12.17 | -11.57 | -12.58 | His ³³⁶ , Gly ³⁶¹ , Asn ⁴¹⁸ |
| 4-135627 | -10.45 | -12.19 | -11.55 | -11.26 | Gly ³⁶¹ |
| 9-1573 | -10.89 | -12.72 | -11.44 | -13.24 | His ³³² , His ³³⁵ , His ³³⁶ , Gly ³⁶¹ |
| 3-137443 | -10.6 | -13.43 | -11.31 | -14.26 | Gly ³³¹ , His ³³⁵ , Gln ³⁶³ |

| | | | | | |
|----------|--------|--------|--------|--------|--|
| 1-168108 | -10.43 | -12.08 | -11.24 | -13.89 | Gly ³³⁵ |
| 9-134343 | -10.85 | -12.52 | -11.22 | -12.89 | Asn ³²⁹ , His ³³² , His ³³⁵ , Gly ³⁶¹ , Gln ³⁶³ , Tyr ³³³ , Tyr ⁴⁴⁴ , Tyr ⁶⁰⁹ |
| 1-180918 | -10.3 | -11.99 | -11.22 | -12.58 | Gly ³⁶¹ , Gln ³⁶³ , Glu ⁴⁵³ |
| 9-1674 | -10.98 | -13.39 | -11,2 | -13,6 | --- |
| 2-12104 | -10.72 | -13.38 | -11.2 | -14.74 | Gly ³³¹ |
| 1-102877 | -10,65 | -13,22 | -11.18 | -14.32 | Gly ³³¹ , His ³³² , Gln ³⁶³ |
| 8-456 | -9.59 | -12.17 | -11.18 | -13.59 | Gly ³³¹ , His ³³⁵ , Gly ³³⁹ , Glu ³⁴¹ , Gly ³⁶¹ |
| 3-110732 | -10.47 | -12.76 | -11.16 | -13.15 | Gly ³³⁵ , Gly ³³⁹ , Gly ³⁶¹ , Gln ³⁶³ , Tyr ⁶⁰⁹ |
| 1-11351 | -9.9 | -10.83 | -11.13 | -11.6 | His ³³² , His ³³⁶ , Asn ⁴¹⁸ |
| 4-106854 | -9.16 | -10.96 | -11.13 | -14.77 | Gly ³³¹ , His ³³⁶ , Glu ³⁴¹ , Val ³⁶⁰ , Gln ³⁶³ |
| 1-180914 | -10.53 | -11.68 | -11.12 | -13.9 | His ³³² , Tyr ⁶⁰⁹ |
| 3-114848 | -9.37 | -10.71 | -11.13 | -13.11 | His ³³⁶ , Gly ³⁶¹ , Glu ⁴⁵³ , Tyr ⁶⁰⁹ |
| 9-102548 | -10.52 | -12.45 | -11.11 | -13.04 | His ³³² |
| 2-114522 | -10.62 | -11.94 | -11.08 | -12.45 | Gly ³³¹ , His ³³⁵ , His ³³⁶ , Gln ³⁶³ |
| 1-11728 | -10.02 | -11.59 | -11.01 | -12.33 | His ³³² , His ³³⁶ , Gly ³³⁹ , Gly ³⁶¹ , Asn ⁴¹⁸ , Tyr ⁶⁰⁹ |
| 4-131363 | -10.29 | -13.07 | -10.95 | -13.78 | His ³³² |
| 4-100665 | -9.8 | -12.37 | -10.85 | -13.29 | --- |
| 5-11207 | -10.09 | -12.61 | -10,75 | -13,09 | Gly ³⁶¹ |

Compounds shown on Table 4.3 are the possible candidates for the regulation of IDE; but at the first glance, a detailed analysis is conducted in order to evaluate their drug-likeness and their tendency to make interactions with the exosite. Therefore, these compounds are then analyzed according to some features concerning the docking positions; hydrogen bonding with exosite residues (336-342 and 359-363) and close proximity, van

der Waals interactions, exposed surface area, pocket occupancy. In addition to this analysis protocol, Lipinski's rules [154] and the rules defined by Ghose et al. [183] are applied to evaluate drug-likeness of the candidate molecules, and then to filter hits. As the drug must pass through lipid bilayers during cellular transportation, the selected compound must be hydrophobic enough to pass through the bilayer membrane; but at the same time it should not be so hydrophobic in order not to be accumulated in the cytosol [184]. Additionally, hydrophobic drugs are found to be more toxic due to their non selective binding patterns and higher retention time within the body. In pharmacokinetics, logP, the distribution coefficient is accepted as the hydrophobicity measure, which should have an optimum value for an efficient transport.

Lipinski's rule of 5 [154] is not a definite guarantee for a compound to be a drug-like. In the physicochemical properties suggested by the study of Ghose et al.[183], calculated log P is between -4 and 5.6, molecular weight, is between 160 and 480, molar refractivity, is between 40 and 130, the total number of atoms, is between 20 and 70. Exceptionally, the molecular weight upper limit is set at 550 Da instead of 500 Da suggested by Lipinski [154] or 480 Da suggested by Ghose [183], due to the fact that the exosite covers a considerably larger space. Poor permeation or absorption is more likely to occur when drug molecule properties are not in these ranges. For instance, oral bioavailability which is an important criterion for drug likeness depends on the log P, molecular weight, and the number of hydrogen bonding groups. Basic Lipinski's rule of 5 determines the acceptable aqueous solubility and intestinal permeability which are relevant with oral bioavailability [151]. Other important aspects of drug-likeness such as molecular lipophilicity and molar refractivity of drug molecules put an important act on receptor binding, cellular uptake, and bioavailability [183].

The 38 selected compounds are tabulated according to their physicochemical properties in Table 4.4 provide insight into the estimation of their drug-likeness. MW represents the

molecular weight, N_{AT} is the total number of atoms, N_{CLC} is number of rings, N_{HDON} represents the number of donor atoms for H-bonds (with N and O), while N_{HACC} is number of acceptor atoms for H-bonds (N, O, F). AMR and ALOGP are the properties reported by Ghose et al [183], which are Ghose-Crippen molar refractivity and Ghose-Crippen octanol-water partition coefficient (logP), respectively.

The ones that are eliminated are given in blue color and bold font, and the values that are colored red represent the off-limits. The main criteria behind the elimination process are the docking positions and polar interactions; therefore some compounds that do not exceed the limits are also eliminated due to their ineligible binding patterns. On the other hand, some of few that are off-limits are selected, because these properties mainly have impact on oral bioavailability. However our first concern is to discover the potential hits. These features should be concerned more during *in vivo* testing studies.

Table 4.4: Physicochemical properties of top selected candidates. (Blue color represents the eliminated compounds, and the values that are colored in red represent the off-limits)

| COMPOUND ID | MW | NAT | NCIC | NHDON | NHACC | AMR | ALOGP |
|-----------------|--------|-----|------|-------|-------|---------|-------|
| 8-171972 | 430.56 | 56 | 7 | 0 | 0 | 142.131 | 8.5 |
| 8-141267 | 509.97 | 57 | 5 | 1 | 6 | 141.41 | 7.353 |
| 1-100872 | 471.6 | 56 | 7 | 2 | 7 | 132.148 | 3.997 |
| 8-171299 | 520.68 | 71 | 7 | 0 | 6 | 149.45 | 5.996 |
| 4-131929 | 461.61 | 62 | 6 | 0 | 5 | 137.995 | 5.91 |
| 9-151914 | 438.48 | 46 | 4 | 2 | 8 | 115.88 | 4.192 |
| 3-122109 | 504.51 | 56 | 6 | 1 | 7 | 137.725 | 7.158 |
| 9-147338 | 497.7 | 61 | 5 | 0 | 7 | 136.177 | 4.028 |
| 3-114154 | 448.47 | 50 | 6 | 0 | 7 | 125.621 | 5.201 |
| 1-16588 | 448.37 | 45 | 4 | 0 | 8 | 119.308 | 5.047 |
| 8-141265 | 506.5 | 56 | 5 | 1 | 8 | 138.889 | 6.097 |
| 9-14137 | 443.26 | 42 | 4 | 0 | 5 | 113.35 | 6.178 |
| 1-16593 | 450.34 | 43 | 4 | 1 | 9 | 115.961 | 4.293 |
| 3-116810 | 460.59 | 60 | 7 | 0 | 1 | 149.74 | 8.175 |
| 5-108909 | 448.51 | 54 | 4 | 3 | 7 | 130.509 | 4.825 |
| 9-151856 | 498.64 | 56 | 5 | 0 | 8 | 133.992 | 4.448 |
| 3-113780 | 438.47 | 51 | 5 | 0 | 7 | 123.779 | 4.556 |
| 4-135627 | 479.68 | 69 | 6 | 0 | 5 | 143.888 | 5.88 |
| 9-1573 | 520.69 | 74 | 3 | 0 | 7 | 154.821 | 6.733 |
| 3-137443 | 490.65 | 62 | 6 | 0 | 6 | 138.961 | 6.333 |
| 1-168108 | 545 | 100 | 8 | 0 | 0 | 166.793 | 9.687 |
| 9-134343 | 416.42 | 47 | 4 | 1 | 7 | 112.472 | 4.195 |

| | | | | | | | |
|-----------------|--------|----|---|---|---|---------|-------|
| 1-180918 | 493.75 | 70 | 7 | 0 | 7 | 140.873 | 3.994 |
| 9-1674 | 477.61 | 63 | 6 | 0 | 7 | 141.815 | 3.987 |
| 2-12104 | 487.69 | 59 | 6 | 0 | 4 | 141.385 | 6.777 |
| 1-102877 | 524.11 | 68 | 6 | 2 | 4 | 152.009 | 7.713 |
| 8-456 | 519.62 | 59 | 5 | 2 | 8 | 147.325 | 4.723 |
| 3-110732 | 427.51 | 54 | 5 | 3 | 5 | 122.837 | 5.676 |
| 1-11351 | 460.48 | 54 | 4 | 1 | 8 | 125.668 | 5.799 |
| 4-106854 | 409.51 | 55 | 4 | 0 | 6 | 112.054 | 1.754 |
| 1-180914 | 490.65 | 64 | 5 | 0 | 9 | 129.923 | 2.746 |
| 3-114848 | 499.64 | 61 | 5 | 1 | 7 | 143.186 | 3.949 |
| 9-102548 | 477.53 | 53 | 5 | 0 | 8 | 126.89 | 4.863 |
| 2-114522 | 412.45 | 47 | 5 | 3 | 9 | 109.24 | 1.531 |
| 1-11728 | 477.45 | 51 | 6 | 0 | 6 | 135.758 | 6.329 |
| 4-131363 | 399.56 | 58 | 4 | 2 | 9 | 112.82 | 4.024 |
| 4-100665 | 430.99 | 49 | 5 | 1 | 2 | 126.442 | 7.013 |
| 5-11207 | 512.77 | 73 | 6 | 0 | 4 | 152.414 | 6.353 |

Docking positions and the polar interactions of the eliminated compounds are illustrated in Figures 4.5 - 4.22.

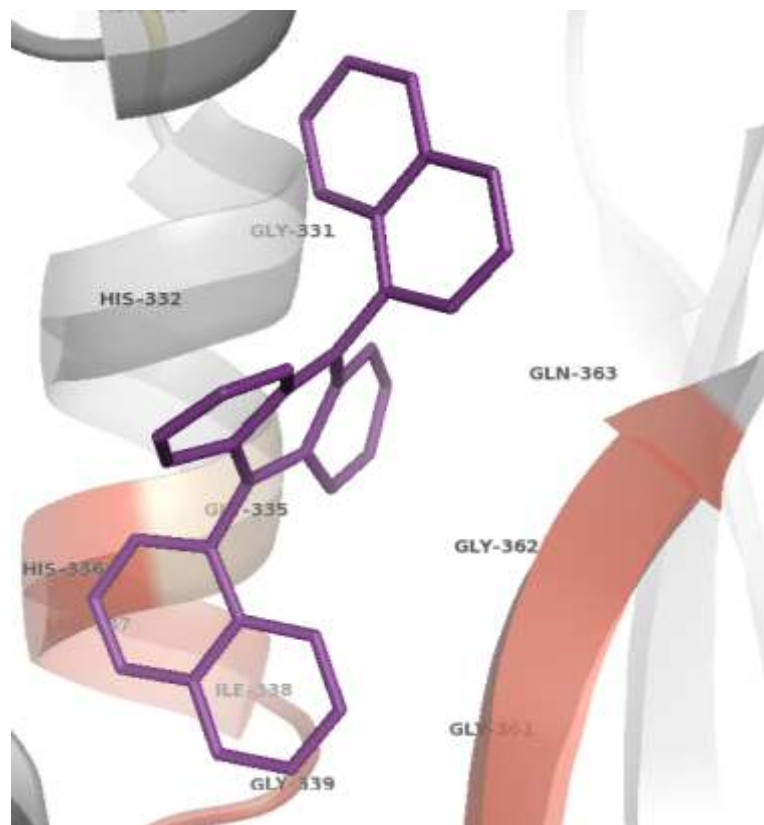


Figure 4.5: Docked Conformation of compound 8-171972 within IDE exosite. The exosite residues are shown as red.

In the cocrystal structure shown in Figure 4.5, no amino acid residues interacts with the drug candidate. The compound 8-171972 occupies the exosite; however due to the lack of any reactive species, no polar contacts are formed. In addition to that, high AMR and ALOGP (142.131 and 8.5, respectively) values also influenced this decision process.

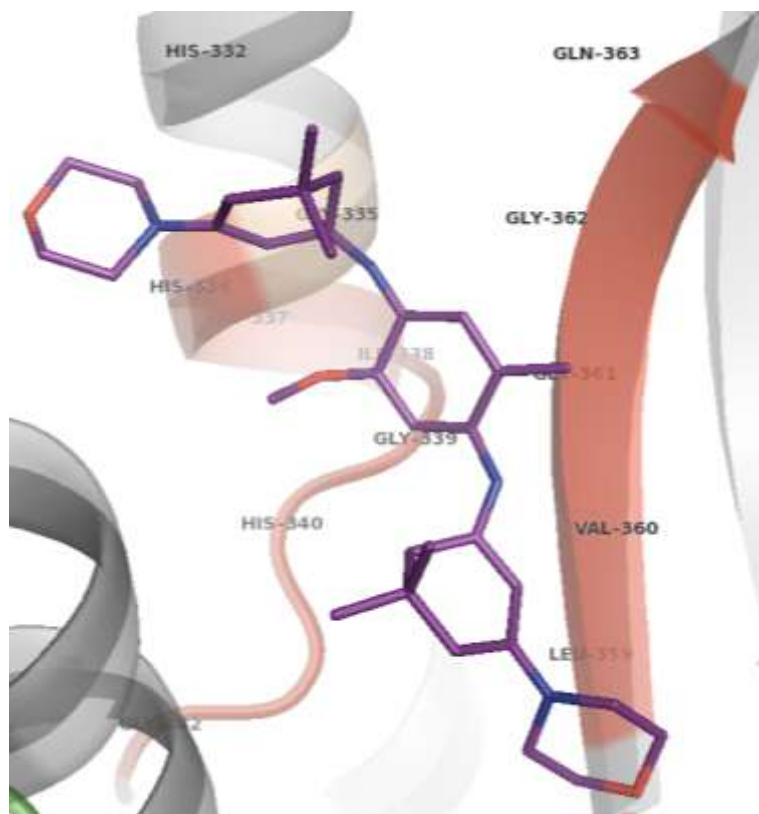


Figure 4.6: Docked Conformation of compound 1-100872 within IDE exosite. The exosite residues are shown as red.

Compound 1-100872 shown in Figure 4.6 occupies the exosite; however again no hydrogen bonding exists between this compound and the exosite or any other IDE residues. AMR value, 132.148, exceeds the limit of 130; but it is quite acceptable. If the docking position and the polar interactions were reasonable, this high value would be ignored.

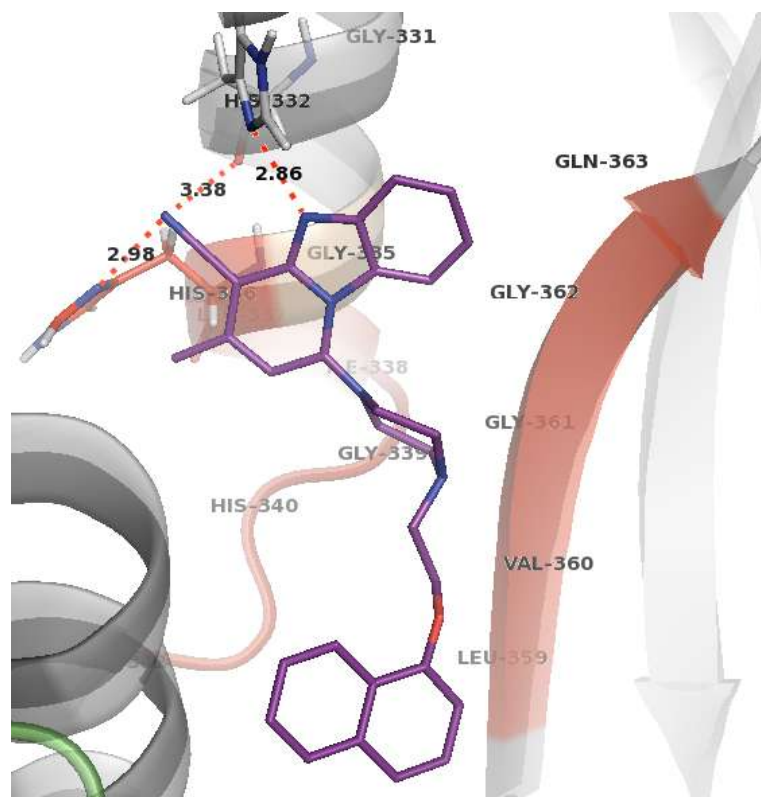


Figure 4.7: Docked Conformation of compound 4-131929 within IDE exosite. The exosite residues are shown as red. Hydrogen bonds are shown as red dashed lines.

The compound 4-131929 covers the exosite and have some reactive species allows to form hydrogen bonding with two IDE residues, one of which belongs to the exosite region. N atom of the imidazole ring makes hydrogen bonding with His³³² and another N atom bounded to the pyridine ring interacts with both His³³² and His³³⁶. However, as can be seen from Figure 4.8 that only one part of the compound interacts with IDE, and low docking energy may be due to this high torsional freedom. In addition to that AMR and ALOGP values are slightly higher than those of the limiting conditions.

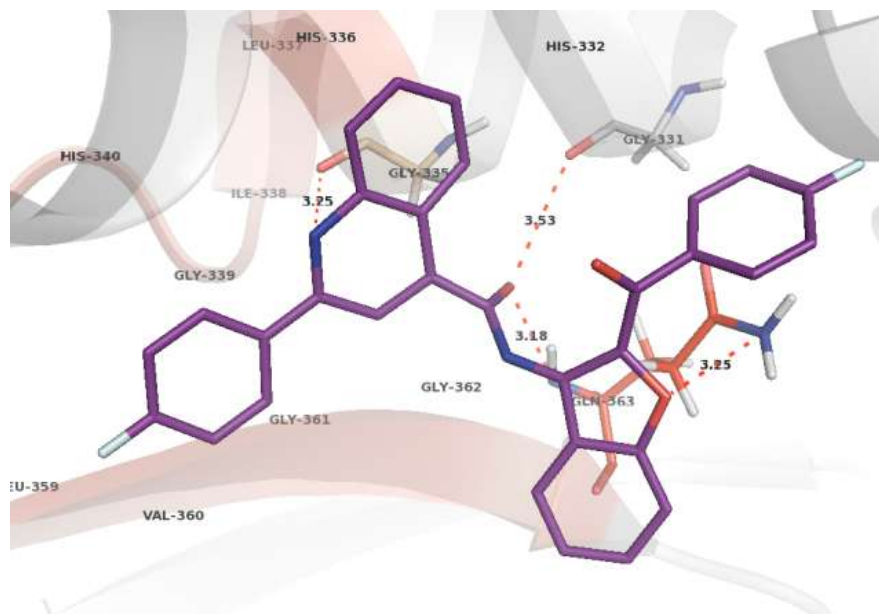


Figure 4.8: Docked Conformation of compound 3-122109 within IDE exosite. The exosite residues are shown as red. Hydrogen bonds are shown as red dashed lines.

The compound 3-122109 occupies partly the exosite region and makes polar interactions with one exosite residue, Gln³⁶³, and two other close ones, Gly³³¹ and Gly³³⁵. However this compound contains a furan ring which is toxic and may be carcinogenic; the O atom in the furan ring interacts with the Gln³⁶³. Additionally, high AMR and ALOGP values which are 137.725 and 7.158, respectively, have influences on this elimination procedure.

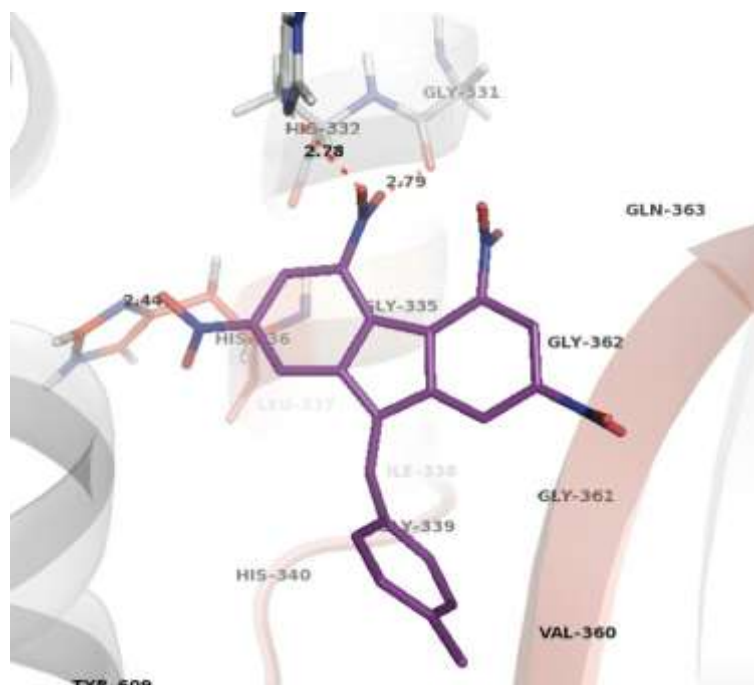


Figure 4.9: Docked Conformation of compound 1-16588 within IDE exosite. The exosite residues are shown as red. Hydrogen bonds are shown as red dashed lines.

Figure 4.9 shows the lowest-energy AutoDock conformation of the compound 1-16588 in the exosite of IDE. It has only three polar interactions between the O atoms of the nitrobenzene ring and amino acid residues Gly³³¹, His³³² and His³³⁶. Only His336 corresponds to the exosite region. Unfortunately, other nitrobenzene groups of the compound are not able to establish additional interactions; therefore the compound is free to rotate. The smaller value of the calculated docking energy might be the reason for this situation.

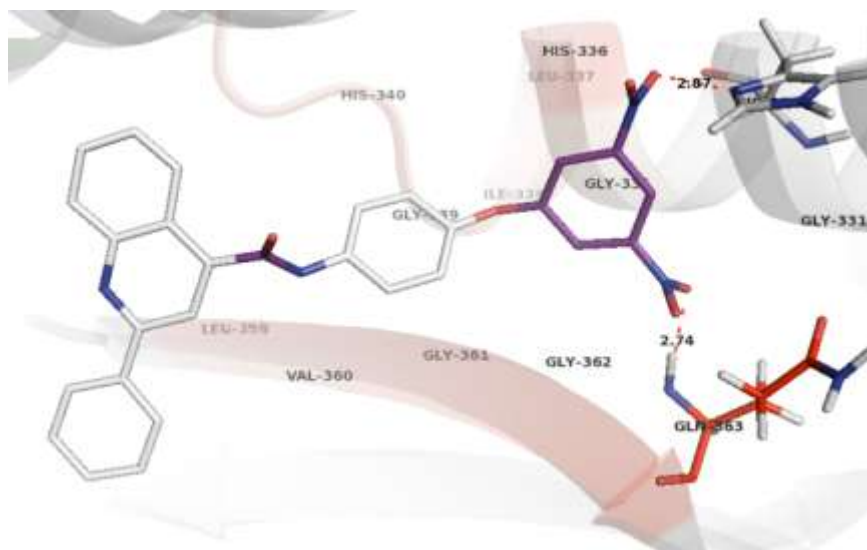


Figure 4.10: Docked Conformation of compound 8-141265 within IDE exosite. The exosite residues are shown as red. Hydrogen bonds are shown as red dashed lines.

The compound 8-141265 covers the whole exosite region by interacting one exosite and one other close residue; however only one terminal of this compound makes these polar interactions. Other part is therefore free to rotate which will then involve in the minimum docking energy. Besides, AMR and ALOGP values, 137.725 and 7.158, respectively, are found to be higher than limiting conditions.

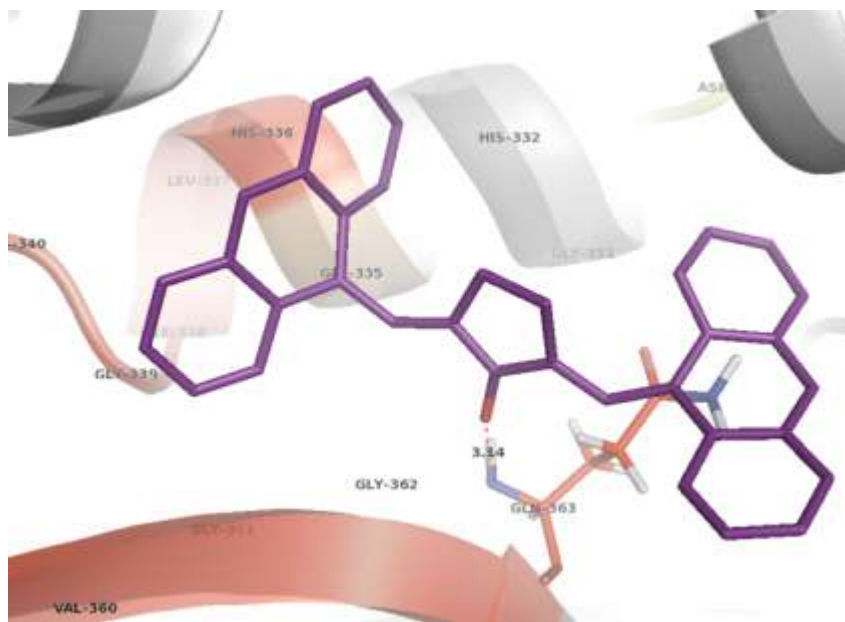


Figure 4.11: Docked Conformation of compound 3-116810 within IDE exosite. The exosite residues are shown as red. Hydrogen bonds are shown as red dashed lines.

The main reason behind the elimination of compound 3-116810 is its docking position which is a bit far from the exact exosite region. That is to say, it does not cover all the exosite residues. Other reason is that the AMR and ALOGP values exceed the limitation conditions with values of 149.74 and 8.175, respectively. All these reasons along with only one polar interaction with IDE caused the elimination of this compound.

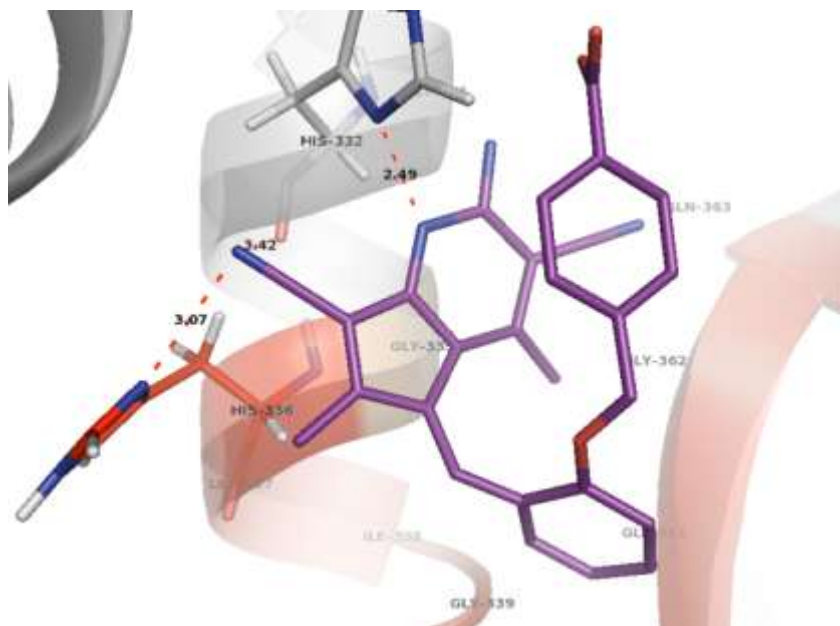


Figure 4.12: Docked Conformation of compound 5-108909 within IDE exosite. The exosite residues are shown as red. Hydrogen bonds are shown as red dashed lines.

The compound 5-108909 is eliminated particularly due to its docking position. This lead forms hydrogen bonding with one exosite residue, His³³⁶ and, His³³²; however due to high torsional freedom, one end of this compound is oriented to itself instead of sterically covering the exosite.

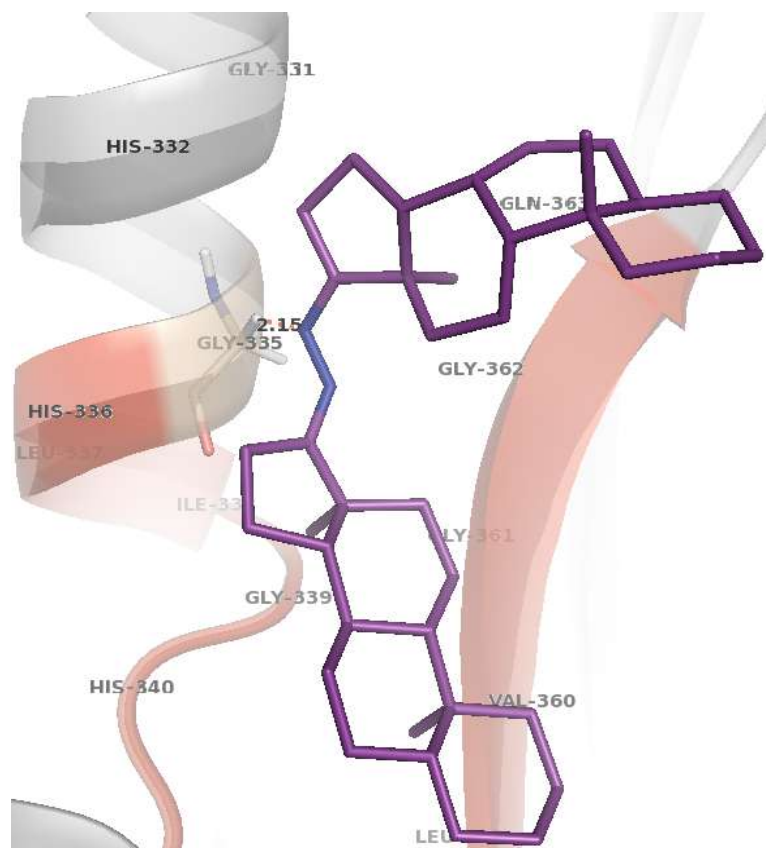


Figure 4.13: Docked Conformation of compound 1-168108 within IDE exosite. The exosite residues are shown as red. Hydrogen bonds are shown as red dashed lines.

The docking position shown in Figure 4.13 indicates that the compound 1-168108 is able to cover the exosite by forming polar interaction with only one residue, Gly³³⁵, which does not locate in the exosite region; however it is at the same α -helix segment. This low binding ability is resulted from the fact that this compound contains only two N atoms as reactive species. Other than these disadvantages, log P value is also extremely high.

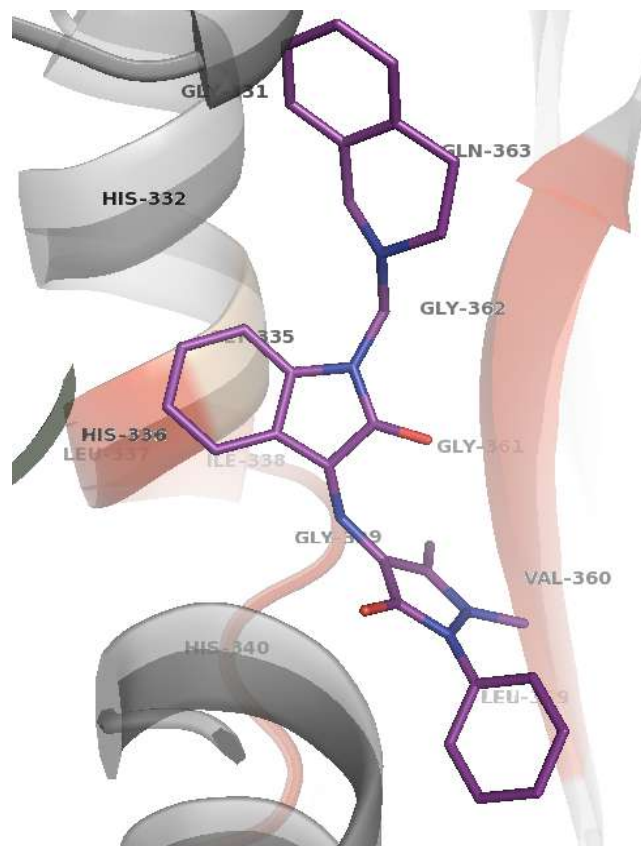


Figure 4.14: Docked Conformation of compound 9-1674 within IDE exosite. The exosite residues are shown as red. Hydrogen bonds are shown as red dashed lines.

As can be observed from Figure 4.14 that even though the compound 9-1674 has reasonably low binding and docking energies; no polar interactions are occurred with IDE residues. Except from AMR value, other physicochemical properties are acceptable for a drug candidate; however binding interactions are much more important than these drug-like properties. Therefore the compound 9-1674 is also eliminated.

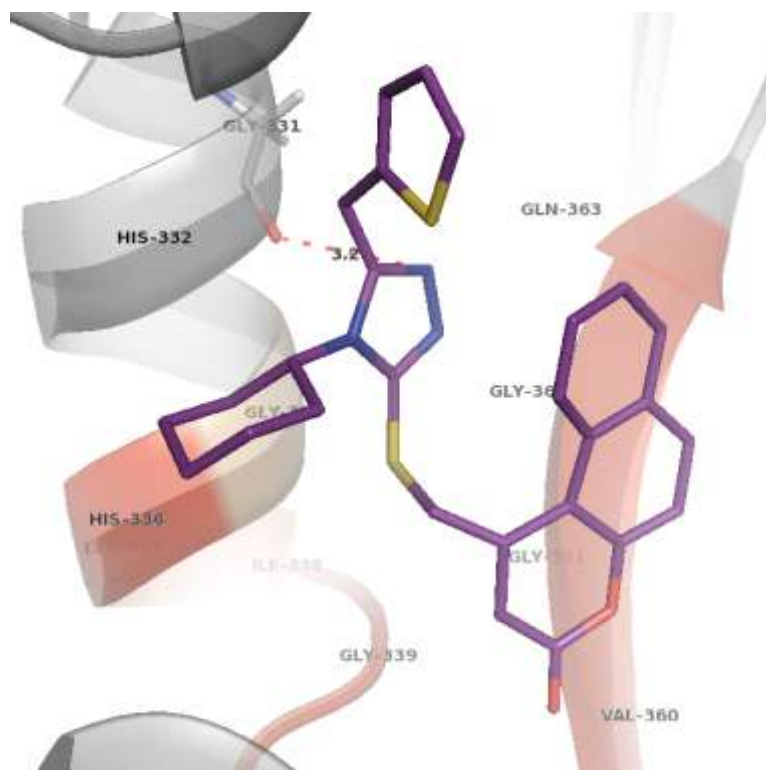


Figure 4.15: Docked Conformation of compound 2-12104 within IDE exosite. The exosite residues are shown as red. Hydrogen bonds are shown as red dashed lines.

In compound 2-12104, N atom of triazole ring form hydrogen bonding with O atom of Gly³³¹, and no other interaction has been observed. Even though it partially covers the exosite, this compound is also eliminated due to low binding interactions with IDE. Lower docking energy might come from high torsional freedom. AMR value of 141.385, and ALOGP value of 6.777 also exceed the limitations.

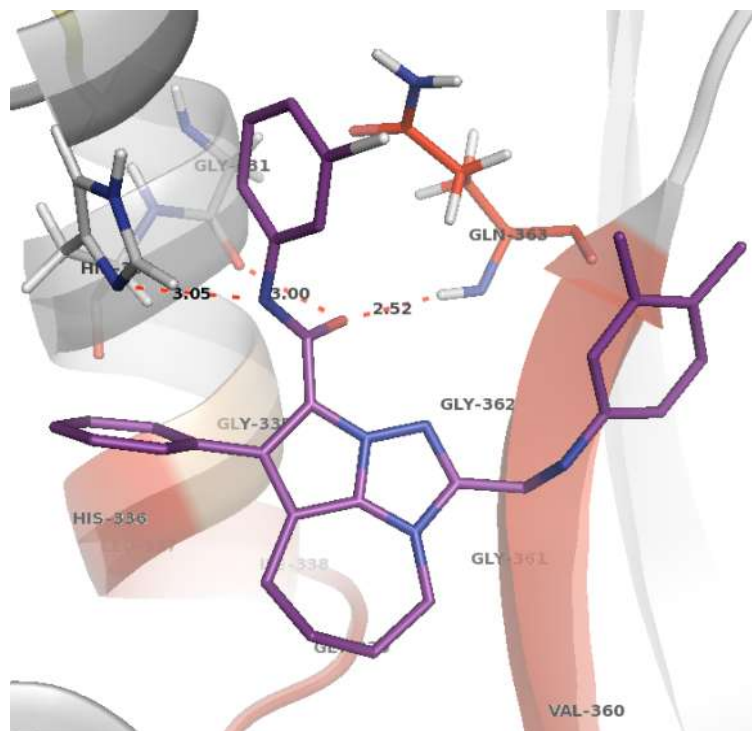


Figure 4.16: Docked Conformation of compound 1-102877 within IDE exosite. The exosite residues are shown as red. Hydrogen bonds are shown as red dashed lines.

The compound 1-102877 covers the upper part of the exosite region by interacting with one exosite residue, Gln³⁶³ and two other close residues, Gly³³¹, His³³². However, as can be seen from Figure 4.16 that these interactions are only governed by only one part of the compound, whereas the other part is unable to form any hydrogen bonding. Therefore, this docking position is unfavorable. In addition, high AMR and ALOGP values are also considered during this elimination period.

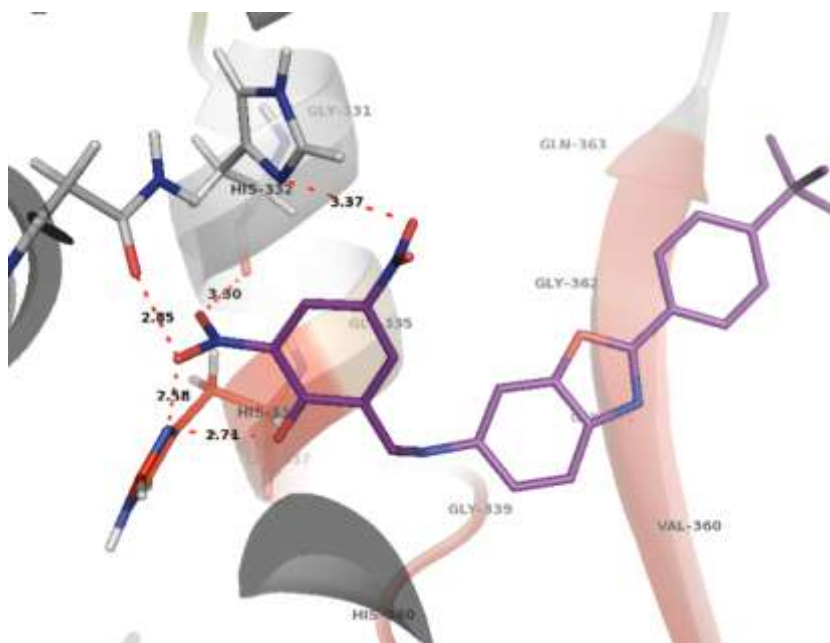


Figure 4.17: Docked Conformation of compound 1-11351 within IDE exosite. The exosite residues are shown as red. Hydrogen bonds are shown as red dashed lines.

Figure 4.17 illustrates the docking position of the compound 1-11351. Interactions with exosite residue His³³⁶ and two other residues, His³³² and Asn⁴¹⁸, that are located on the same α -helix segment with His³³⁶ and located on a close another α -helix segment, respectively, are only yielded by the O atoms at the one terminal of the compound. Therefore the other end is flexible which might end up binding to another side in the real biological environment. This uncertainty is the main cause of eliminating this compound. ALOGP value of this compound is found to be 5.799; this is higher than the limiting value which is 5.6, However if the docking position and binding interactions are acceptable, this slightly high value would be ignored.

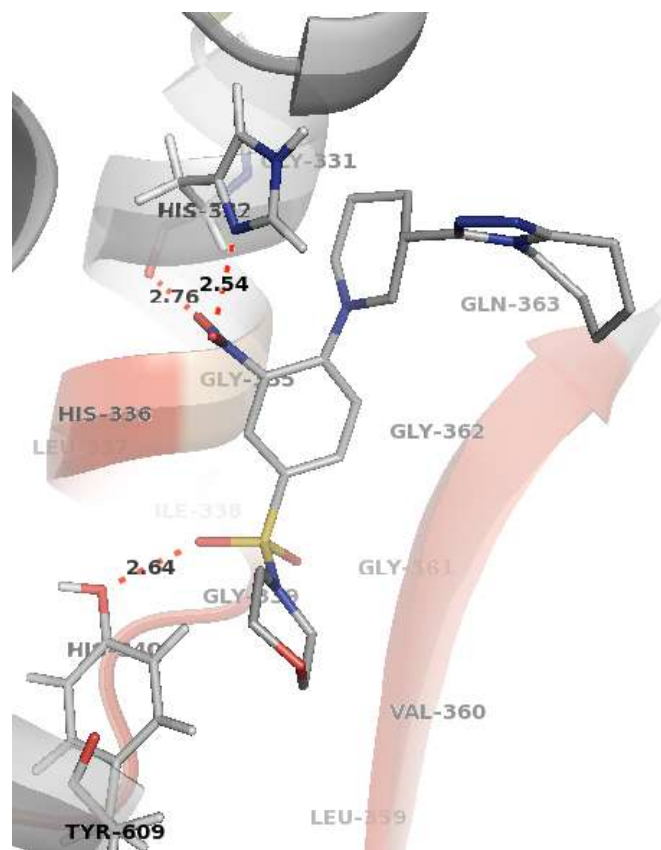


Figure 4.18: Docked Conformation of compound 1-180914 within IDE exosite. The exosite residues are shown as red. Hydrogen bonds are shown as red dashed lines.

The compound 1-180914 has only two polar interactions with IDE; however none of them locate in the exosite region. The end where triazole and benzene rings exist is slightly twisted; this indicates high torsional degrees of freedom of that end. However, it should have planar docking position. That is to say, the lack of polar interactions with exosite residues, and unusual docking position are the fundamental causes for the elimination of this compound.

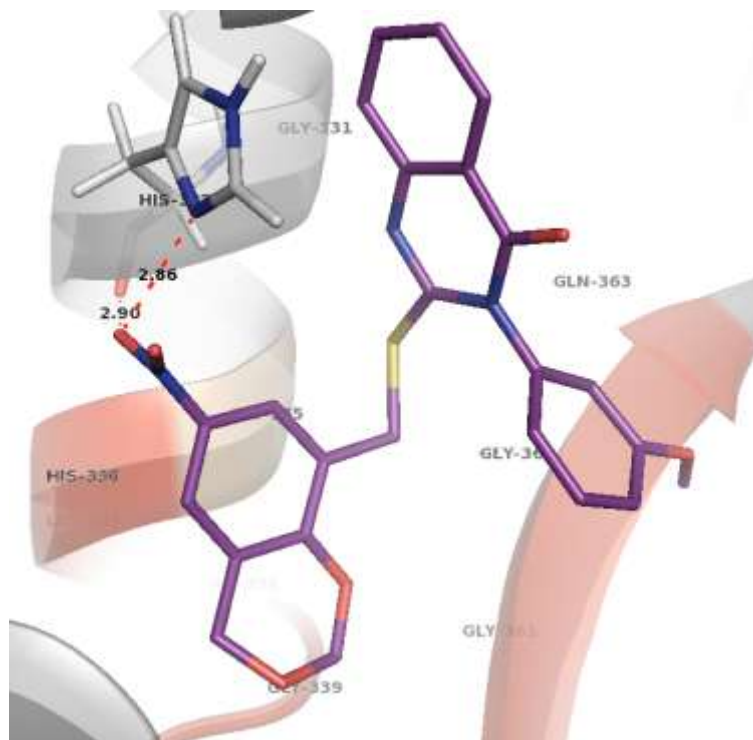


Figure 4.19: Docked Conformation of compound 9-102548 within IDE exosite. The exosite residues are shown as red. Hydrogen bonds are shown as red dashed lines.

As in the case for compound 1-180914, compound 9-102548 has only one polar interaction with IDE, His³³², and no other interactions with IDE exosite, which renders it unfavorable.

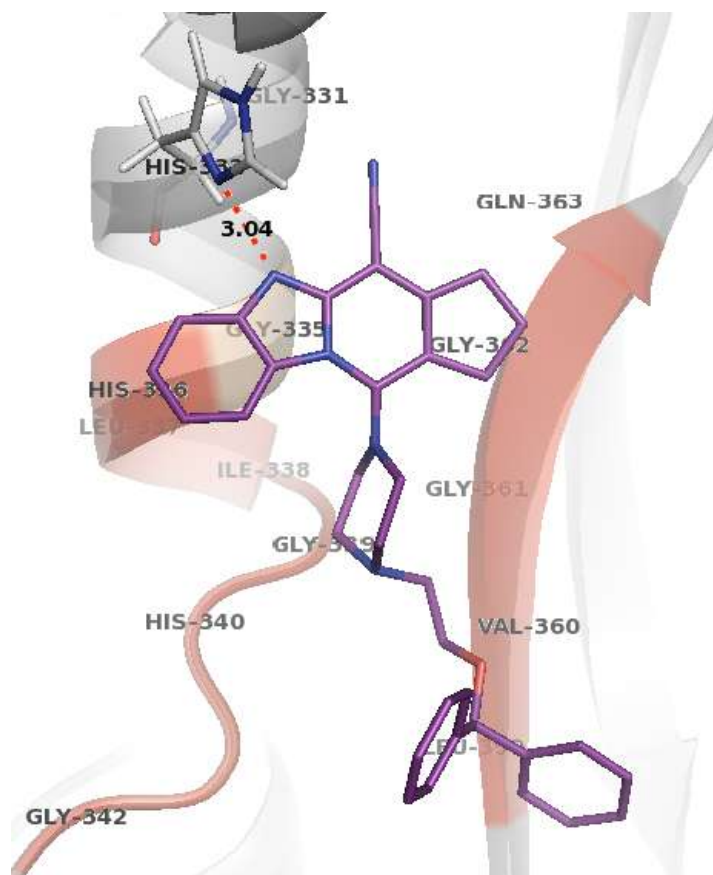


Figure 4.20: Docked Conformation of compound 4-131363 within IDE exosite. The exosite residues are shown as red. Hydrogen bonds are shown as red dashed lines.

All the physicochemical properties of the compound 4-131363 fit well for a drug like compound; however the sole polar interaction with the residue His³³² renders it inadequate for required selection criteria. The other end has no interactions with exosite residues which might end up binding to another side in the real biological environment.

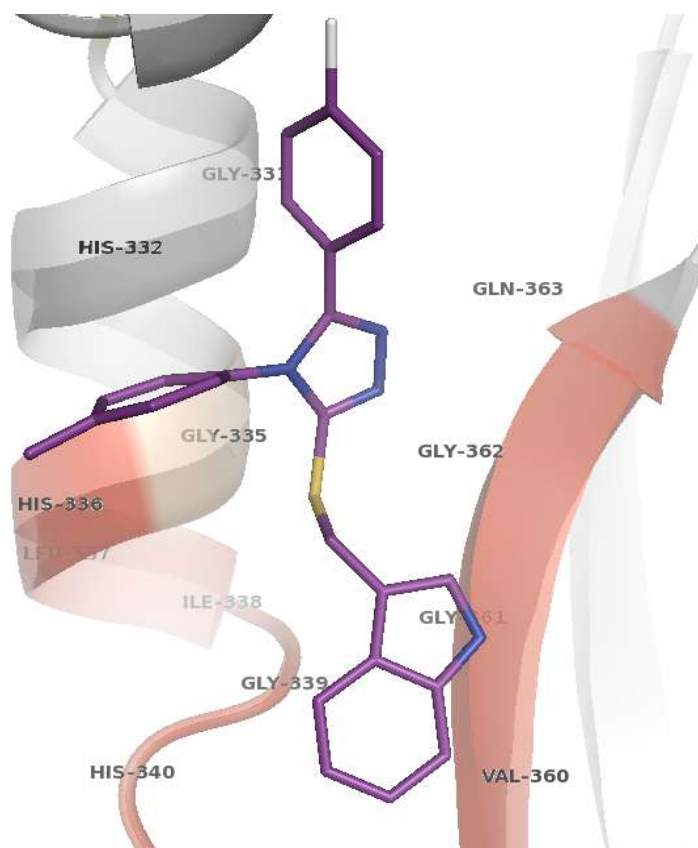


Figure 4.21: Docked Conformation of compound 4-100665 within IDE exosite. The exosite residues are shown as red. Hydrogen bonds are shown as red dashed lines.

The compound 4-100665 has no valid polar interaction with IDE residues at the exosite or any other part. Regardless of its drug-like properties, it is eliminated due to this unfavorable docking pattern.

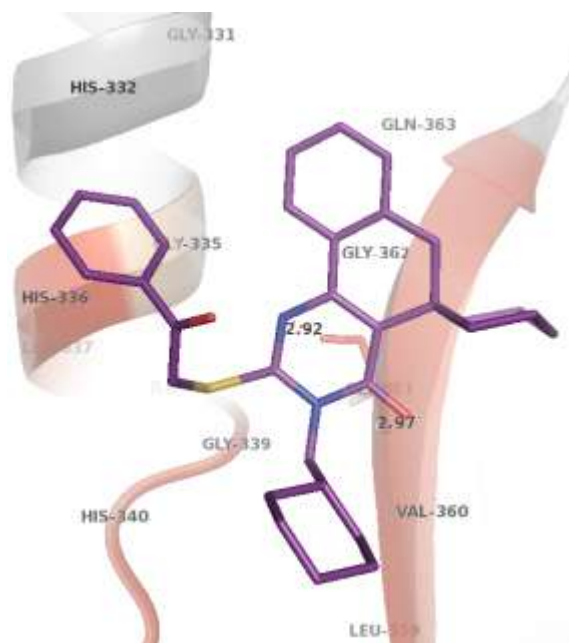


Figure 4.22: Docked Conformation of compound 1-11207 within IDE exosite. The exosite residues are shown as red. Hydrogen bonds are shown as red dashed lines.

The compound 1-11207 has one polar interaction with Gly³⁶¹, which belongs to exosite region. It has 152.414, 6.353 and 73 for AMR, ALOGP and NAT values, respectively. All these values exceed the limits. Few interactions both with exosite and other parts in the enzyme, and higher physicochemical properties than for a normal drug molecule, all cause this compound to be eliminated from the selection list.

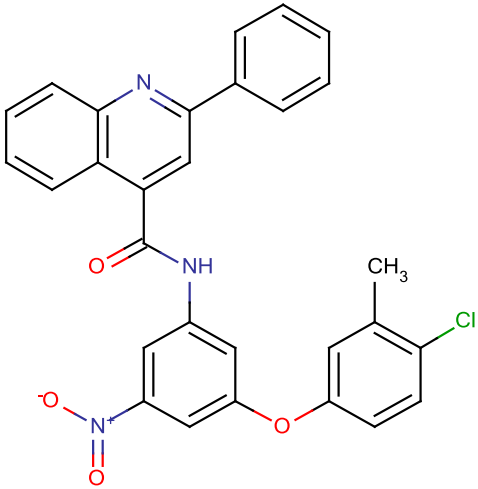
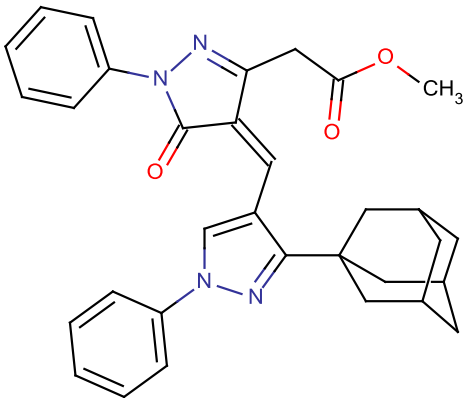
Using this filtering process and visual checking, 18 out of the 38 compounds from the initial ranking list were removed. A list for top 20 compounds with estimated binding and docking energies in both virtual screening and detailed docking were given in Table 4.5. As can be seen, binding and docking energy values of detailed docking were higher than those of the virtual screening, which was found to be reasonable due to the increased resolution of the grid maps.

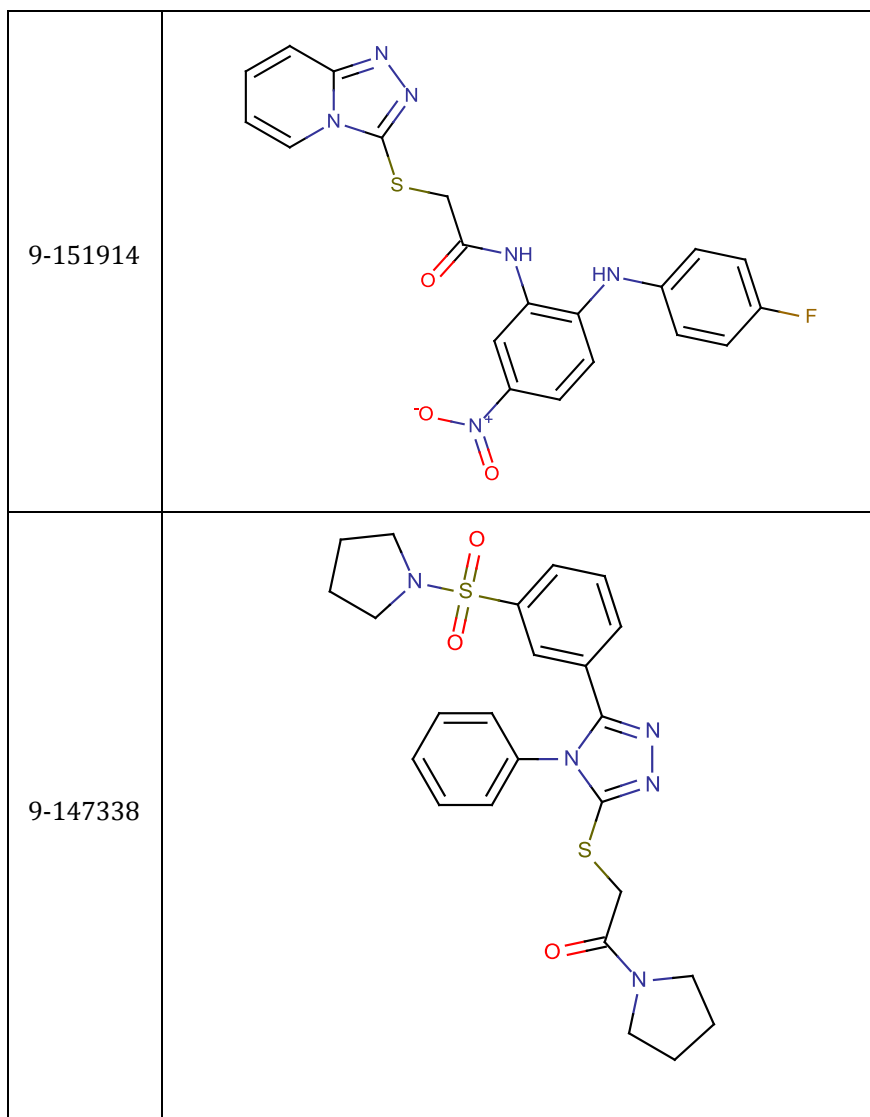
Table 4.5: IDE regulation of compounds selected from Ambinter Compound Library that showed effective binding and docking scores in virtual screening and detailed docking.

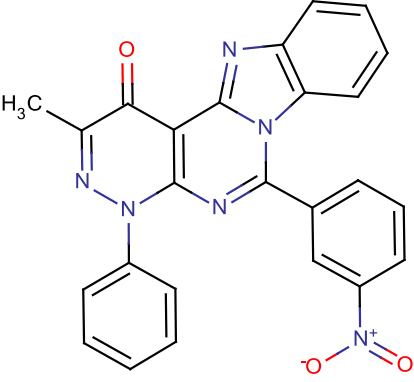
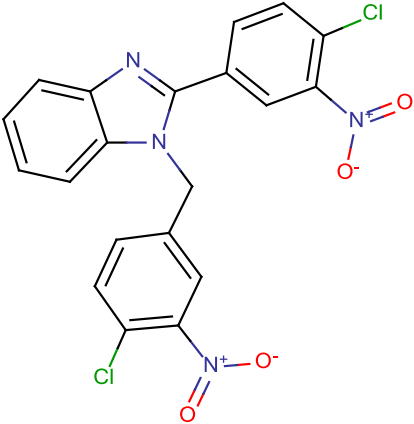
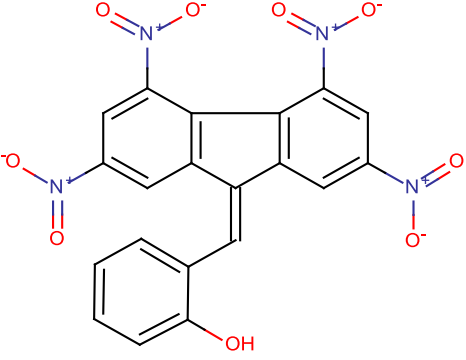
| COMPOUND ID | VIRTUAL SCREENING | | DETAILED DOCKING | | INTERACTIONS |
|-------------|---------------------------|---------------------------|---------------------------|---------------------------|---|
| | BINDING ENERGY (KCAL/MOL) | DOCKING ENERGY (KCAL/MOL) | BINDING ENERGY (KCAL/MOL) | DOCKING ENERGY (KCAL/MOL) | |
| 8-141267 | -10.64 | -11.97 | -12.99 | -14.89 | His ³³² , His ³³⁵ , His ³³⁶ , Gly ³⁶¹ |
| 8-171299 | -11.34 | -14.14 | -12.22 | -14.9 | Gly ³³¹ , His ³³² , Gln ³⁶³ |
| 9-151914 | -10.92 | -13.6 | -12.18 | -15.26 | Asn ³²⁹ , Gly ³³¹ , His ³³² , His ³³⁶ , Gly ³⁶¹ , Gln ³⁶³ , Asn ⁴¹⁸ |
| 9-147338 | -9.71 | -13.85 | -12.06 | -15.14 | Gly ³³⁹ , Gly ³⁶¹ , Gln ³⁶³ |
| 3-114154 | -11.48 | -11.11 | -11.84 | -11.54 | His ³³² , Gln ³⁶³ |
| 9-14137 | -11.08 | -12.67 | -11.77 | -14.23 | His ³³² , Gly ³⁶¹ , Gln ³⁶³ |
| 1-16593 | -10.86 | -13.24 | -11.76 | -14.06 | Gly ³³¹ , His ³³² , His ³³⁶ , Gly ³³⁹ , Gly ³⁶¹ , Gln ³⁶³ , Tyr ⁶⁰⁹ |
| 9-151856 | -10.57 | -13.2 | -11.57 | -13.95 | His ³³² , Gly ³³⁹ , Gln ³⁶³ , Tyr ⁶⁰⁹ |
| 3-113780 | -11.26 | -12.17 | -11.57 | -12.58 | His ³³⁶ , Gly ³⁶¹ , Asn ⁴¹⁸ |
| 4-135627 | -10.45 | -12.19 | -11.55 | -11.26 | Gly ³⁶¹ |
| 9-1573 | -10.89 | -12.72 | -11.44 | -13.24 | His ³³² , His ³³⁵ , His ³³⁶ , Gly ³⁶¹ |
| 3-137443 | -10.6 | -13.43 | -11.31 | -14.26 | Gly ³³¹ , His ³³⁵ , Gln ³⁶³ |
| 9-134343 | -10.85 | -12.52 | -11.22 | -12.89 | Asn ³²⁹ , His ³³² , His ³³⁵ , Gly ³⁶¹ , Gln ³⁶³ , Tyr ³³³ , Tyr ⁴⁴⁴ , Tyr ⁶⁰⁹ |
| 1-180918 | -10.3 | -11.99 | -11.22 | -12.58 | Gly ³⁶¹ , Gln ³⁶³ , Glu ⁴⁵³ |
| 8-456 | -9.59 | -12.17 | -11.18 | -13.59 | Gly ³³¹ , His ³³⁵ , Gly ³³⁹ , Glu ³⁴¹ , Gly ³⁶¹ |
| 3-110732 | -10.47 | -12.76 | -11.16 | -13.15 | His ³³⁵ , Gly ³³⁹ , Gly ³⁶¹ , Gln ³⁶³ , Tyr ⁶⁰⁹ |
| 4-106854 | -9.16 | -10.96 | -11.13 | -14.77 | Gly ³³¹ , His ³³⁶ , Glu ³⁴¹ , Val ³⁶⁰ , Gln ³⁶³ |
| 3-114848 | -9.37 | -10.71 | -11.13 | -13.11 | His ³³⁶ , Gly ³⁶¹ , Glu ⁴⁵³ , Tyr ⁶⁰⁹ |

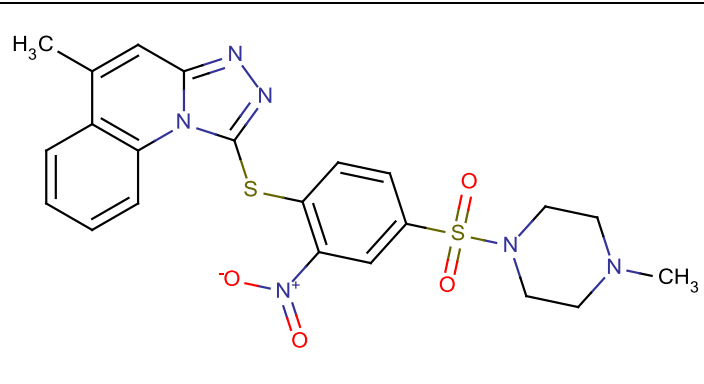
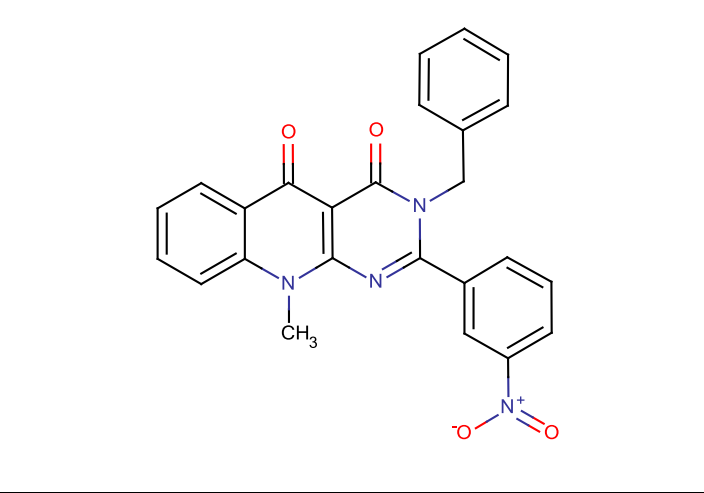
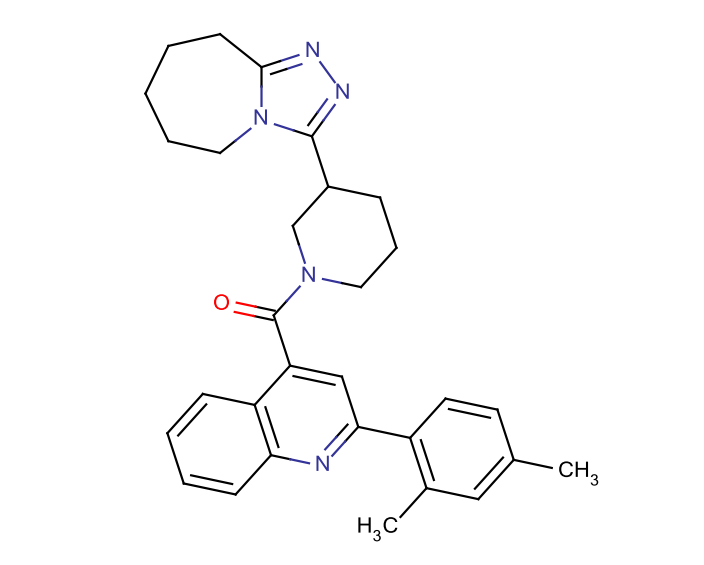
| | | | | | |
|----------|--------|--------|--------|--------|--|
| 2-114522 | -10.62 | -11.94 | -11.08 | -12.45 | Gly ³³¹ , His ³³⁵ , His ³³⁶ , Gln ³⁶³ |
| 1-11728 | -10.02 | -11.59 | -11.01 | -12.33 | His ³³² , His ³³⁶ , Gly ³³⁹ , Gly ³⁶¹ , Asn ⁴¹⁸ , Tyr ⁶⁰⁹ |

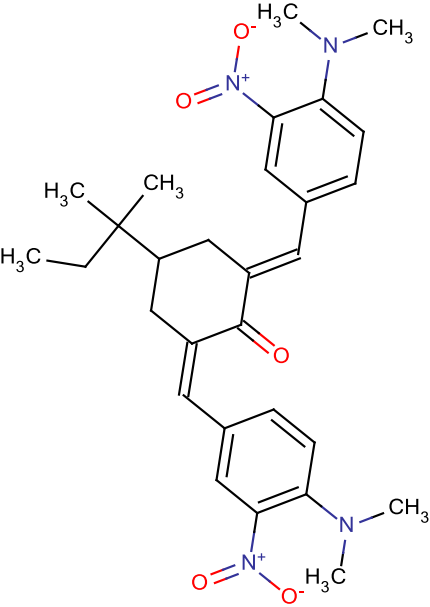
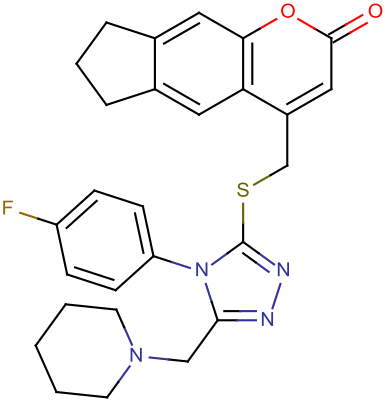
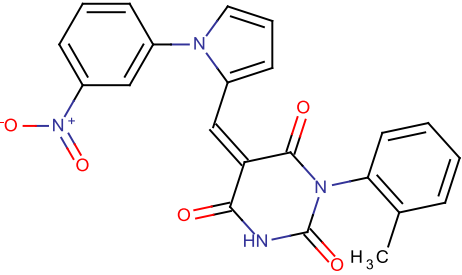
Table 4.6: 2D Structures of the selected candidates.

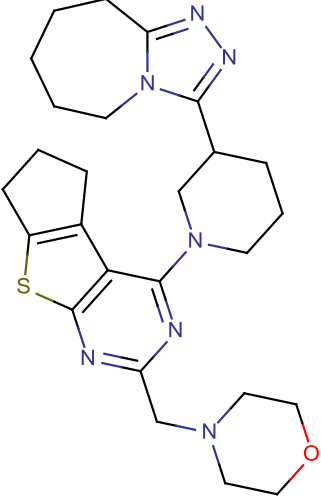
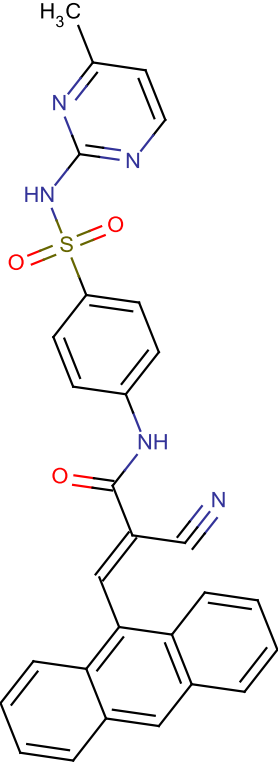
| COMPOUND ID | 2D-STRUCTURE |
|-------------|--|
| 8-141267 |  |
| 8-171299 |  |

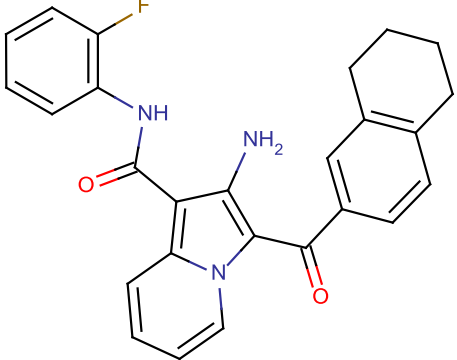
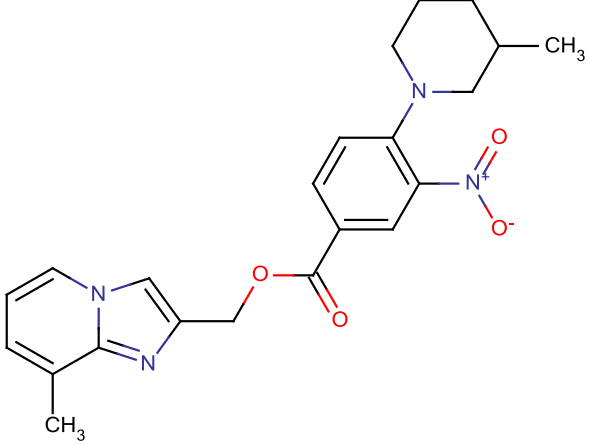
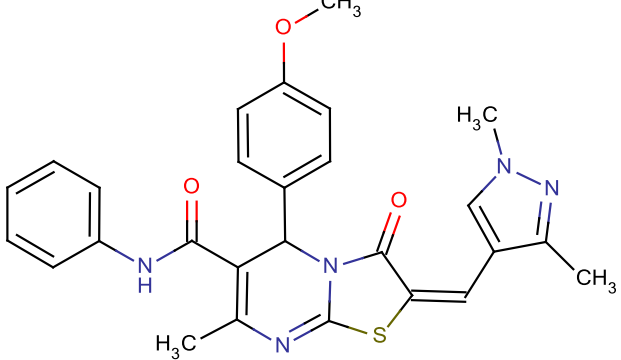


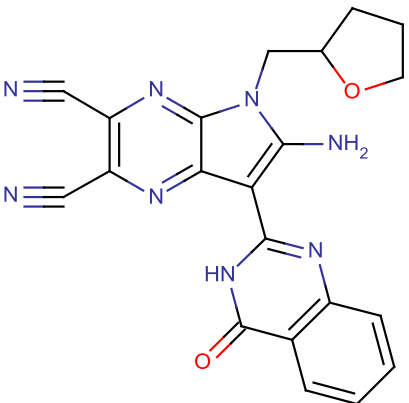
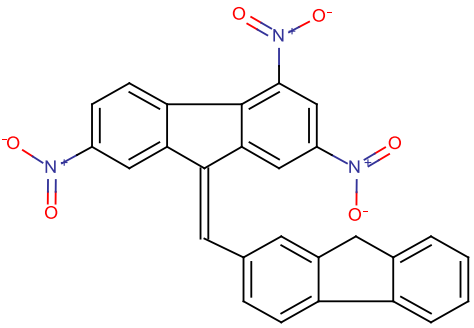
| | |
|----------|--|
| 3-114154 |  |
| 9-14137 |  |
| 1-16593 |  |

| | |
|----------|--|
| 9-151856 |  <p>Chemical structure of compound 9-151856. It features a benzimidazole ring system with a methyl group (H₃C) at the 2-position. The benzimidazole is linked via its sulfur atom to a benzene ring. This benzene ring is substituted with a nitro group (NO₂) at the 3-position and a methanesulfonyl group (SO₂) at the 4-position. The methanesulfonyl group is further linked to a piperidine ring with a methyl group (CH₃) on the nitrogen atom.</p> |
| 3-113780 |  <p>Chemical structure of compound 3-113780. It consists of a pyrimidopyrimidinone bicyclic core. The core has a methyl group (CH₃) on one of the nitrogen atoms and a carbonyl group (C=O) at the 2-position. The 4-position of the core is substituted with a benzyl group (CH₂-C₆H₅) and a 4-nitrophenyl group (C₆H₄-NO₂).</p> |
| 4-135627 |  <p>Chemical structure of compound 4-135627. It features a benzimidazole ring system where the nitrogen atom is part of a bicyclic system fused to a seven-membered ring. The benzimidazole is linked via its sulfur atom to a piperidine ring. The piperidine ring is further linked to a pyridine ring, which is substituted with a carbonyl group (C=O) at the 2-position and a 3,5-dimethylphenyl group (C₆H₃(CH₃)₂) at the 4-position.</p> |

| | |
|----------|--|
| 9-1573 |  <p>Chemical structure 9-1573: A complex molecule featuring a central six-membered ring with a carbonyl group and two exocyclic double bonds. One double bond is attached to a 4-(dimethylamino)phenyl group, and the other is attached to a 2-(dimethylamino)phenyl group. A tert-butyl group is also attached to the six-membered ring.</p> |
| 3-137443 |  <p>Chemical structure 3-137443: A complex molecule featuring a central benzimidazole ring system. One nitrogen is substituted with a piperidine ring, and the other with a 4-fluorophenyl group. A sulfur atom is attached to the benzimidazole ring, which is further connected to a fused bicyclic system consisting of a benzene ring and a five-membered ring containing an oxygen atom and a carbonyl group.</p> |
| 9-134343 |  <p>Chemical structure 9-134343: A complex molecule featuring a central six-membered ring with a carbonyl group and two exocyclic double bonds. One double bond is attached to a 4-(dimethylamino)phenyl group, and the other is attached to a 2-(dimethylamino)phenyl group. A tert-butyl group is also attached to the six-membered ring.</p> |

| | |
|----------|---|
| 1-180918 |  <p>Chemical structure of compound 1-180918, featuring a central benzimidazole ring system. The benzimidazole is substituted with a 7-membered azepane ring, a 6-membered piperidine ring, and a 6-membered morpholine ring. A sulfur atom is also present in the structure.</p> |
| 8-456 |  <p>Chemical structure of compound 8-456, featuring a central benzimidazole ring system. The benzimidazole is substituted with a 4-methylpyridin-2-ylamino group, a sulfonamide group, and a cyano group. The structure also includes a benzene ring and a naphthalene-like fused ring system.</p> |

| | |
|----------|--|
| 3-110732 |  |
| 4-106854 |  |
| 3-114848 |  |

| | |
|----------|---|
| 2-114522 |  <p>The chemical structure of compound 2-114522 features a central imidazole ring. At the 2-position of the imidazole, there is a 1,2,4-triazole ring substituted with two cyano groups (-C≡N). At the 4-position of the imidazole, there is a 2-aminoethyl group (-CH₂CH₂NH₂). At the 5-position of the imidazole, there is a 2-oxo-1H-benzimidazole ring system. The nitrogen atom of the imidazole ring is substituted with a tetrahydrofuran ring.</p> |
| 1-11728 |  <p>The chemical structure of compound 1-11728 consists of a central benzimidazole ring system. The benzimidazole core is substituted with three nitro groups (-NO₂) at the 2, 4, and 6 positions. A styryl group (-CH=CH-C₆H₄-) is attached to the 5-position of the benzimidazole ring, where the phenyl ring of the styryl group is fused to an indole ring system.</p> |

4.3.3. Computational analysis of the novel compounds

According to the AutoDock energy calculations and ligand conformations, all molecules favorably and sterically fit into the IDE exosite with multiple polar interactions. Most of the hits make at least one hydrogen bond with the exosite residues of IDE.

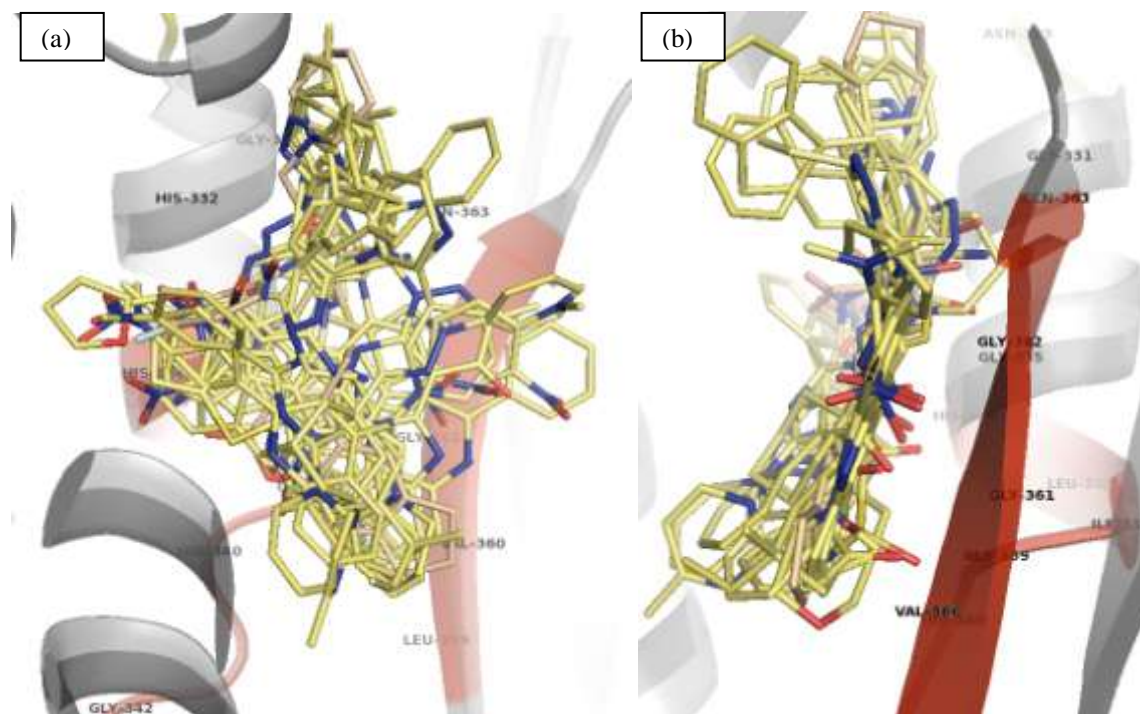


Figure 4.23: Selected IDE regulators (light yellow sticks colored by elements; blue for N, red for O, white for H atoms) at the exosite (red cartoon) (a) front view, (b) side view.

As can be seen from Figure 4.23, the top ranked compounds show several common motifs; docking positions at the exosite, having reactive species as O and N atoms that locate generally at the same part of exosite. Apart from the common motifs, it should also be noted that the compounds shown in Figure 4.23 and Table 4.6 are structurally diverse; therefore each of them can be considered as new basis in order to further improve by optimization studies.

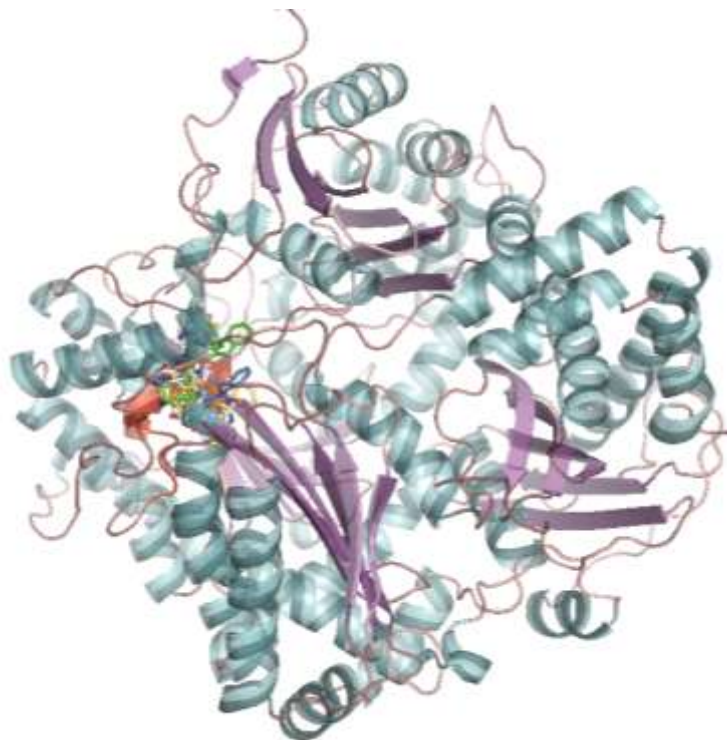


Figure 4.24: The structure of IDE catalytic chamber and selected representative compounds (colorful sticks) docked to the IDE exosite (red cartoon).

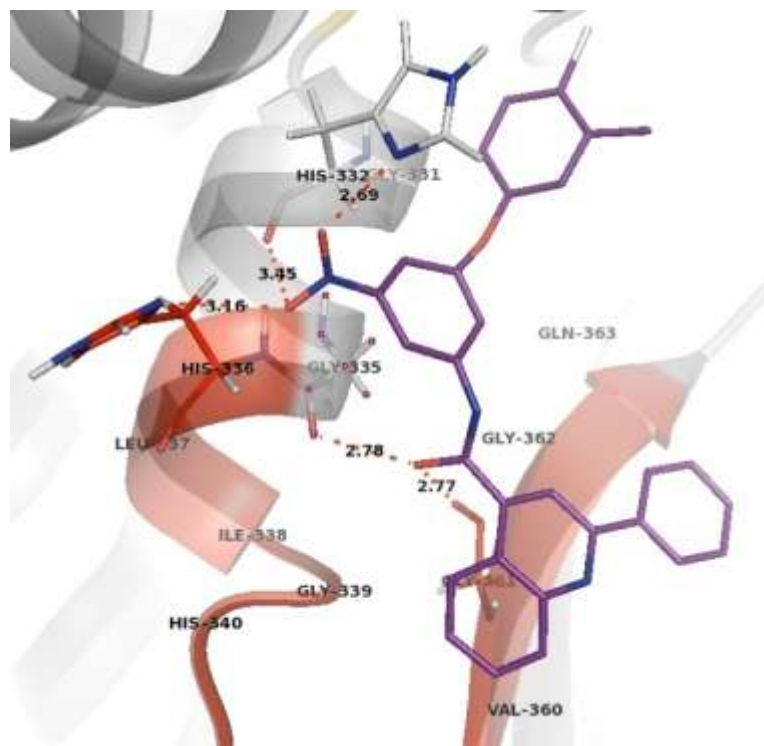


Figure 4.25: Docked Conformation of compound 8-141267 within IDE exosite. The exosite residues are shown as red. Hydrogen bonds are shown as red dashed lines.

The calculated binding mode of compound 8-141267 in the exosite of IDE is shown in Figure 4.25. The docking position shows that, this new candidate covers the exosite by interacting with four IDE amino acids; two of them belong to the exosite region. Two of the required physicochemical properties, 141.41 and 7.353 for AMR and ALOGP values, respectively, are quite higher than those of a drug-like compound; however the lower binding and docking energies render this compound as a potential candidate.

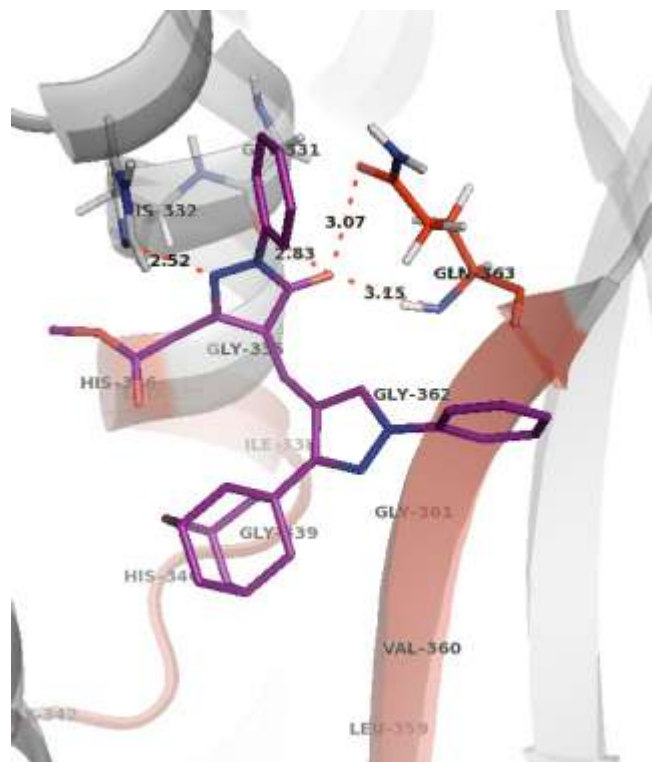


Figure 4.26: Docked Conformation of compound 8-171299 within IDE exosite. The exosite residues are shown as red. Hydrogen bonds are shown as red dashed lines.

The calculated binding mode of compound 8-171299 shows that polar interactions with one exosite residue and two other closer residues are responsible for its higher rank with minimum docking and binding energy scores. It can be seen that the oxygen atom that is connected to pyrazole ring accepts hydrogen bonds from the side chains of Gln³⁶³ and Gly³³¹. One of the nitrogen atoms of the pyrazole ring also forms a hydrogen bond with His³³². Unfortunately, some physicochemical properties of this candidate are higher than those of a drug-like compound. Even though the upper limit of number of atoms that should exist is said to be 70, AMR is 130 and ALOGP value is +5.6, the calculated values are as follows; 71, 149.45, and 5.996, respectively. It can be noticed that these values

higher than the reference values can be neglected with respect to minimum binding and docking energy scores of the compound, and its docking position at the exosite with multiple polar interactions. Even though these physicochemical properties are important for oral bioavailability, the foremost important step is the discovery of candidates.

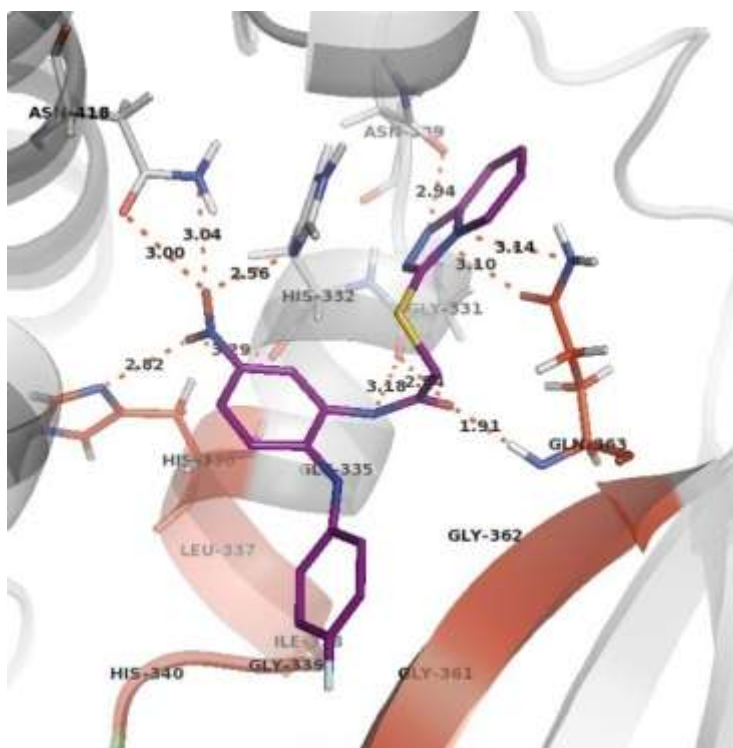


Figure 4.27: Docked Conformation of compound 9-151914 within IDE exosite. The exosite residues are shown as red. Hydrogen bonds are shown as red dashed lines.

Figure 4.27 shows the lowest-energy AutoDock conformation of the compound 9-151914 in the exosite of IDE. Two N atoms in the triazole ring make polar interactions with Asn³²⁹ and Gln³⁶³. Other than these, two O atoms of the nitrobenzene group both accept and donate hydrogen bonds from and to His³³² and Asn⁴¹⁸; while one of the O atoms donates one to His³³⁶. Besides, carboxylic O atom of Gly³³¹ donates another

hydrogen bond to the candidate molecule. Moreover, the physicochemical properties that this compound possesses are suitable for a drug-like compound.

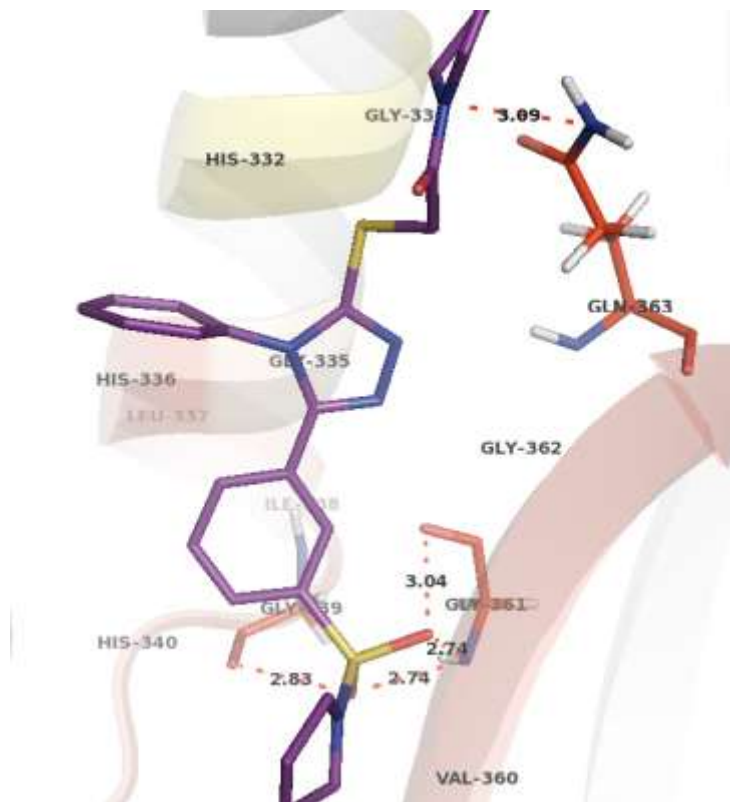


Figure 4.28: Docked Conformation of compound 9-147338 within IDE exosite. The exosite residues are shown as red. Hydrogen bonds are shown as red dashed lines.

In the cocrystal structure shown in Figure 4.28, several exosite amino acid residues interact with the regulatory compound 9-147338. Exosite residues Gly³³⁹, Gly³⁶¹ and Gln³⁶³ are predicted to give hydrogen bonds to this candidate molecule. These residues are believed to contribute to the catalytic action of IDE. In addition to that, high number of O-H-O bond than N-H-N one provides better stability; due to the fact that the former is

stronger than the latter. The sole negative physicochemical property is its higher AMR value, 136.77, than the limiting value, 130,.

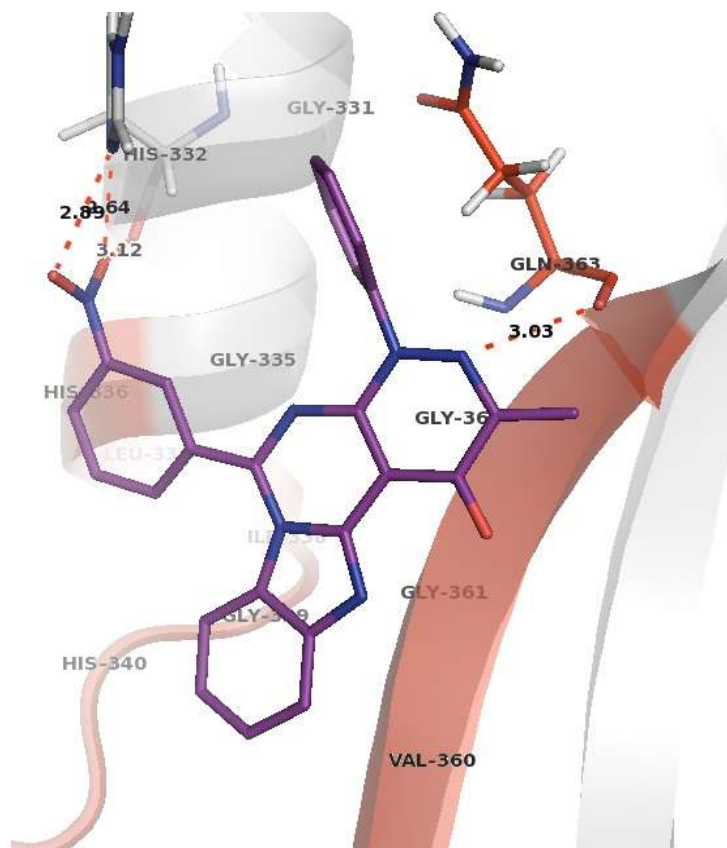


Figure 4.29: Docked Conformation of compound 3-114154 within IDE exosite. The exosite residues are shown as red. Hydrogen bonds are shown as red dashed lines.

Figure 4.29 shows the predicted orientation of the identified hit, 3-114154, on the exosite. It has two interactions with IDE; one is the exosite residue, Gln³⁶³. An important electrostatic bond exists between one of the N atoms of the pyridazine ring and the O atom of the Glu³⁶³. Additionally, terminal COOH group of compound interacts with His³³² which locates at the same helix segment of the exosite region. The minimum binding and docking

energies, docking position covering the exosite, and the optimum physicochemical properties render this compound favorable.

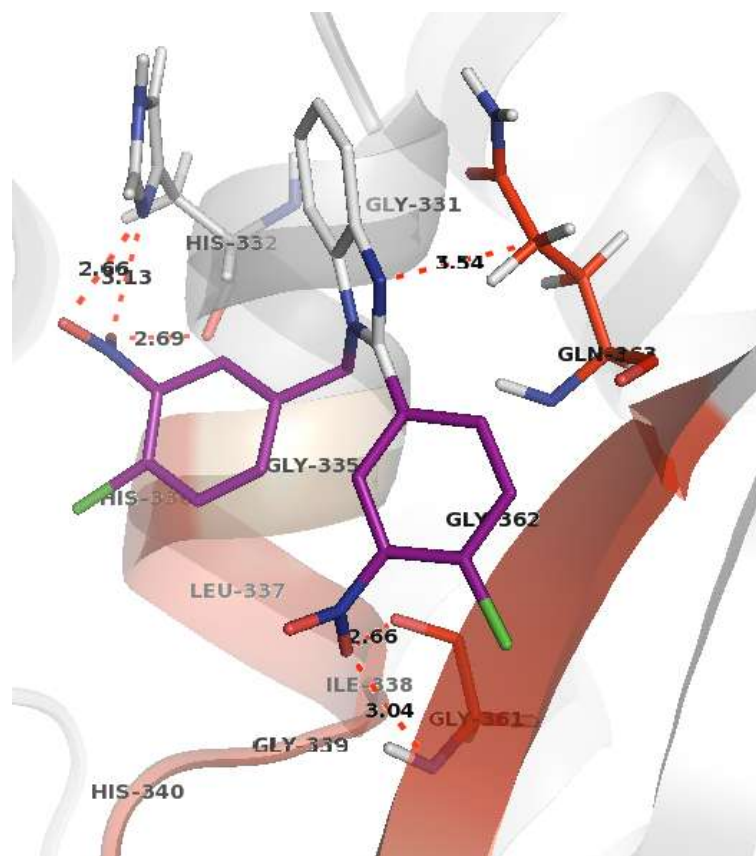


Figure 4.30: Docked Conformation of compound 9-14137 within IDE exosite. The exosite residues are shown as red. Hydrogen bonds are shown as red dashed lines.

The docking result, illustrated in Figure 4.30, indicated that the compound is found to dock well and established interactions with important amino acid residues of IDE exosite. N atom of the benzimidazole ring forms polar interaction with Gln³⁶³; and the nitrobenzene groups of the compound also interact with residues His³³² and Gly³⁶¹. The physicochemical features, except ALOGP which is found as 6.178, obey the drug-like compound properties.

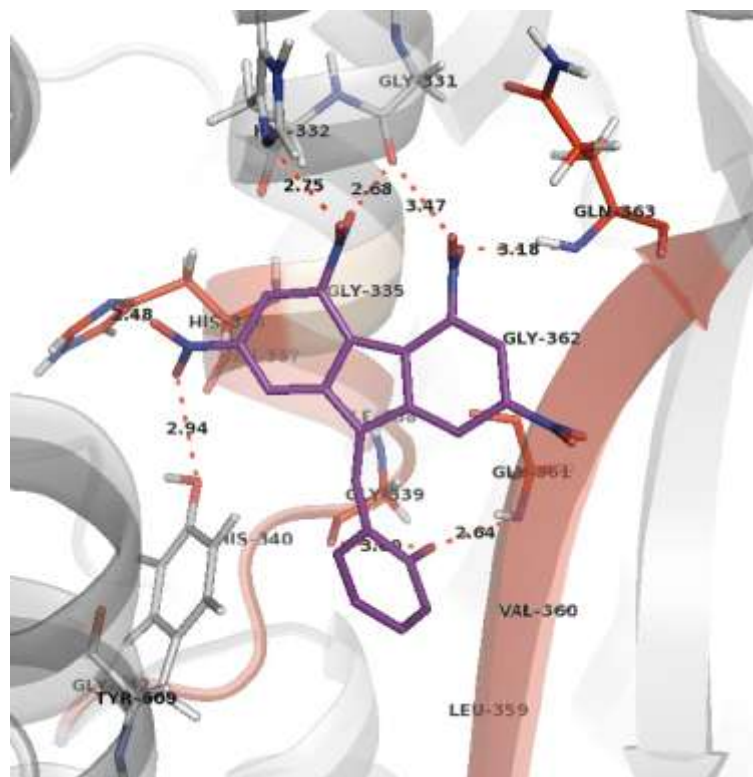


Figure 4.31: Docked Conformation of compound 1-16593 within IDE exosite. Interactions with the exosite of IDE. The exosite residues are shown as red. Hydrogen bonds are shown as red dashed lines.

The nitrobenzene groups of the compound interact with residues Gly³³¹, His³³², His³³⁶, Gln³⁶³ and Tyr⁶⁰⁹. The phenolic oxygen of the compound is hydrogen bonded to the exosite residues of Gly³⁶¹ and Gln³³⁹. There are totally seven polar interactions with IDE residues where four of them locate in the exosite region. This binding mode and optimum drug-like properties render this compound favorable as an IDE regulator.

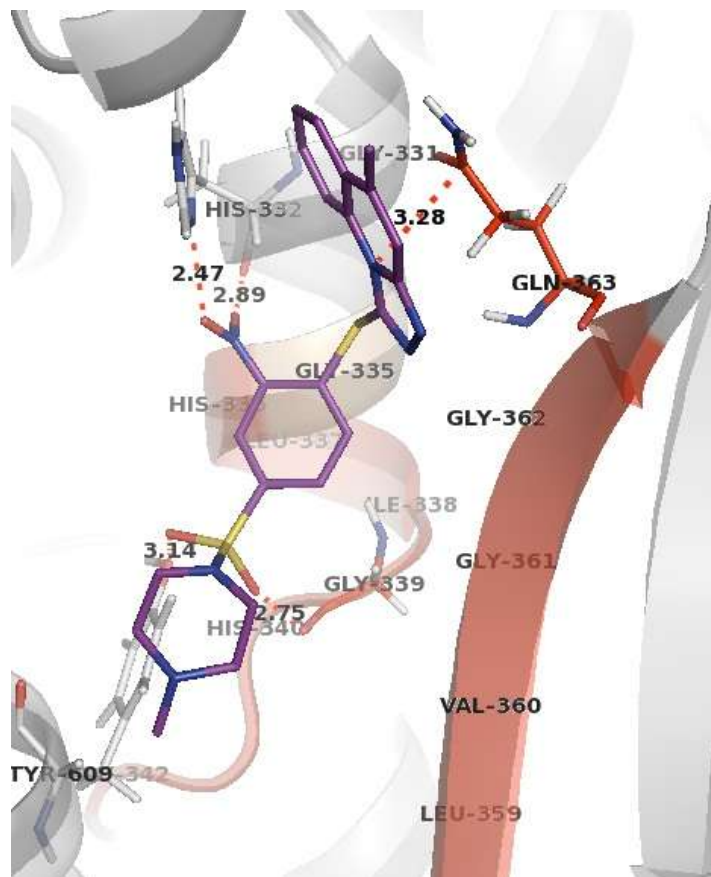


Figure 4.32: Docked Conformation of compound 9-151856 within IDE exosite. Interactions with exosite of IDE. The exosite residues are shown as red. Hydrogen bonds are shown as red dashed lines.

The representative docked conformation of the compound 9-151856 is shown in Figure 4.32. This candidate is able to occupy the exosite region by establishing polar interactions. Residues His³³², Gly³³⁹ and Tyr⁶⁰⁹ are found to donate hydrogen bonds with the candidate molecule. Additionally, N atom of the pyridine ring is hydrogen bonded to the exosite residue of Gln³⁶³. The calculated AMR value, 133.992, is nonetheless quite higher than the limiting value, 130.

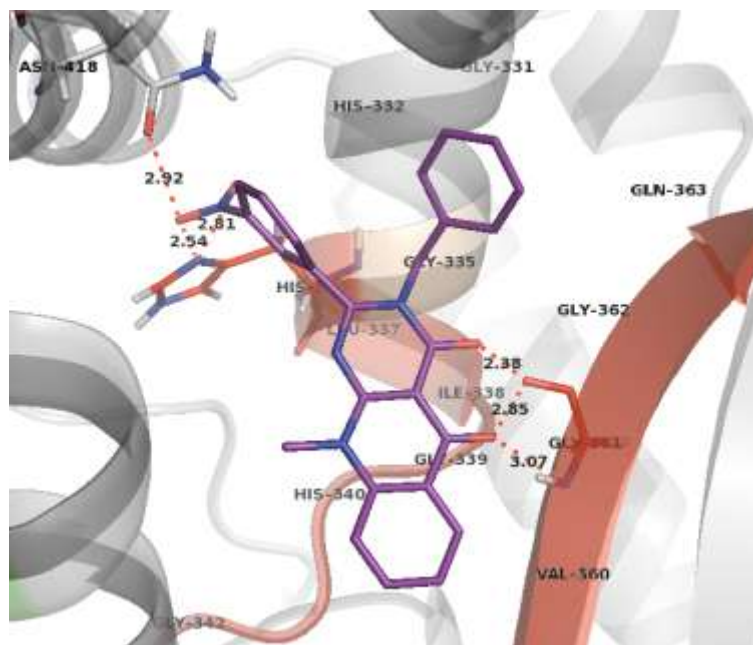


Figure 4.33: Docked Conformation of compound 3-113780 within IDE exosite. The exosite residues are shown as red. Hydrogen bonds are shown as red dashed lines.

As can be seen from the docked conformation illustrated in Figure 4.33, the compound 3-113780 occupies the exosite by interacting with several IDE residues. His³³⁶ is predicted to accept hydrogen bonds; whereas the residues Gly³⁶¹ and Asn⁴¹⁸ donate hydrogen bonds to the candidate molecule. Another important point to note is that all the physicochemical properties are within accepted limits.

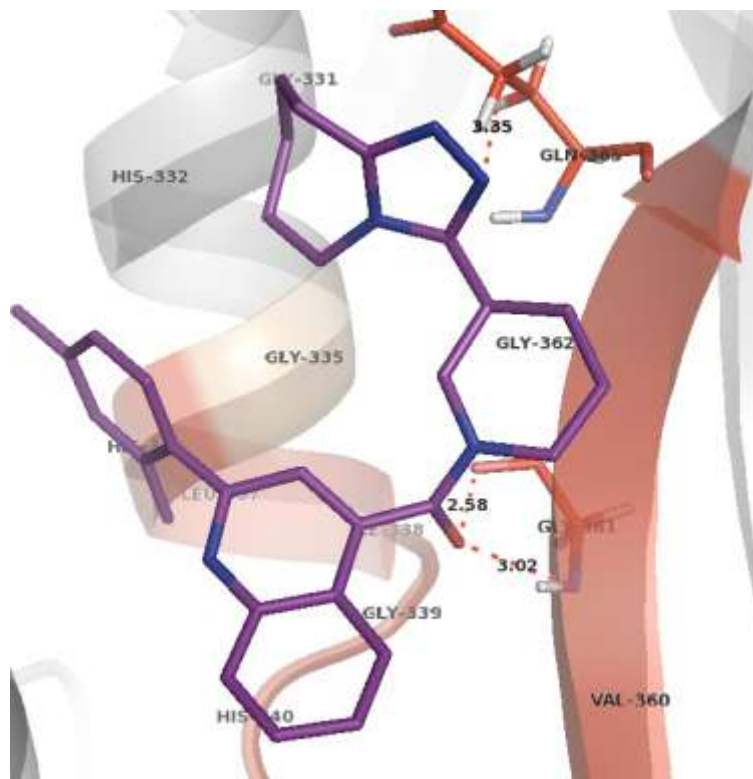


Figure 4.34: Docked Conformation of compound 3-135627 within IDE exosite. The exosite residues are shown as red. Hydrogen bonds are shown as red dashed lines.

The structure of IDE complex with the compound 3-135627 is shown in Figure 4.34. It covers the exosite region by interacting with two exosite residues, Gly³⁶¹ and Gln³⁶³. One of the N atoms in the triazole ring is found to accept a hydrogen bond from the Gln³⁶³ side chain, and the sole O atom also forms two hydrogen bonds with residue Gly³⁶¹. Nevertheless, it has some physicochemical properties beyond the limits, 143.888 for AMR and 5.88 for ALOGP.

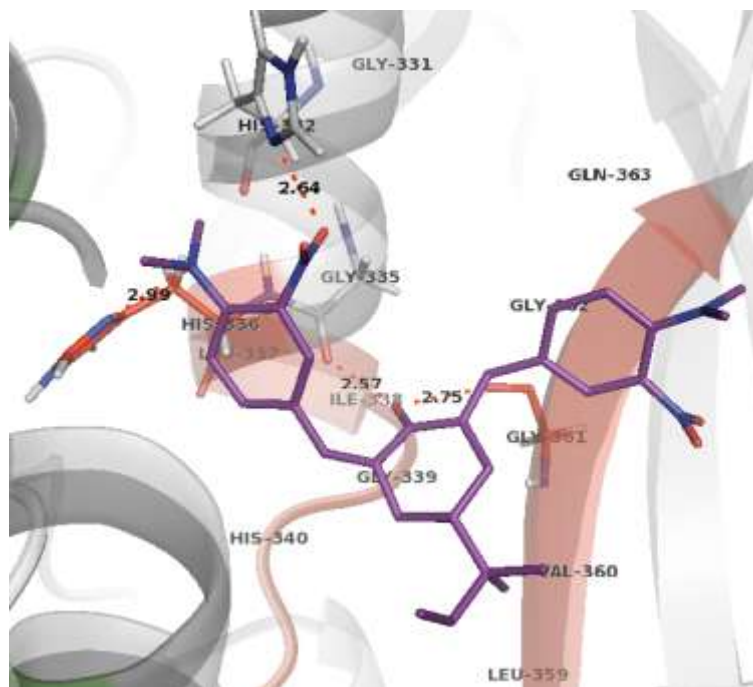


Figure 4.35: Docked Conformation of compound 9-1573 within IDE exosite. The exosite residues are shown as red. Hydrogen bonds are shown as red dashed lines.

The representative docked conformation of the compound 9-1573 that occupies the exosite region of IDE by interacting with four amino acid residues is shown in Figure 4.35. The phenolic oxygen of the candidate molecule is hydrogen bonded to the residues of Gly³⁶¹ and Gly³³⁵; at the same time nitrogen atoms of His³³² and His³³⁶ are predicted to receive hydrogen bonds from the nitrobenzene oxygen atoms. There are two O-H-O bonds and one N-H-N bond; in which the former is stronger. Therefore the stability of this compound is reasonable. The sole disadvantage of this hit is its physicochemical properties that exceed the limiting values for a drug-like compound. However, at a first instance, it is worth testing due its docking position and smaller binding and docking energies.

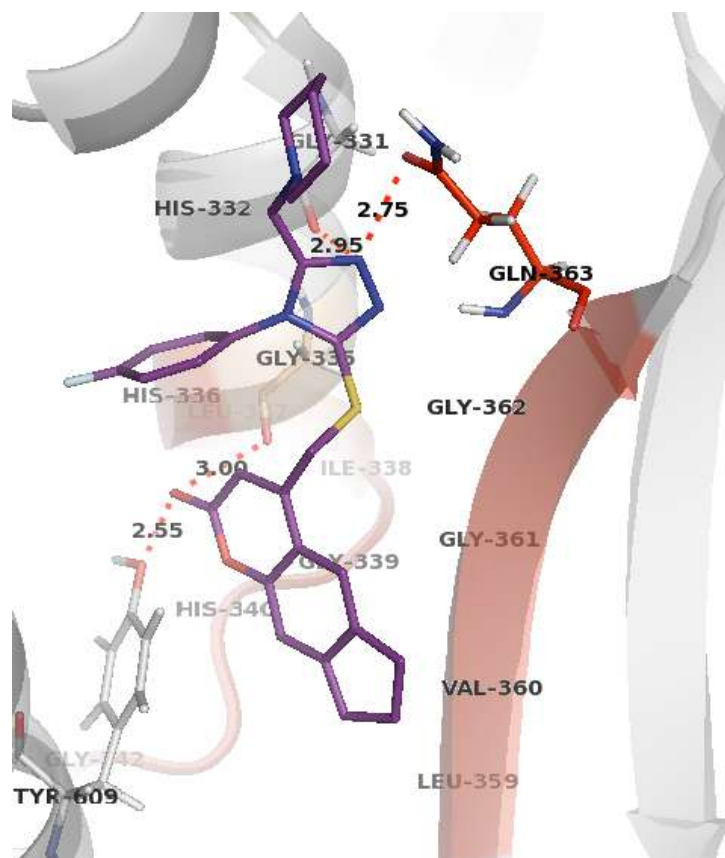


Figure 4.36: Docked Conformation of compound 3-137443 within IDE exosite. The exosite residues are shown as red. Hydrogen bonds are shown as red dashed lines.

As illustrated in Figure 4.36 compound 3-137443 binds to several IDE residues. Gln³⁶³ and Gly³³¹ are predicted to donate hydrogen bonds to the nitrogen atom of the triazole ring. Additional hydrogen bonds with Tyr⁶⁰⁹ and Gly³³⁵ are also established. Nevertheless, it has some physicochemical properties beyond the limits, 138.961 for AMR and 6.33 for ALOGP.

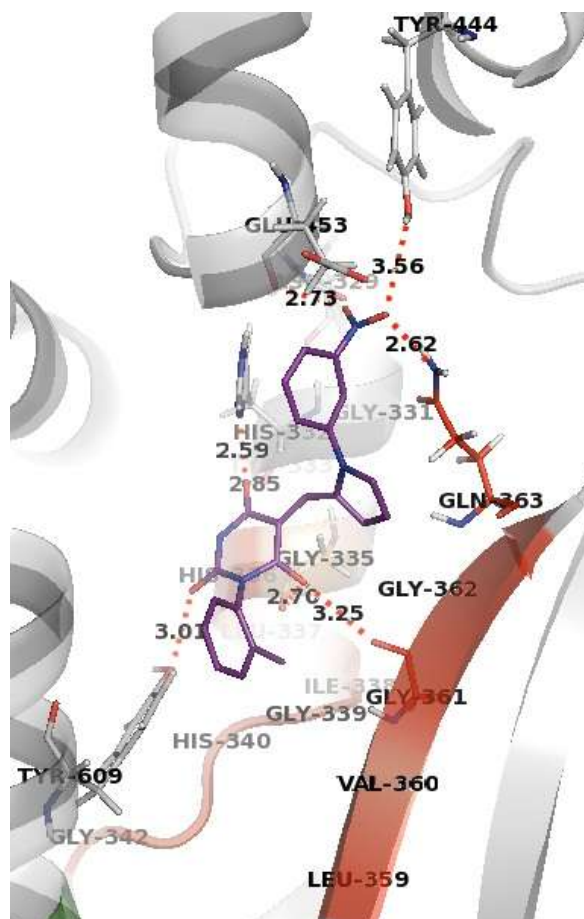


Figure 4.37: Docked Conformation of compound 9-134343 within IDE exosite. The exosite residues are shown as red. Hydrogen bonds are shown as red dashed lines.

Compound 9-134343 is predicted to bind to several exosite residues. The oxygen atoms that are connected to the pyrimidine ring and the O atoms of the nitrobenzene group can accept hydrogen bonds from Asn³²⁹, His³³², Tyr³³³, Gly³³⁵, Gly³⁶¹, Glu⁴⁵³, Tyr⁴⁴⁴ and Tyr⁶⁰⁹; whereas side chain N atom of Gln³⁶³ receives a hydrogen bond from the candidate molecule. Additionally, all the physicochemical properties are within accepted limits.

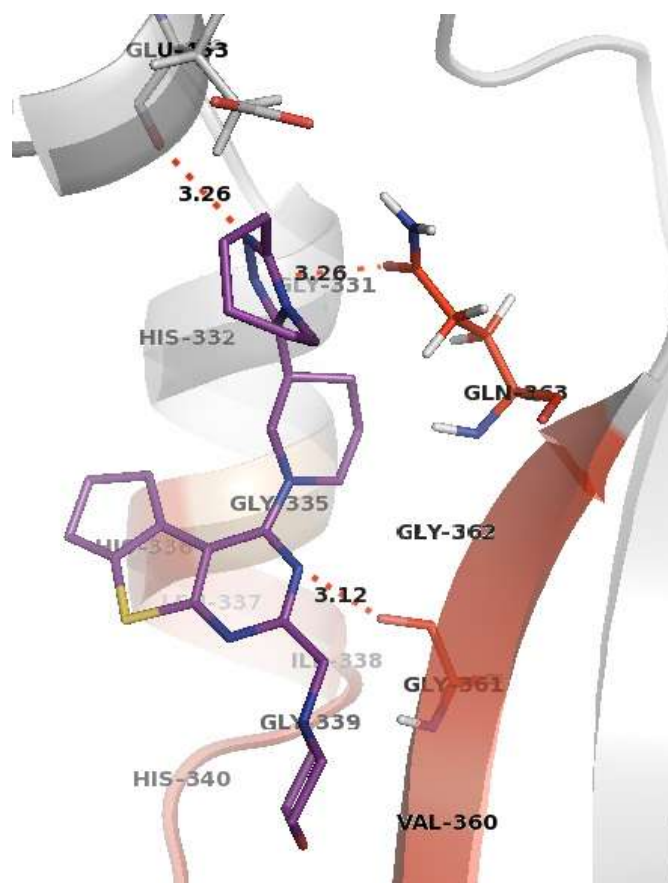


Figure 4.38: Docked Conformation of compound 1-180918 within IDE exosite. The exosite residues are shown as red. Hydrogen bonds are shown as red dashed lines.

Compound 1-180918 appears to interact with two exosite residues which are important for the catalytic activity. Glu⁴⁵³, Gln³⁶³ are predicted to donate hydrogen bonds to the N atoms of the triazole ring; and Gly³⁶¹ is also found to donate one to the N atom of the pyrimidine ring. For the physicochemical properties, only the AMR value exceeds the limits.

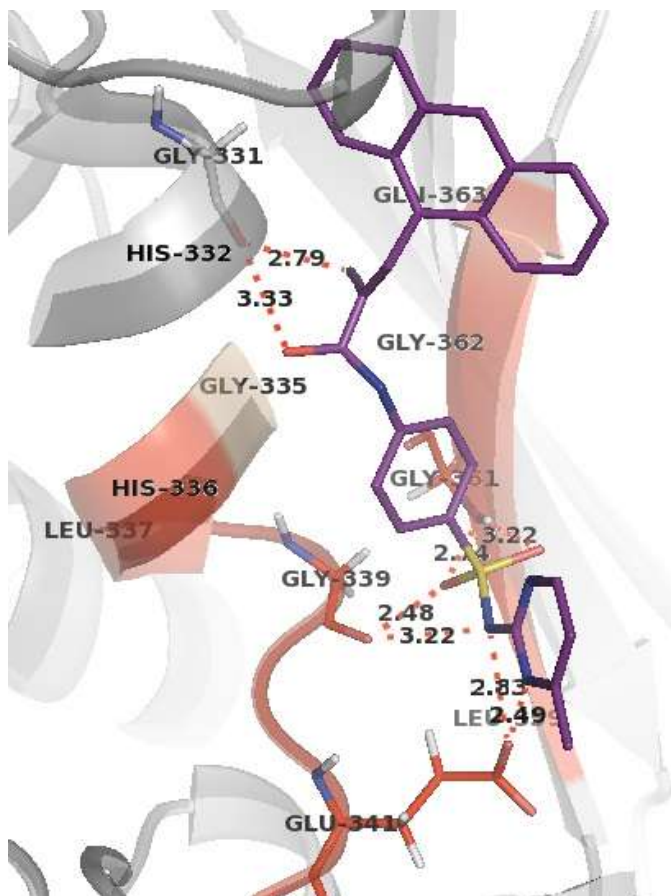


Figure 4.39: Docked Conformation of compound 8-456 within IDE exosite. The exosite residues are shown as red. Hydrogen bonds are shown as red dashed lines.

The docked structure of the molecule 8-456 is mostly positioned in the evolutionarily conserved exosite by establishing contacts with three exosite residues and one other IDE residue that is located at the same α -helix segment of exosite. Glu³⁴¹ is predicted to donate a hydrogen bond to one of the pyrimidine nitrogen atom. Additional hydrogen bonds are established between this anthracene ring containing compound and residues Gly³³¹, Gly³³⁹, Gly³⁶¹. For the physicochemical properties, only the AMR value exceeds the limits.

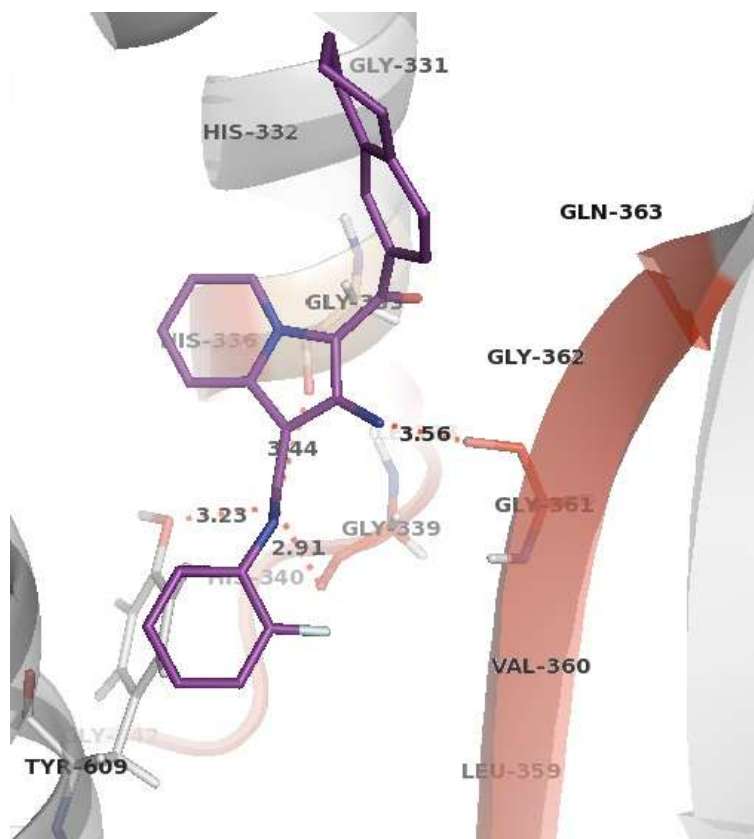


Figure 4.40: Docked Conformation of compound 3-110732 within IDE exosite. The exosite residues are shown as red. Hydrogen bonds are shown as red dashed lines.

The docking position shown in Figure 4.40 indicates that the compound 3.110732 is docked sterically well and established interactions with important amino acid residues of IDE exosite. Gly³⁶¹ is predicted to donate a hydrogen bond to the N atom that is bounded to pyrrole ring, and the compound also accepts two hydrogen bonds from Gly³³⁵, Gly³³⁹ and Tyr⁶⁰⁹. All physicochemical properties are in the range for a drug-like compound, which render this compound as a potential candidate for IDE regulator.

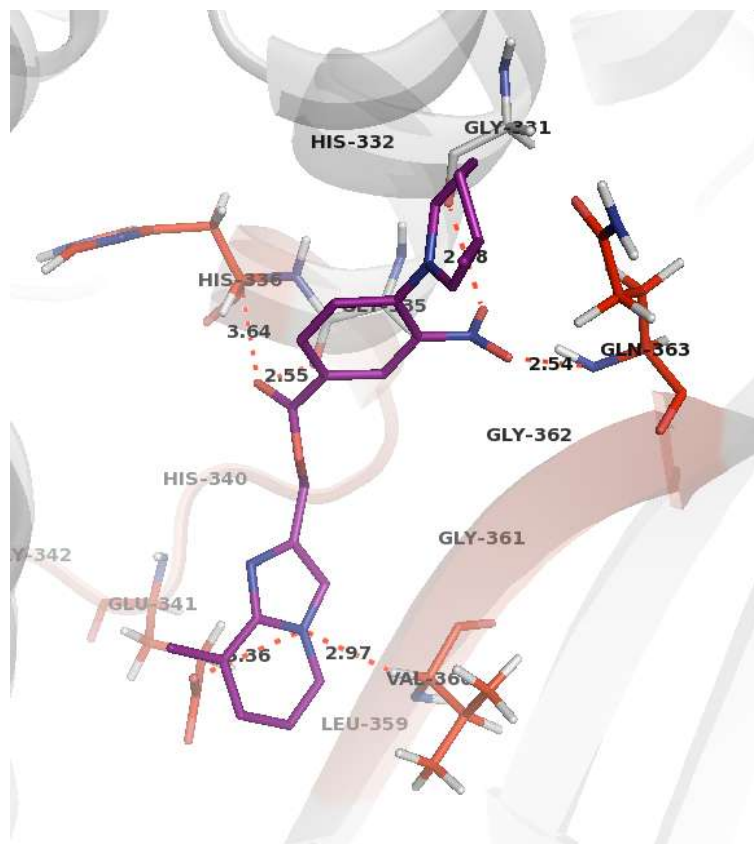


Figure 4.41: Docked Conformation of compound 4-106854 within IDE exosite. The exosite residues are shown as red. Hydrogen bonds are shown as red dashed lines.

The calculated binding mode of the compound 4-106854 in the exosite of IDE is shown in Figure 4.41. Oxygen atoms of the nitrobenzene group donate and receive hydrogen bonds to and from Gln³⁶³ and Gly³³¹, respectively. Besides, amino acid residues Val³⁶⁰ and Glu³⁴¹, which locate in the exosite region, donate hydrogen bonds to the nitrogen atom of the pyrazole ring. Additionally, another hydrogen bond is established between the residue His³³⁶ and the hit. All its molecular properties obey the drug likeness criteria.

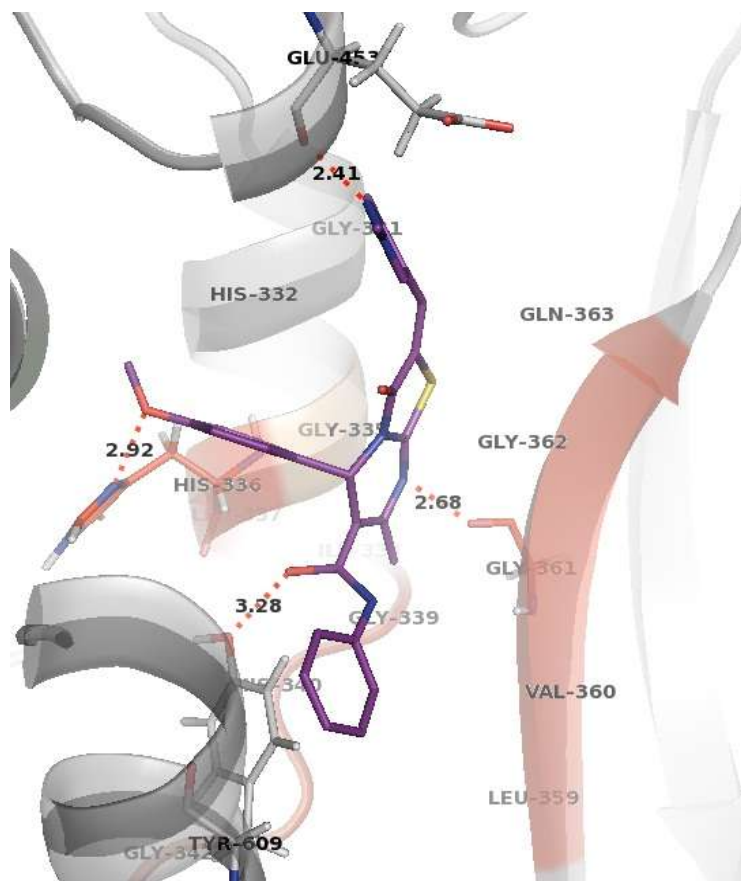


Figure 4.42: Docked Conformation of compound 3-114848 within IDE exosite. The exosite residues are shown as red. Hydrogen bonds are shown as red dashed lines.

The compound 3-114848 is docked along the exosite region and is hydrogen bonded to some IDE amino acid residues. Nitrogen atoms of the triazole ring and the pyrazole ring are predicted to receive two hydrogen bonds from Glu⁴⁵³ and Gly³⁶¹, respectively. On the other hand His³³⁶ accepts a hydrogen bond from the phenolic oxygen atom. Even though this compound has a molar refractivity value of 143.186, which is higher than the accepted value of 130, it is still acceptable due to its other desirable properties.

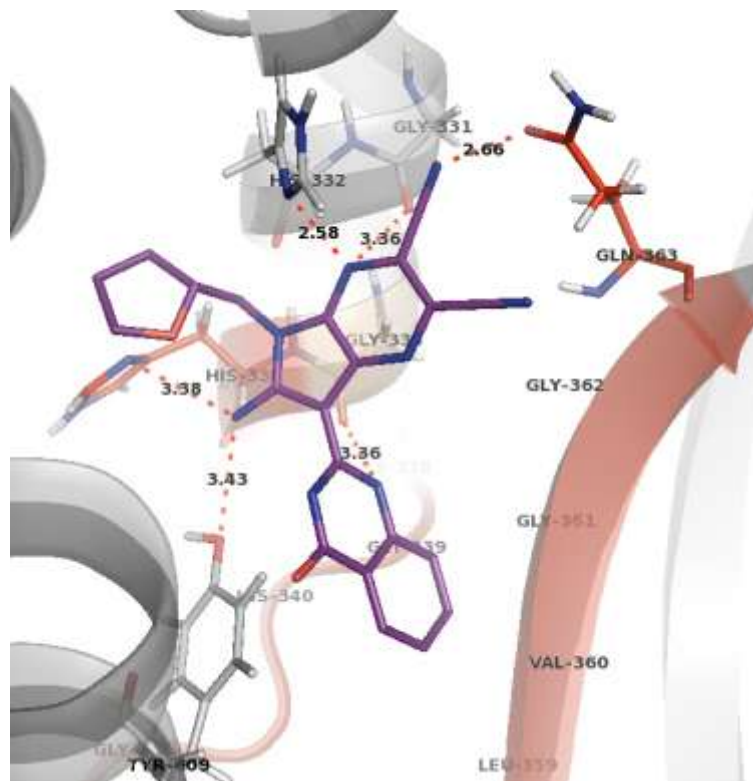


Figure 4.43: Docked Conformation of compound 2-114522 within IDE exosite. The exosite residues are shown as red. Hydrogen bonds are shown as red dashed lines.

The docking position shown in Figure 4.43 indicates that the compound 2-114522 is docked on the exosite and is predicted to interact with two exosite amino acid residues and four other IDE residues. Nitrogen atom of the quinazoline ring is hydrogen bonded to residue Gly³³⁵. Amino acid residues Gln³⁶³, Gly³³¹ and Tyr⁶⁰⁹ are found to donate hydrogen bonds to the N atom that is connected to the pyrazine ring, pyrazine N atom and N atom that is connected to pyrrole ring of the compound, respectively. On the other hand all the physicochemical properties obey the drug likeness criteria.

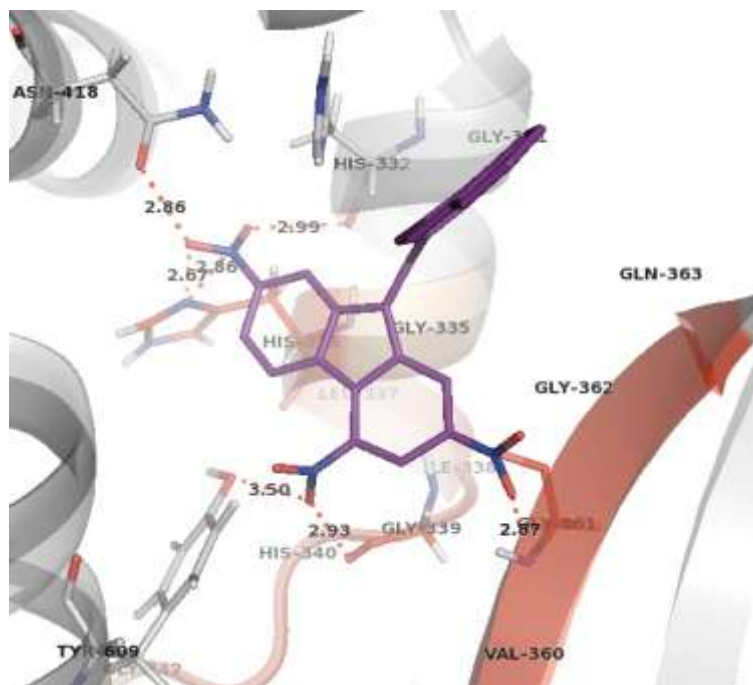


Figure 4.44: Docked Conformation of compound 1-11728 within IDE exosite. The exosite residues are shown as red. Hydrogen bonds are shown as red dashed lines.

Exosite residues His³³⁶ and Gly³⁶¹ are found to accept hydrogen bonds from the nitrobenzene oxygen atoms that are located at the terminal ends of the compound. Amino acid residues His³³², Gly³³⁹, Asn⁴¹⁸ and Tyr⁶⁰⁹ are all predicted to donate hydrogen bonds to the compound. Except from the molar refractivity value, all other molecular properties are in the range of a drug-like compound. And the excess value for the AMR value from the limiting point is considerably small.

Subject to the structural features derived from docking simulations, the selected compounds should be capable of regulating the catalytic activity of IDE by binding in the exosite. Therefore, 20 top-ranked compounds were selected for their virtual ability to regulate IDE. This virtual screening process would decrease the cost required to identify

these novel candidates in a wet-lab experiment. The applied computational procedure for the discovery of these novel compounds is illustrated in Figure 4.45.

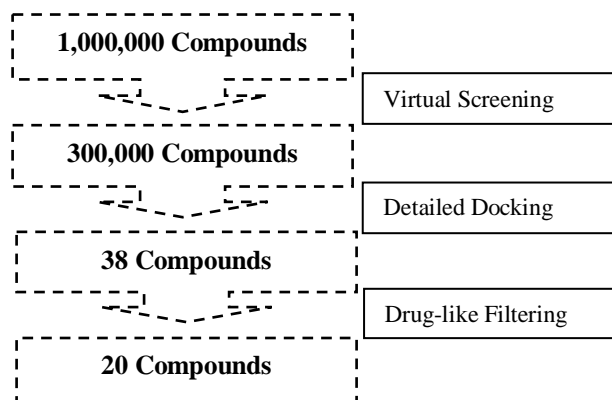


Figure 4.45: Adopted computational strategy for the discovery of Alzheimer and T2DM regulators.

4.5. Discussion

In the present study, we conducted a structure based drug discovery strategy to identify IDE activators. The protocol includes the molecular dynamics simulations of IDE, structure based virtual screening, and selection of the IDE regulators based on specific criteria described in previous sections. Consequently, we describe the use of virtual ligand screening for successful identification of several novel compounds that might enhance the activity of IDE.

Virtual screening, which is a much faster, cheaper and more efficient strategy compared to HTS, is becoming the major component of drug discovery process in the last few years [185]. There are two types of virtual screening: structure based and ligand based. When 3D structure of the protein is known, structure based screening is preferred, whereas ligand based screening is utilized when there is an experimental inhibition/activation data in the literature [186]. Since we have a crystal structure of IDE and there is not sufficient activator/inhibitor compounds discovered for IDE, we employed structure based virtual

screening. We used the AutoDock program in the structure based virtual screening protocol because its outperformance subject to its scoring function over the other docking programs had been displayed in several studies. [181]

The novel compounds that we discovered constitute an important new tool for the experimental manipulation of IDE, which might be critical for routine experimental and clinical applications that involve short peptide substrates of IDE. Detailed binding mode analysis with docking simulation show that the selected candidates are stabilized at the IDE exosite by the formation of hydrogen bonds with both exosite residues and with others that locate in the close proximity.

It has been shown that a small peptide substrate bradykinin increases the activity of IDE when this peptide binds to exosite region of IDE with a low affinity [18]. Hence, the discovery of a therapeutic molecule that binds to the IDE exosite with higher affinity can be a novel approach for the efficient A β clearance. Since the full bradykinin sequence bound IDE complex could not be obtained experimentally, we investigated the binding interactions for bradykinin as a full length peptide substrate. After the chemical screening, molecular docking and computational analysis were performed to gain insight into the binding of bradykinin to the IDE exosite. Crystal structure experiments revealed that the residues 336-342 and 359-363 of IDE are involved in interactions with bradykinin [18]. Molecular docking simulations confirmed the interactions of bradykinin with the residues 341-361 of IDE. The docking conformation of the N-terminus three residues (Arg¹, Pro², Pro³) of bradykinin is found to interact with the similar IDE residues within exosite. In addition, further interactions, which could not be observed from the crystal structure experiments, have been found with Ala⁴²¹, Ala⁶¹¹, Leu⁶¹⁶, Ser⁶¹⁷, Lys⁶³² of IDE and bradykinin. Binding free energy of bradykinin is considerably higher than those of the recently published chemical compounds (Ia1, Ia2), whereas docking energy of bradykinin is the lowest among others. This fact may be due to the high number of torsional freedom

of bradykinin molecule that creates high entropic contribution. This verification is also consistent with the previous study, where bradykinin was found to have low binding affinity to the IDE exosite [18]. It can be postulated that, binding of bradykinin at the exosite stimulates the switch from close to open state; however the stability and duration of open state can be increased using more efficient compounds. Similarly, binding of reference compounds (Ia1, Ia2) at the exosite are investigated. Cabrol *et al.* suggest that both Ia1 and Ia2 interact with a common domain within the IDE molecule [16]. Therefore we investigate whether Ia1, Ia2 exert their action through binding to the residues at the IDE exosite. Since their exact binding region is not known, we start by docking these compounds onto this evolutionarily conserved site. According to the binding energy calculations and ligand conformations, recently published IDE activators favorably fit into the IDE exosite with multiple polar interactions. Compound Ia1 was previously found to exert stronger effect on the degradation of A β by IDE compared to compound Ia2 [16]. Molecular docking simulation results also confirm this result, as lower binding and docking energies were obtained for Ia1-IDE interaction than Ia2-IDE as shown in Table 4.2. Even though the polar interactions between these compounds and IDE are not same as those between bradykinin and IDE; their conformations within the exosite region are quite similar. Since binding of these compounds to the same site with lower binding energies than that of bradykinin, they might have a similar regulatory role with bradykinin with higher stability.

It is known that IDE has a distinct allostericity. It can be suggested that the modulatory effects of these hit compounds can be due to this allosteric mechanism. Binding of these leads to the exosite of IDE might induce the proteolytic activity of IDE towards its substrates. The conformational change for IDE is required to enhance the catalytic activity due to this complex allosteric nature. This conformation change at the active site that is important for catalysis is linked to a structural change at the exosite interface. It can be

speculated that our lead compounds can even enter into a partially opened chamber due to their small sizes; therefore they can interact with exosite residues. This may result in a conformational change of IDE by reducing its catalytic chamber size, and this shift may yield the open state to allow substrates interact with the catalytic site [18, 119].

According to the virtual screening and detailed docking results, selected leads bind to IDE exosite by establishing polar interactions with IDE exosite residues. However, this method is not completely reliable; therefore the combination of molecular docking and experimental activity testing is required for reliable and satisfactory outcomes. Another problematic issue appears at this step. Even though the experimental assay results agree with the virtual screening results, it can not be said that these compounds show this regulatory effect by binding to IDE exosite. In order to gain insight into the functions of this regulatory site, exosite, and the binding interactions between exosite and the lead compounds, site directed mutagenesis approach can be performed as future studies. Several point mutations should be performed to the IDE exosite residues, and the mutated enzyme then allows the cleavage of its selected substrates where the mixture contains both the substrate and the lead compounds. Cleavage rate by the nonmutated wild type IDE would serve as a control. Effects of mutagenesis at the IDE exosite would be noted by an increase or decrease in the IDE catalytic activity by comparing with the wild type IDE proteolytic activity.

IDE substrate recognition mechanism does not depend on the amino acid sequence; but remarkably all IDE substrates have amyloidogenic parts which are recognized by IDE somehow. IDE regulation is also related with its cellular compartmentalization. As mentioned before, IDE exist mainly in cytosol (~95%), on the other hand small amount is also present in endosomes, peroxisomes, mitochondria, cell surface and the extracellular milieu (1-5%). There are several hypotheses that IDE degrade its substrates either within cytosol or endosome, at the cell surface or extracellularly by the secreted IDE [120]. The

clearance of the internalized insulin located within the endosomes is assumed not to be consistent with the cytosolic/peroxisomal localization of IDE. IDE is also present in the soluble fractions of the brain, and degrades A β both extracellularly and also at the cell surface. Additionally, IDE selectively recognizes and degrades insulin rather than the other substrates due to its high affinity to insulin. As it has an atypically moving active site, structural flexibility from α -helix to β -sheet, size, shape and charge distribution of the peptide substrates are involved in substrate recognition mechanism which elucidate its substrate specificity [119, 159]. IDE has multiple substrates with different binding affinities resulting in the competition with each other for IDE. That's why IDE catalytic activity depends on the balance between these substrates. IDE substrate recognition mechanism is therefore related to the pathogenesis of both AD and T2DM [125]. Understanding of this mechanism is crucial for the development of IDE regulators.

Chapter 5

CONCLUSIONS

At the outset of this study, 20 different possible candidates that might increase the activity of IDE are identified using molecular dynamics simulation and structure based virtual screening targeting to exosite of IDE. Molecular dynamics simulation is used to improve the structure of IDE to be utilized in molecular docking and virtual screening studies. The proposed compounds probably bind to exosite region that plays an important role in activity regulation of IDE by orienting the peptides to the catalytic site. Considering the minimum binding and docking energies and the exosite pocket occupancy of these lead compounds, they all have strong affinity to IDE. In order to validate our computational studies, these selected IDE regulators should be tested by *in vitro* enzymatic and cell viability assays for the further study. In addition to that, they should also be optimized to obtain efficient drug-like IDE activators. Future efforts will be undertaken to improve the activity of IDE by following the goal of lead optimization of these selected novel compounds. Considering the structural diversity and binding affinity of these leads, it is worth optimizing these compounds based on potency and low toxicity measurements to obtain an efficient drug-like IDE activator.

By the virtue of virtual screenin strategy, a library of randomly selected 1,000,000 compounds was docked to the previously modeled binding site, exosite of IDE. At the initial step, the number of compounds was reduced by applying molecular weight filter to save from the computational time. The molecular weight cut-off was set at 550g/mol, up to which the drug-like properties of a compound would decrease. The docked compounds were then ranked according to their minimum binding and docking energy conformation

scores. Based on energy scores, and visual analysis which comprise both the ligand docking conformation at the exosite and established polar interaction with both IDE residue, 300,000 compounds were selected for post analysis. These promising candidates were then redocked to the same site with higher resolution to increase the accuracy. As expected, the docking scores were improved with higher resolution grids and wider search parameters. By again applying the same analysis strategy, only 20 top selected compounds were subjected to experimental testing. The ones having long hydrocarbon chains, less reactive species, docking position far from the exosite, and inadequate interactions with IDE residues were eliminated. The physicochemical properties of these selected hits were also computed to understand their drug-like ability that is important for oral bioavailability, receptor binding and cellular uptake. Most of them can be considered as efficient drug-like compounds, the ones that are not within the accepted region can be further chemically modified to increase their regulation efficiency during experimental testing. Throughout this study, virtual screening, fast conformational search of the ligands, enabled us to save both time and resources. The cost required for the wet-lab experiments were minimized efficiently.

We also performed molecular docking calculations to validate the activity of the compounds used in the previous studies (Ia1, Ia2). Short peptide substrate bradykinin was previously found to be an activator by only binding to the exosite of IDE, and believed to stimulate the activity of IDE through allosteric effect. The low affinity of this peptide to IDE was confirmed by docking the full length of bradykinin to this region. Interactions between the N-terminal three residues of bradykinin with the exosite residues of IDE were also demonstrated through computational analysis. Introduced low binding affinity of bradykinin to IDE was also validated with respect to its binding energy, -5.66 kcal/mol. In addition, binding ability of the recently published compounds to IDE with respect to one another had also justified our study; higher degradation effect towards A β achieved with

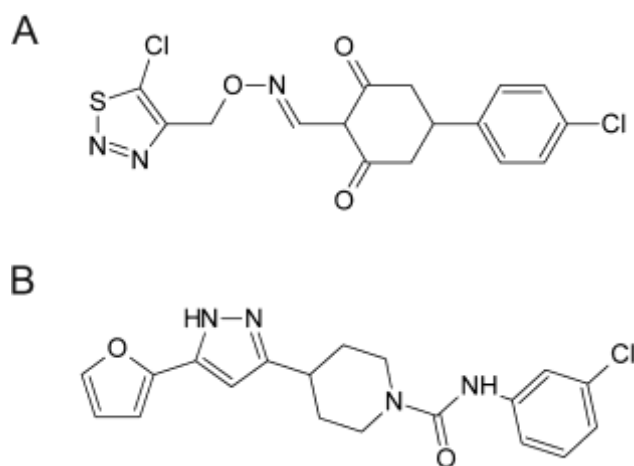
compound Ia1 was found reasonable depending on their smaller binding and docking energy than those of compound Ia2.

In future studies, the same virtual screening protocol can be conducted to screen new virtual libraries. In order to increase the success rate, more realistic docking algorithms involving both the ligand and the target macromolecule flexibility can be used. In order to maximize the chances of finding new drugs, MD simulations can be used for the refinement of docked complexes after virtual screening, and to understand the interaction in between better. Important to note that, each selected candidate has diverse structure, so that they can all be considered as new basis in order to further improve by optimization studies. By doing so, their binding affinity to IDE can be increased while keeping their toxicity minimum and selectivity maximum. Similarity search based on steric and electrostatic analogy can be also conducted to identify new molecules which might have regulatory effects on IDE by comparing them with the selected hits.

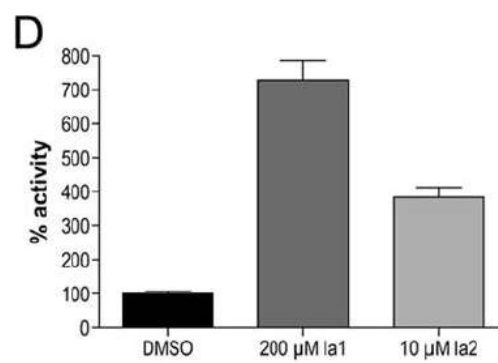
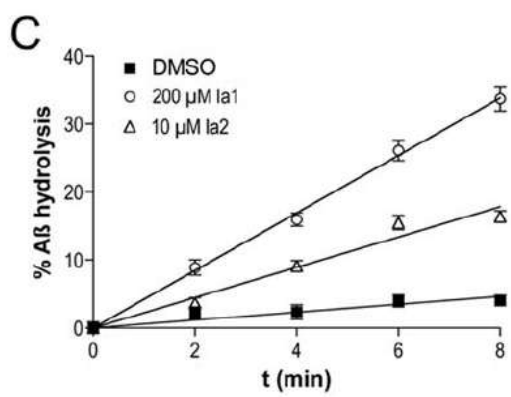
Selected IDE regulators after optimization studies to further attain appropriate pharmacokinetic properties may be useful for Alzheimer's disease by virtue of enhancing the clearance of amyloid- β from blood, or could be referred as potential molecules for development of IDE regulators with higher affinity. Additionally, they can constitute the promising candidates useful for the anti-diabetic therapy by modulation of the insulin degradation by IDE.

SUPPLEMENTARY

Supplementary 1: Chemical structures of reference paper compounds Ia1 (A), Ia2 (B) [16].



Supplementary 2: Reference paper compounds, Ia1 and Ia2, strongly activate A β degradation when presented together with a short substrate (FRET1; 10 mM). Representative timecourse of A β activation by Ia1 and Ia2 (C). Results of 4 independent experiments showing results normalized to DMSO-only controls (D).



BIBLIOGRAPHY

1. Myers S, Baker A: **Drug discovery – an operating model for a new era.** *Nat. Biotechnol* 2001, **19**:727–730.
2. Lyne PD: **Structure-based virtual screening: an overview.** *reviews research focus, DDT* 2002, Vol. **7**, No. 20.
3. Ghosh S, Nie A, An J, Huang Z: **Structure-based virtual screening of chemical libraries for drug discovery.** *Current Opinion in Chemical Biology* 2006, **10**:194–202.
4. Reddy AS, Pati SP, Kumar PP, Pradeep HN, Sastry GN: **Virtual Screening in Drug Discovery – A Computational Perspective.** *Current Protein and Peptide Science* 2007, **8**:329-351.
5. McInnes C: **Virtual screening strategies in drug discovery.** *Current Opinion in Chemical Biology* 2007, **11**:494–502.
6. Manly CJ, May SL, Hammer JD: **The impact of informatics and computational chemistry on synthesis and screening.** *reviews research focus DDT* 2001, Vol. **6**, No. 21.
7. Marrone TJ, Briggs JM, McCammon J: **Structure-Based Drug Design: Computational Advances.** *Annu. Rev. Pharmacol. Toxicol* 1997, **37**:71-90.
8. Leissring MA, Lu A, Condrón MM, Teplow DB, Stein RL, Farris W, Selkoe DJ: **Kinetics of amyloid beta protein degradation determined by novel fluorescence- and fluorescence polarization-based assays.** *J. Biol. Chem.* 2003, **278**:37314-37320.
9. Findeis MA: **The role of amyloid β peptide 42 in Alzheimer's Disease.** *Pharmacology & Therapeutics* 2007, **116**:266 – 286.

10. Bush AI: **The metallobiology of Alzheimer's Disease.** *TRENDS in Neurosciences* 2003, Vol.26 No.4.
11. Cole AR, Astell A, Green C, Sutherland C: **Molecular connexions between dementia and diabetes.** *Neuroscience and Biobehavioral Reviews* 2007, **31**:1046 – 1063.
12. Li L, Hölscher C: **Common pathological processes in Alzheimer disease and type 2 diabetes: A review.** *Brain Research Reviews* 2007, **56**:384– 402.
13. Hamaguchi T, Ono K, Yamada M: **Review: Anti-amyloidogenic therapies: strategies for prevention and treatment of Alzheimer's Disease.** *Cell. Mol. Life Sci.* 2006, **63**:1538–1552.
14. Eckman EA, Eckman CB: **Abeta-degrading enzymes: modulators of Alzheimer's disease pathogenesis and targets for therapeutic intervention.** *Biochem Soc Trans* 2005, **33**:1101 –1105.
15. Gasparini L, Xu H: **Potential roles of insulin and IGF- 1 i n Alzheimer 's Disease.** *Trends Neurosci.* 2003, **26**:404 – 406.
16. Cabrol C, Huzarska MA, Dinolfo C, Rodriguez MC, Reinstatler L: **Small-molecule activators of insulin-degrading enzyme discovered through high-throughput compound screening.** *PLoS One* 2009, **4**: e5274.
17. Leissring MA, Malito E, Hedouin S, Reinstatler L, Sahara T, Abdul-Hay SO, Choudhry S, Maharvi GM, Fauq AH, Huzarska M, May PS, Choi S, Logan TP, Turk BE, Cantley LC, Manolopoulou M, Tang WJ, Stein RL, Cuny GD, Selkoe DJ: **Designed inhibitors of insulin-degrading enzyme regulate the catabolism and activity of insulin.** *Plos One* 2010, **5**:e10504.
18. Malito E, Ralat LA, Manolopoulou M, Tsay JL, Wadlington NL, Tang WJ, **Molecular Bases for the Recognition of Short Peptide Substrates and Cysteine-**

- Directed Modifications of Human Insulin-Degrading Enzyme.** *Biochemistry* 2008, 47 (48), 12822-12834.
19. Mechlin H: **Dementia and Physical Activity.** *Eur Rev Aging Phys Act* 2008, 5:1-3.
 20. Tanzi RE, Bertram L: **New frontiers in Alzheimer's disease genetics.** *Neuron* 2001, 32: 181–184.
 21. Berchtold NC, Cotman CW: **Evolution in the conceptualization of dementia and Alzheimer's disease: Greco-Roman period to the 1960s.** *Neurobiol. Aging* 1998, 19 (3): 173–89.
 22. Selkoe DJ: **The molecular pathology of Alzheimer's Disease.** *Neuron* 1991, 6, 487–498.
 23. Evin G, Weidemann A: **Biogenesis and metabolism of Alzheimer's disease A β amyloid peptides.** *Peptides* 2002, 23:1285–1297.
 24. Iwata N, Higuchi M, Saido TC: **Metabolism of amyloid- β peptide and Alzheimer's disease.** *Pharmacology & Therapeutics* 2005, 108:129 – 148
 25. Zheng WH, Bastianetto S, Mennicken F, Ma W, Kar S: **Amyloid beta peptide induces tau phosphorylation and loss of cholinergic neurons in rat primary septal cultures.** *Neuroscience* 2002, 115:201–211.
 26. Perez RG, Zheng H, Van der Ploeg LH, Koo EH: **The beta-amyloid precursor protein of Alzheimer's Disease enhances neuron viability and modulates neuronal polarity.** *Journal of Neuroscience* 1997, 17:9407–9414.
 27. Yankner BA: **Mechanisms of Neuronal Degeneration in Alzheimer's Disease.** *Neuron* 1996, Vol. 16, 921–932.
 28. Pearson HA, Peers C: **Physiological roles for amyloid β peptides.** *J Physiol* 2006, 575.1, pp 5–10.

29. Ling Y, Morgan K, Kalsheker N: **Amyloid precursor protein (APP) and the biology of proteolytic processing: relevance to Alzheimer's Disease.** *The International Journal of Biochemistry & Cell Biology* 2003, **35**:1505–1535.
30. Buxbaum JD, Koo EH, Greengard P: **Protein phosphorylation inhibits production of Alzheimer amyloid beta/A4 peptide.** *Proceedings of the National Academy of Sciences of the United States of America* 1993, **90**:9195–9201.
31. Gouras GK, Xu H, Jovanovic JN, Buxbaum JD, Wang R, Greengard P, Relkin NR, Gandy S: **Generation and regulation of beta-amyloid peptide variants by neurons.** *Journal of Neurochemistry* 1998, **71**:1920–1925.
32. Turner PR, O'Connor K, Tate WP, Abraham WC: **Roles of amyloid precursor protein and its fragments in regulating neural activity, plasticity and memory.** *Progress in Neurobiology* 2003, **71**:1–32.
33. Selkoe DJ, Podlisny MB, Joachim CL, Vickers EA, Lee G, Fritz LC, Oltersdorf T: **Beta-amyloid precursor protein of Alzheimer disease occurs as 110–135-kilodalton membrane-associated proteins in neural and non-neural tissues.** *Proc. Natl. Acad. Sci. U.S.A.* 1988, **85**:7341–7345.
34. Morgan C, Colombres M, Nunez MT, Inestros NC: **Structure and function of amyloid in Alzheimer's Disease.** *Progress in Neurobiology* 2004, **74**:323–349.
35. Kuo YM, Emmerling MR, Vigo-Pelfrey C, Kasunic TC, Kirkpatrick JB, Murdoch GH, Ball MJ, Roher AE: **Water-soluble A β (N-40, N-42) oligomers in normal and Alzheimer disease brains.** *J. Biol. Chem.* 1996, **271**:4077–4081.
36. Vickers JC, Dickson TC, Adlard PA, Saunders HL, King CE, McCormack G: **The cause of neuronal degeneration in Alzheimer's disease.** *Progress in Neurobiology* 2000, **60**:139-165.

37. Bateman, RJ, Munsell, LY, Morris, JC, Swarm R, Yarasheski KE, Holtzman DM: **Human amyloid-beta synthesis and clearance rates as measured in cerebrospinal fluid in vivo.** *Nature Medicine* 2006, **12**:856–861.
38. Selkoe DJ: **Clearing the brain's amyloid cobwebs.** *Neuron* 2001, **32**:177–180.
39. Vekrellis K, Ye Z, Qiu WQ, Walsh D, Hartley D, Chesneau V, Rosner MR, Selkoe DJ: **Neurons regulate extracellular levels of amyloid b-protein via proteolysis by insulin-degrading enzyme.** *J. Neurosci.* 2000, **20**:1657–1665.
40. Lue LF, Kuo YM, Roher AE, Brachova L, Shen Y, Sue L, Beach T, Kurth JH, Rydel RE, Rogers J: **Soluble amyloid peptide concentration as a predictor of synaptic change in Alzheimer's disease.** *Am. J. Pathol.* 1999, **155**:853–862.
41. Graff-Radford NR, Lucas JA, Crook JE, Boeve BF, Knopman DS, Ivnik RJ: **Plasma A β Levels as a Premorbid Biomarker for Cognitive Decline, Mild Cognitive Impairment (MCI) and Alzheimer Disease (AD).** *Abstracts of the Alzheimer's Association International Conference on Prevention of Dementia, June 18-21, Washington, DC. Presentation P-011, 2005.*
42. Kim J, Onstead L, Yu C, Golde T, McGowan E: **A β 40 inhibits amyloid deposition and modulates premature death phenotype in vivo.** *Society for Neuroscience 35th Annual Meeting 2005, Program number 817.2.*
43. Mattson MP, Cheng B, Davis D, Bryant K, Lieberburg I, Rydel RE: **β -Amyloid peptides destabilize calcium homeostasis and render human cortical neurons vulnerable to excitotoxicity.** *J. Neurosci.* 1992, **12**, 376–389.
44. Yan SD, Chen X, Fu J, Chen M, Zhu H, Roher A, Slattery T, Zhao L, Nagashima M, Morser J, Migheli A, Nawroth P, Stern D, Schmidt AM: **RAGE and amyloid-beta peptide neurotoxicity in Alzheimer's disease.** *Nature* 1996, **382**:685– 691.
45. Hensley K, Carney JM, Mattson MP, Aksenova M, Harris M, Wu JF, Floyd RA, Butterfield DA: **A model for beta-amyloid aggregation and neurotoxicity based**

- on free radical generation by the peptide: relevance to Alzheimer disease.** *Proc. Natl Acad. Sci.* 1994, **91**:3270–3274.
46. Koh JY, Yang LL, Cotman CW: **Beta-amyloid protein increases the vulnerability of cultured cortical neurons to excitotoxic damage.** *Brain Res.* 1990, **533**:315–320.
47. St George Hyslop PH, Petit A: **Molecular biology and genetics of Alzheimer's Disease.** *C. R. Biologies* 2004, **328**:119–130.
48. Blennow K, Leon MJ, Zetterberg H: **Alzheimer's disease.** *Lancet* 2006, **368**:387–403.
49. Scheuner D, Eckman C, Jensen M, Song X, Citron M, Suzuki N, Bird TD, Hardy J, Hutton M, Kukull W, Larson E, Levy-Lahad E, Vitanen M, Peskind E, Poorkaj P, Schellenberg G, Tanzi R, Wasco W, Lannfelt L, Selkoe D, Younkin S: **Secreted amyloid beta-protein similar to that in the senile plaques of Alzheimer's disease is increased in vivo by the presenilin 1 and 2 and APP mutations linked to familial Alzheimer's disease.** *Nat. Med.* 1996, **2**:864–870.
50. Citron M: *Nat Rev Drug Discov*, **9**:387, 2010.
51. Wang DS, Dickson DW, Malter JS: **β -Amyloid Degradation and Alzheimer's Disease.** *Journal of Biomedicine and Biotechnology* 2006, Article ID 58406, 1–12, DOI 10.1155.
52. McGeer PL, McGeer E: *Neurobiol. Aging* 2007, **28**:639.
53. Schneider A, Mandelkow E: *Neurotherapeutics* 2008, **5**:443.
54. Mahley RW, Weisgraber KH, Huang Y: *Proc. Natl Acad. Sci. USA* 2006, **103**:5644.
55. Wolozin B: *Neuron* 2004, **41**, 7.
56. Puglielli L, Konopka G, Pack-Chung E, Ingano LA, Berezovska O, Hyman BT, Chang TY, Tanzi RE, Kovacs DM. *Nat Cell Biol* 2001, **3**:905.

57. Doerfler P, Shearman MS, Perlmutter RM: **Presenilin-dependent gamma-secretase activity modulates thymocyte development.** *Proc. Natl. Acad. Sci. USA* 2001, **98**:9312–7.
58. Clausen T, Bullock R: **Medical treatment and neuroprotection in traumatic brain injury.** *Curr. Pharm. Des.* 2001, **7**:1517–32.
59. Helmuth L: **New therapies. New Alzheimer's treatments that may ease the mind.** *Science* 2002, **297**:1260–2.
60. Scarpini E, Scheltens P, Feldman H: **Treatment of Alzheimer's disease: current status and new perspectives.** *Lancet Neurol* 2003, **2**:539–47.
61. Sonkusare SK, Kaul CL, Ramarao KP: **Dementia of Alzheimer's disease and other neurodegenerative disorders—memantine, a new hope.** *Pharmacological Research* 2005, **51**:1–17.
62. Selkoe DJ, Schenk D: **Alzheimer's disease: molecular understanding predicts amyloid-based therapeutics.** *Annu Rev Pharmacol Toxicol* 2003, **43**:545–584.
63. Imbimbo BP: *Drug Discov Today* 2008, **5**:169.
64. Milano J, McKay J, Dagenais C, Foster-Brown L, Pognan F, Gadiant R, Jacobs RT, Zacco A, Greenberg B, Ciaccio PJ: *Toxicol Sci* 2004, **82**:341.
65. Wong GT, Manfra D, Poulet FM, Zhang Q, Josien H, Bara T, Engstrom L, Pinzon-Ortiz M, Fine JS, Lee HJ, Zhang L, Higgins GA, Parker EM: *J Biol Chem* 2004, **279**: 12876.
66. Durham TB, Shepherd TA: *Curr Opin Drug Discov Devel* 2006, **9**:776.
67. Gervais F, Paquette J, Morissette C, Krzywkowski P, Yu M, Azzi M, Lacombe D, Kong X, Aman A, Laurin J, Szarek WA, Tremblay P: *Neurobiol Aging* 2007, **28**:537.
68. Aisen PA, Mehran M, Poole R, Lavoie I, Gervais F, Briand R, Garceau D: *Neurobiol. Aging* 2004, **25**:S20.

69. Bard F, Cannon C, Barbour R, Burke RL, Games D, Grajeda H, Guido T, Hu K, Huang J, Johnson-Wood K, Khan K, Kholodenko D, Lee M, Lieberburg I, Motter R, Nguyen M, Soriano F, Vasquez N, Weiss K, Welch B, Seubert P, Schenk D, Yednock T: *Nat Med* 2000, **6**:916.
70. Salloway S, Sperling R, Gilman S, Fox NC, Blennow K, Raskind M, Sabbagh M, Honig LS, Doody R, van Dyck CH, Mulnard R, Barakos J, Gregg KM, Liu E, Lieberburg I, Schenk D, Black R, Grundman M: *Neurology* 2009, **73**:2061.
71. DeMattos RB, Bales KR, Cummins DJ, Dodart JC, Paul SM, Holtzman DM: *Proc Natl Acad Sci U S A* 2001, **98**:8850.
72. Dodel R, Hampel H, Depboylu C, Lin S, Gao F, Schock S, Jackel S, Wei X, Buerger K, Hoft C, Hemmer B, Moller HJ, Farlow M, Oertel WH, Sommer N, Du YA: *Neurol* 2002, **52**:253.
73. Tsakanikas D, Shah K, Flores C, Assuras S, Relkin NR: *Alzheimers Dement.* 2008, **4**: T776.
74. Ott A, Stolk RP, Hofman A, van Harskamp F, Grobbee DE, Breteler MM: **Association of diabetes mellitus and dementia: the Rotterdam Study.** *Diabetologia* 1996, **39**:1392–1397.
75. Ott A, Stolk RP, van Harskamp F, Pols HA, Hofman A, Breteler MM: **Diabetes mellitus and the risk of dementia: The Rotterdam Study.** *Neurology* 1999 **53**: 1937–1942.
76. Leibson CL, Rocca WA, Hanson VA, Cha R, Kokmen E, O'Brien PC, Palumbo PJ: **The risk of dementia among persons with diabetes mellitus: a population-based cohort study.** *Ann. N.Y. Acad. Sci.* 1997, 826, 422–427.
77. Miklossy J, Qing H, Radenovic A, Kis A, Vilenó B, László F, Miller L, Martins RN, Waeber G, Mooser V, Bosmang F, Khalili K, Darbinia N, McGeera PL: **Beta**

- amyloid and hyperphosphorylated tau deposits in the pancreas in type 2 diabetes.** *Neurobiology of Aging* 2009,xxx xxx–xxx.
78. Zhang T, Pan BS, Zhao B, Zhang LM, Huang YL, Sun FY: **Exacerbation of Poststroke Dementia by Type 2 Diabetes is Associated with Synergistic Increases of β -secretase Activation and β -amyloid Generation in Rat Brains.** *Neuroscience* 2009, **161**:1045–1056.
79. Watson GS, Craef S: **Insulin resistance, inflammation, and cognition in Alzheimer's Disease: Lessons for multiple sclerosis”** *Journal of the Neurological Sciences* 2006, Issues 1-2, **245**:21-33.
80. Luchsinger JA: **Adiposity, hyperinsulinemia, diabetes and Alzheimer's disease An epidemiological perspective.** *European Journal of Pharmacology* 2008, **585**:119–129.
81. Lizcano JM, Alessi DR: **The insulin signalling pathway.** *Current Biology* 2002, **12**: R236–R238.
82. Pearl LH, Barford D: **Regulation of protein kinases in insulin, growth factor and Wnt signalling.** *Current Opinion in Structural Biology* 2002, **12**:761–767.
83. Roriz-Filho JS, Sá-Roriz TM, Rosset I, Camozzato AL, Santos AC, Chaves MLF, Moriguti JC, Roriz-Cruz M: **(Pre)diabetes, brain aging, and cognition.** *Biochimica et Biophysica Acta* 2009, **1792**:432–443.
84. Zhao WQ, Townsend M: **Insulin resistance and amyloidogenesis as common molecular foundation for type 2 diabetes and Alzheimer's disease.** *Biochimica et Biophysica Acta* 2009, **1792**:482–496.
85. Allen KV, Frier BM, Strachan MWJ: **The relationship between type 2 diabetes and cognitive dysfunction: longitudinal studies and their methodological limitations.** *European Journal of Pharmacology* 2004, **490**:169– 175.

86. Ryan CM, Geckle MO: **Circumscribed cognitive dysfunction in middle-aged adults with type 2 diabetes.** *Diabetes Care* 2000, **23**:1486–1493.
87. Xu WL, Qiu CX, Wahlin A, Winblad B, Fratiglioni L: **Diabetes mellitus and risk of dementia in the Kungsholmen project: a 6-year follow-up study.** *Neurology* 2004, **63**:1181–1186.
88. Luchsinger JA, Tang MX, Shea S, Mayeux R: **Hyperinsulinemia and risk of Alzheimer disease.** *Neurology* 2004, **63**:1187–1192.
89. Bruehl H, Wolf OT, Sweat V, Tirsi A, Richardson S, Convit A: **Modifiers of cognitive function and brain structure in middle-aged and elderly individuals with type 2 diabetes mellitus.** *Brain Research* 2009, **1280**:186 – 194.
90. Gerozissis K: **Brain insulin, energy and glucose homeostasis; genes, environment and metabolic pathologies.** *European Journal of Pharmacology* 2008, **585**:38–49
91. Diaz B, Serna J, De Pablo F, de la Rosa EJ: **In vivo regulation of cell death by embryonic (pro)insulin and the insulin receptor during early retinal neurogenesis.** *Development* 2000, **127**:1641–1649.
92. Craft S: **Insulin resistance syndrome and Alzheimer's disease: Age- and obesity-related effects on memory, amyloid, and inflammation.** *Neurobiology of Aging* 2005, **26S**:S65–S69
93. Mielke JG, Taghibiglou C, Liu L, Zhang Y, Jia Z, Adeli K, Wang YT: **A biochemical and functional characterization of diet-induced brain insulin resistance.** *Journal of Neurochemistry* 2005, **93**:1568–1578.
94. Luchsinger JA: **Evidence Linking The Continuum of Hyperinsulinemia to Alzheimer's Disease.** *Alzheimer's and Dementia* 2009, Volume 5, Issue 4, Supplement 1, Page P122.

95. Craft S, Asthana S, Cook DG, Baker LD, Cherrier M, Purganan K: **Insulin dose–response effects on memory and plasma amyloid precursor protein in Alzheimer’s disease: interactions with apolipoprotein E genotype.** *Psychoneuroendocrinology* 2003, 28(6):809–22.
96. Ho L, Qin W, Pompl PN, Xiang Z, Wang J, Zhao Z, Peng Y, Cambareri G, Rocher A, Mobbs CV, Hof PR, Pasinetti GM: **Diet-induced insulin resistance promotes amyloidosis in a transgenic mouse model of Alzheimer’s disease.** *FASEB Journal* 2004, 18, 902–904.
97. Freude S, Plum L, Schnitker J, Leeser U, Udelhoven M, Krone W, Bruning JC, Schubert M: **Peripheral hyperinsulinemia promotes tau phosphorylation in vivo.** *Diabetes* 2005, 54:3343–3348.
98. Kompoti M, Mariolis A, Alevizos A, Kyrazis I, Protopsaltis I, Dimou E, Lentzas I, Levisianou D, Gova A, Melidonis A: **Elevated serum triglycerides is the strongest single indicator for the presence of metabolic syndrome in patients with type 2 diabetes.** *Cardiovasc. Diabetol.* 2006, 5, 21.
99. Kaiyala KJ, Prigeon RL, Kahn SE, Woods SC, Schwartz MW: **Obesity induced by a high-fat diet is associated with reduced brain insulin transport in dogs.** *Diabetes* 2000, 49, 1525–1533.
100. Schubert D: **Glucose metabolism and Alzheimer’s disease.** *Ageing Research Reviews* 2005, 4:240–257.
101. Festa A, Williams K, D’Agostino R Jr, Wagenknecht LE, Haffner SM: **The Natural Course of {beta}-Cell Function in Nondiabetic and Diabetic Individuals: The Insulin Resistance Atherosclerosis Study.** *Diabetes* 2006, 55:1114–1120.
102. Prodi E, Obici S: **Minireview: the brain as a molecular target for diabetic therapy.** *Endocrinology* 2006, 147:2664–2669.

103. Janson J, Laedtke T, Parisi JE, O'Brien P, Petersen RC, Butler PC: **Increased risk of type 2 diabetes in Alzheimer disease.** *Diabetes* 2004, 53:474.
104. Munch G, Schinzel R, Loske C, Wong A, Durany N, Li JJ, Vlassara H, Smith MA, Perry G, Riederer P: **Alzheimer's disease—synergistic effects of glucose deficit, oxidative stress and advanced glycation endproducts.** *J. Neural. Transm.* 1998, **105**:439–461.
105. Wada R, Nishizawa Y, Yagihashi N, Takeuchi M, Ishikawa Y, Yasumura K, Nakano M, Yagihashi S: **Effects of OPB-9195, anti-glycation agent, on experimental diabetic neuropathy.** *Eur. J. Clin. Invest.* 2001, 31:513–520.
106. Clark A, Wells CA, Buley ID, Cruickshank JK, Vanhegan RI, Matthews DR, Cooper GJ, Holman RR, Turner RC: **Islet amyloid, increased A-cells, reduced B-cells and exocrine fibrosis: quantitative changes in the pancreas in type 2 diabetes.** *Diabetes Res.* 1988, **9**:151–159.
107. Porat Y, Kolusheva S, Jelinek R, Gazit E: **The human islet amyloid polypeptide forms transient membrane-active prefibrillar assemblies.** *Biochemistry* 2003, **42**:10971.
108. Hoppener JW, Ahren B, Lips CJ: **Islet amyloid and type 2 diabetes mellitus.** *N. Engl. J. Med.* 2000, **343**:411–419.
109. Hoppener JW, Lips, CJ: **Role of islet amyloid in type 2 diabetes mellitus.** *Int. J. Biochem. Cell Biol.* 2006, **38**:726–736.
110. Westermark P: **Fine structure of islets of Langerhans in insular amyloidosis.** *A Pathol. Pathol. Anat.* 1973, **359**:1.
111. Watson GS, Peskind ER, Asthana S, Purganan K, Wait C, Chapman D: **Insulin increases CSF Abeta42 levels in normal older adults.** *Neurology* 2003;60(12):1899–903.

112. Runz H, Rietdorf J, Tomic I, de Bernard M, Beyreuther K, Pepperkok R, Hartmann TJ: **Inhibition of intracellular cholesterol transport alters presenilin localization and APP processing in neuronal cells.** *Neuroscience* 2002, **22(5)**:1679-89,.
113. Fassbender K, Simons M, Bergmann C, Stroick M, Lutjohann D, Keller P, Runz H, Kuhl S, Bertsch T, von Bergmann K, Hennerici M, Beyreuther K, Hartmann T: **Simvastatin strongly reduces levels of Alzheimer's Disease beta-amyloid peptides Abeta 42 and Abeta 40 in vitro and in vivo.** *Proc. Natl.Acad. Sci. U.S.A.* 2001, **98**: 5856–5861.
114. Jick H, Zornberg GL, Jick SS, Seshadri S, Drachman DA: **Statins and the risk of dementia.** *Lancet* 2000, **356**:1627–1631.
115. Leroy K, Boutajangout A, Authelet M, Woodgett JR, Anderton BH, Brion JP: **The active form of glycogen synthase kinase-3beta is associated with granulovacuolar degeneration in neurons in Alzheimer's disease.** *Acta Neuropathology* 2002, **103**:91–99.
116. Cross DA, Alessi DR, Cohen P, Andjelkovich M, Hemmings BA: **Inhibition of glycogen synthase kinase-3 by insulin mediated by protein kinase B.** *Nature* 1995, **378**:785–789.
117. Salkovic - Petrisic M, Tribl F, Schmidt M, Hoyer S, Riederer P: **Alzheimer-like changes in protein kinase B and glycogen synthase kinase-3 in rat frontal cortex and hippocampus after damage to the insulin signalling pathway.** *Journal of Neurochemistry* 2006, **96**:1005–1015.
118. Mirsky IA, Broh-Kahn RH, Perisutti G, Brand J: **Inactivation of insulin by tissue extracts I. The distribution and properties of insulin inactivating extracts (insulinase).** *Biochem.* 1949, **20**:1–9.

119. Malito E, Hulse RE, Tang WJ: **Amyloid β -degrading cryptidases : insulin degrading enzyme,presequence peptidase, and neprilysin.** *Cell. Mol. Life Sci.* 2008, **65**:2574–2585.
120. Hulse RE, Ralat LA, Tang WJ: **Structure, function, and regulation of insulin-degrading enzyme.** *Vitam. Horm.* 2009, **80**:635–648.
121. Shii K, Roth RA: **Inhibition of insulin degradation by hepatoma cells after microinjection of monoclonal antibodies to a specific cytosolic protease.** *Proceedings of the National Academy of Sciences of the United States of America* 1986, **83**:4147–4151.
122. Kuo WL, Gehm BD, Rosner MR, Li W, Keller G: **Inducible expression and cellular localization of insulin-degrading enzyme in a stably transfected cell line.** *Journal of Biological Chemistry* 1994, **269**:22599–22606.
123. Yao H, Hersh LB: **Characterization of the binding of the fluorescent ATP analog TNP-ATP to insulysin.** *Archives of Biochemistry and Biophysics* 2006, **451**:175–181.
124. Kurochkin IV: **Insulin-degrading enzyme: embarking on amyloid destruction.** *Trends Biochem. Sci.* 2001, **26**:421–425.
125. Qiu WQ, Folstein MF: **Insulin, insulin-degrading enzyme and amyloid-beta peptide in Alzheimer's disease: review and hypothesis.** *Neurobiol. Aging* 2006, **27**:190-198.
126. Morelli L, Llovera RE, Mathov I, Lue LF, Frangione B, Ghiso J, Castaño EM: **Insulin degrading enzyme in brain microvessels: proteolysis of amyloid {beta} vasculotropic variants and reduced activity in cerebral amyloid angiopathy.** *Biol. Chem.* 2004, **279**:56004–56013.
127. Kim M, Hersh LB, Leissring MA, Ingelsson M, Matsui T, Farris W, Lu A, Hyman BT, Selkoe DJ, Bertram L, Tanzi RE: **Decreased Catalytic Activity of the Insulin-**

- degrading Enzyme in Chromosome 10-Linked Alzheimer Disease Families.** *The Journal of Biological Chemistry* 2007, VOL. **282**, NO. 11, pp. 7825–7832.
128. Qiu, WQ, Walsh DM, Ye Z, Vekrellis K, Zhang J, Podlisny MB, Rosner MR, Safavi A, Hersh LB, Selkoe DJ: **Insulin-degrading enzyme regulates extracellular levels of amyloid beta-protein by degradation.** *Journal of Biological Chemistry* 1998, **273**:32730–32738.
129. Song ES, Juliano MA, Juliano L, Fried MG, Wagner SL, Hersh LB: **ATP Effects on Insulin-degrading Enzyme Are Mediated Primarily through Its Triphosphate Moiety.** *The Journal of Biological Chemistry* 2004, Vol. **279**, No. 52, pp. 54216–54220.
130. Karamohamed S, Demissie S, Volcjak J, Liu C, Heard-Costa N, Liu J, Shoemaker CM, Panhuysen CI, Meigs JB, Wilson P, Atwood LD, Cupples LA, Herbert A: **Polymorphisms in the insulin-degrading enzyme gene are associated with type 2 diabetes in men from the NHLBI Framingham Heart Study.** *Diabetes* 2003, **52**:1562–1567.
131. Gu HF, Efendic S, Nordman S, Ostenson CG, Brismar K, Brookes AJ, Prince JA: **Quantitative Trait Loci near the Insulin-Degrading Enzyme Gene (IDE) Contribute to Variation in Plasma Insulin Levels.** *Diabetes* 2004, **53**:2137–2142.
132. Zhao Z, Xiang Z, Haroutunian V, Buxbaum JD, Stetka B, Pasinetti GM: **Insulin degrading enzyme activity selectively decreases in the hippocampal formation of cases at high risk to develop Alzheimer's disease.** *Neurobiol. Aging* 2007, **28**:824–830.
133. Farris W, Mansourian S, Leissring MA, Eckman EA, Bertram L, Eckman CB, Tanzi, RE, Selkoe DJ: **Partial loss-of-function mutations in insulin-degrading enzyme that induce diabetes also impair degradation of amyloid β -protein.** *American Journal of Pathology.* 2004, **164**:1425-1434.

134. Fakhrai-Rad H, Nikoshkov A, Kamel A, Fernstrom M, Zierath JR, Norgren S, Luthman H, Galli J: **Insulin-degrading enzyme identified as a candidate diabetes susceptibility gene in GK rats.** *Human Molecular Genetics* 2000, **9**:2149–2158.
135. Farris W, Mansourian S, Chang Y, Lindsley L, Eckman EA, Frosch MP, Eckman CB, Tanzi RE, Selkoe DJ, Guenette S: **Insulin degrading enzyme regulates the level of insulin, amyloid beta-protein, and the beta-amyloid precursor protein intracellular domain in vivo.** *Proc. Natl. Acad. Sci. U. S. A.* 2003, **100**:4162–4167.
136. Sladek R, Rocheleau G, Rung J, Dina C, Shen L, Serre D, Boutin P, Vincent D, Belisle A, Hadjadj S, Balkau B, Heude B, Charpentier G, Hudson TJ, Montpetit A, Pshezhetsky AV, Prentki M, Posner BI, Balding DJ, Meyre D, Polychronakos C, Froguel P: **A genome-wide association study identifies novel risk loci for type 2 diabetes.** *Nature* 2007, **445**:881–885.
137. Refolo LM, Malester B, LaFrancois J, Bryant-Thomas T, Wang R, Tint GS, Sambamurti K, Duff K, Pappolla MA: **Hypercholesterolemia upon differentiation-associated increases in tau and cyclin-dependent kinase accelerates the Alzheimer's amyloid pathology in a transgenic mouse model.** *Neurobiol.Dis.* 2000, **7**:321–331.
138. Fassbender K, Simons M, Bergmann C, Stroick M, Lutjohann D, Keller P, Runz H, Kuhl S, Bertsch T, von Bergmann K, Hennerici M, Beyreuther K, Hartmann T: Simvastatin strongly reduces levels of Alzheimer's Disease beta-amyloid peptides Abeta 42 and Abeta 40 in vitro and in vivo. *Proc. Natl. Acad. Sci. U.S.A.* 2001, **98**: 5856–5861.
139. Sharma S, Prasanthi RPJ, Schommer E, Feist G, Ghribi O: **Hypercholesterolemia-induced A β accumulation in rabbit brain is associated with alteration in IGF-1 signaling.** *Neurobiology of Disease* 2008, **32**:426–432.

140. Burns MP, Noble WJ, Olm V., Gaynor K, Casey, E, LaFrancois J, Wang L, Duff K: **Co-localization of cholesterol, apolipoprotein E and fibrillar A β in amyloid plaques.** *Brain Res. Mol. Brain Res.* 2003, **110**:119–125.
141. Cook DG, Leverenz JB, McMillan PJ, Kulstad JJ, Ericksen S, Roth RA, Schellenberg GD, Jin LW, Kovacina KS, Craft S: **Reduced hippocampal insulin-degrading enzyme in late-onset Alzheimer's disease is associated with the apolipoprotein E-epsilon4 allele.** *Am. J. Pathol.* 2003, **162**:313–319.
142. Peila R, Rodriguez BL, Launer LJ: **Type 2 diabetes, APOE gene, and the risk for dementia and related pathologies: The Honolulu–Asia Aging Study.** *Diabetes* 2002, **51**:1256–1262.
143. Alonso H, Bliznyuk AA, Gready JE: **Combining Docking and Molecular Dynamic Simulations in Drug Design.** *Medicinal Research Reviews* 2006, Vol. 26, No. 5, 531-568.
144. Muthas D, Sabnis YA, Lundborg M, Karlén A: **Is it possible to increase hit rates in structure-based virtual screening by pharmacophore filtering? An investigation of the advantages and pitfalls of post-filtering.** *Journal of Molecular Graphics and Modelling* 2008, **26**:1237–1251.
145. Guido RVC, Oliva G, Andricopulo AD: **Virtual Screening and Its Integration with Modern Drug Design Technologies.** *Current Medicinal Chemistry*, 2008, **15**:37-46.
146. Shoichet BK: **Virtual screening of chemical libraries.** *Nature* 2004, **432**:862–865.
147. Klebe G: **Foundation review: Virtual ligand screening: strategies, perspectives and limitations.** *Drug Discovery Today* 2006, Volume **11**, Numbers 13/14.
148. Muegge I, Oloff S: **Advances in virtual screening.** *Drug Discovery Today: Technologies* 2006, Vol. 3, No. 4.

149. Anderson AC: The Process of Structure-Based Drug Design. *Chemistry & Biology* 2003, Vol. **10**:787–797.
150. McCarthy JD: *Pharma. Thera.* 1999, **8**:179-191.
151. Jansen JM, Martin EJ: **Target-biased scoring approaches and expert systems in structure-based virtual screening.** *Current Opinion in Chemical Biology* 2004, **8**:359–364.
152. Halgren, TA: **Merck molecular force field. II. MMFF94 van der Waals and electrostatic parameters for intermolecular interactions.** *J. Comput. Chem.* 1996, **17**:520-552.
153. Bohm HJ: **Prediction of binding constants of protein ligands: A fast method for the prioritization of hits obtained from de novo design or 3D database search programs.** *Journal of Computer-Aided Molecular Design* 1998, **12**(4):309-323.
154. Lipinski CA, Lombardo F, Dominy BW, Feeney PJ: **Experimental and computational approaches to estimate solubility and permeability in drug discovery and development settings.** *Adv. Drug Deliv. Rev.* 2001, **46**:3–26.
155. Im H, Manolopoulou M, Malito E, Shen Y, Zhao J, Fery MN, Sun CY, Meredith SC, Sisodia SS, Leissring MA, Tang WJ: **Structure of Substrate-free Human Insulin-degrading Enzyme (IDE) and Biophysical Analysis of ATP-induced Conformational Switch of IDE.** *The Journal of Biological Chemistry* 2007, Vol. 282, No. 35, pp:25453–25463.
156. Shen Y, Joachimiak A, Rosner MR, Tang WJ: **Structures of human insulin-degrading enzyme reveal a new substrate recognition mechanism.** *Nature* 2006, **443**:870-874.
157. Li P, Kuo WL, Yousef M, Rosner MR, Tang WJ: **The C-terminal domain of human insulin degrading enzyme is required for dimerization and substrate**

- recognition.** *Biochemical and Biophysical Research Communications* 2006, **343**:1032–1037.
158. Leissring MA, Selkoe DJ: **Enzyme target to latch on to.** *Nature* 2006, Vol **443**.
159. Manolopoulou M, Guo Q, Malito E, Schilling AB, Tang WJ: **Molecular Basis of Catalytic Chamber-assisted Unfolding and Cleavage of Human Insulin by Human Insulin-degrading Enzyme.** *The Journal of Biological Chemistry* 2009, Vol. **284**, No. 21, pp. 14177–14188.
160. Song ES, Juliano MA, Juliano L, Hersh LB: **Substrate activation of insulin - degrading enzyme (insulysin). A potential target for drug development.** *J. Biol. Chem.* 2003, **278**:49789–49794.
161. Guo Q, Manolopoulou M, Bian Y, Schilling AB, Tang WJ: **Molecular Basis for the Recognition and Cleavages of IGF-II, TGF- α , and Amylin by Human Insulin-Degrading Enzyme.** *J. Mol. Biol.* 2010 **395**:430–443.
162. Kurochkin IV: **Amyloidogenic determinant as a substrate recognition motif of insulin-degrading enzyme.** *FEBS Lett.* 1998, **427**:153–156.
163. Duckworth WC, Bennett RG, Hamel FG: **Insulin Degradation: Progress and Potential.** *Endocr. Rev.* 1998, **19**:608–624.
164. Kitchen DB, Decornez H, Furr JR, Bajorath J: **Docking and Scoring in Virtual Screening for Drug Discovery: Methods and Applications.** *Nature Reviews* 2004, **3**:935-949.
165. Strett WB, Tildesley DJ, Saville G: **Multiple time-step methods in molecular dynamics.** *Molecular Physics* 1978, 35(3):639 – 648.
166. Karplus M, McCammon JA: **Molecular dynamics simulations of biomolecules.** *Nature Structural Biology*, 2002. 9(9):646-652.
167. Adcock SA, McCammon JA: **Molecular Dynamics: Survey of Methods for Simulating the Activity of Proteins.** *Chem Rev.* 2006, 106(5): 1589–1615.

168. Cornell WD, Cieplak P, Bayly CI, Gould IR, Merz KM, Ferguson DM, Spellmeyer DC, Fox T, Caldwell JW, Kollman PA: **A second generation force field for the simulation of proteins, nucleic acids, and organic molecules.** *J Am Chem Soc* 1996, **118**:2309–2309.
169. Brooks BR, Bruccoleri RE, Olafson BD, States DJ, Swaminathan S, Karplus M: **CHARMM—A program for macromolecular energy, minimization, and dynamics calculations.** *J Comput Chem* 1983,**4**:187–217.
170. Scott WRP, Hunenberger PH, Tironi IG, Mark AE, Billeter SR, Fennel J, Torda AE, Huber T, Kruger P, van Gunsteren WF: **The GROMOS biomolecular simulation program package.** *J Phys Chem A* 1999, **103**: 3596–3607.
171. Nelson MT, Humphrey W, Gursoy A, Dalke A, Kale LV, Skeel RD, Schulten K. **NAMD: A parallel, object oriented molecular dynamics program.** *Int J Supercomput Applic* 1996, **10**:251–268.
172. Phillips JC, Braun R, Wang W, Gumbart J, Tajkhorshid E, Villa E, Chipot C, Skeel RD, Kalé L, Schulten K: **Scalable molecular dynamics with namd.** *J Comput Chem* 2005, **26**: 1781-1802.
173. Allen MP, Tildesley DJ: **Computer Simulation of Liquids.** *Oxford University Press* 1987, New York.
174. MacKerell AD: **All-atom empirical potential for molecular modeling and dynamics studies of proteins.** *J Phys Chem B* 1998, **102**:3586-3616.
175. Perlman RK, Rosner MR: **Identification of zinc ligands of the insulin-degrading enzyme.** *J. Biol. Chem.* 1994, **269**:33140-33145.
176. Jorgensen WL: **Rusting of the Lock and Key Model for Protein-Ligand Binding.** *Science*, 1991. 254(**5034**):954-955.

177. Klebe G, Böhm HJ: **Energetic and Entropic Factors Determining Binding Affinity in Protein-Ligand Complexes.** *Journal of Receptors and Signal Transduction* 1997, Vol. **17**, No. 1-3, pp:459-473.
178. Alonso H: **Chapter 2. Computational Approaches for the Study of Enzymes and their Reactions.** *PhD Thesis* 2006.
179. Halperin I, Ma B, Wolfson H, Nussinov R: **Principles of docking: an overview of search algorithms and a guide to scoring functions.** *Proteins* 2002, **47**:409–443.
180. Goodford PJ: **A computational procedure for determining energetically favorable binding sites on biologically important macromolecules.** *J. Med. Chem.* 1985, **28**:849–857.
181. Park H, Lee J, Lee S: **Critical assessment of the automated AutoDock as a new docking tool for virtual screening.** *Proteins* 2006, **65**:549.
182. Morris, GM: **Automated docking using a Lamarckian genetic algorithm and an empirical binding free energy function.** *J. Comput. Chem.* 1998, **19**:1639–1662.
183. Ghose AK, Viswanadhan VN, Wendelowski JJ: **A know- ledge-based approach in designing combinatorial or medicinal chemistry libraries for drug discovery. 1. A qualitative characterization of known drug databases.** *J. Comb. Chem.* 1999, **1**:55–67.
184. Kubinvi H: **Nonlinear dependence of biological activity on hydrophobic character: the bilinear model.** *Farmaco [Sci]* 1979, **34(3)**:248-76.
185. Kruger DM, Evers A: **Comparison of structure- and ligand-based virtual screening protocols considering hit list complementarity and enrichment factors.** *ChemMedChem* 2010, **5**:148-58.
186. Bleicher, KH, Bohm HJ, Muller K, Alanine AI: **Hit and lead generation: beyond high-throughput screening.** *Nature Reviews Drug Discovery* 2003, **2**:369-78.

VITA

Ezgi Dağyıldız was born in Ankara, Turkey, on August 5, 1985. She is a graduate of Saint Joseph French College and she received her B.Sc. Degree in Chemical Engineering from İzmir Institute of Technology, Izmir, Turkey in 2008. She was both research and teaching assistant at Koç University from September 2008 to August 2010.

She is a member of Cell and Tissue Engineering Lab of Dr. Seda Kızılel and *SystemsLab* of Dr. Metin Türkay. Her research interests include computational biology, drug discovery and design.